

**ENHANCING THE SOLUBILITY OF CALCIUM PHOSPHATE CERAMICS BY  
CALCIUM SALT INFILTRATION FOR THE PURPOSE OF HEMATOPOIETIC STEM  
CELL CULTURING**

by

**Qinghao Zhang**

BS, East China University of Science and Technology, 2012

Submitted to the Graduate Faculty of  
The Swanson School of Engineering in partial fulfillment  
of the requirements for the degree of  
Doctor of Philosophy in Materials Science and Engineering

University of Pittsburgh

2016

UNIVERSITY OF PITTSBURGH  
SWANSON SCHOOL OF ENGINEERING

This dissertation was presented

by

Qinghao Zhang

It was defended on

June 30, 2016

and approved by

Chmielus Markus, PhD, Assistant Professor  
Department of Mechanical Engineering and Materials Science

Lee Jung-Kun, PhD, Associate Professor  
Department of Mechanical Engineering and Materials Science

Chun Young Jae, PhD, Assistant Professor  
Department of Industrial Engineering

Dissertation Director: Ian Nettleship, PhD, Associate Professor  
Department of Mechanical Engineering and Materials Science

Copyright © by Qinghao Zhang

2016

**ENHANCING THE SOLUBILITY OF CALCIUM PHOSPHATE CERAMICS BY  
CALCIUM SALT INFILTRATION FOR THE PURPOSE OF HEMATOPOIETIC  
STEM CELL CULTURING**

Qinghao Zhang, PhD

University of Pittsburgh, 2016

The hematopoietic stem cells (HSCs) have been unquestionably important to therapies that involve blood and immune system replacement. However, the in-vitro culture and the expansion of HSCs inhibit their application. This work aims to develop a composite biodegradable 3D scaffold that would simulate key aspects of the in-vivo microenvironment (niche) in which expansion of the hematopoietic stem cells takes place in human bone marrow. Hydroxyapatite (HA) has been chosen as a scaffold material because of its biocompatibility and the ability to create an osteogenic scaffold and thereby simulate trabecular bone that is known to be important to the HSC niche in bone marrow. It is hypothesized that the use of a Ca-rich HA scaffold will create a three dimensional, protective environment for HSCs and further promote their in-vitro expansion by releasing Ca ions into the culture medium. .

The first part of this study examined the processing of Ca-rich HA and the release of calcium ions into saline over time. The Ca-rich phase was introduced into the HA by an infiltration process and has been shown to release calcium into the culture medium over 42 days. The second part of this study examined the effect of the scaffold material on the fate of human umbilical vein endothelial cells (HUVECS), a well-known endothelial progenitor model. The results showed, for the first time, that at least some HUVEC cells have hematopoietic potential and that the scaffold promoted differentiation down the hematopoietic cell lineage. This is

thought to be due to hemangioblast character in the HUVEC cells which is also shared by HSCs. Finally the effects of the scaffold on the in-vitro co-culture of an osteoblast cell line and primary human bone marrow derived HSCs was studied. The infiltrated scaffolds were shown to stimulate the HSC population to differentiate down the hematopoietic lineage and also showed greater potential to differentiate down the HSC lineage in consequent CFU assays.

## TABLE OF CONTENTS

<b>PREFACE.....</b>	<b>XV</b>
<b>1.0       INTRODUCTION.....</b>	<b>1</b>
<b>2.0       BACKGROUND .....</b>	<b>5</b>
<b>2.1       REGENERATIVE MEDICINE .....</b>	<b>5</b>
<b>2.1.1   Cell therapy .....</b>	<b>5</b>
<b>2.1.2   Tissue engineering.....</b>	<b>6</b>
<b>2.1.3   Bioreactor.....</b>	<b>7</b>
<b>2.1.4   Biomaterial scaffold .....</b>	<b>10</b>
<b>2.2       BONE MARROW .....</b>	<b>12</b>
<b>2.2.1   Hematopoietic Stem Cell .....</b>	<b>14</b>
<b>2.2.2   Hematopoietic Stem Cell Applications.....</b>	<b>16</b>
<b>2.2.3   In vitro Hematopoietic Stem Cell Culture .....</b>	<b>18</b>
<b>2.3       CALCIUM PHOSPHATE .....</b>	<b>19</b>
<b>2.3.1   Calcium Phosphate .....</b>	<b>19</b>
<b>2.3.2   Hydroxyapatite.....</b>	<b>21</b>
<b>2.3.3   Tri-calcium phosphate .....</b>	<b>22</b>
<b>2.3.4   Solubility of Calcium Phosphate Phases .....</b>	<b>24</b>
<b>2.3.5   Effect of Calcium on the Bone Marrow Niche.....</b>	<b>26</b>

<b>2.4</b>	<b>CERAMIC FOAM.....</b>	<b>28</b>
<b>2.4.1</b>	<b>Replication .....</b>	<b>29</b>
<b>2.4.2</b>	<b>Templating.....</b>	<b>30</b>
<b>2.4.3</b>	<b>Direct Foaming.....</b>	<b>31</b>
<b>2.4.4</b>	<b>Emulsion Foaming .....</b>	<b>34</b>
<b>2.5</b>	<b>SINTERING.....</b>	<b>34</b>
<b>2.5.1</b>	<b>Infiltration.....</b>	<b>36</b>
<b>3.0</b>	<b>HYPOTHESIS.....</b>	<b>38</b>
<b>4.0</b>	<b>OBJECTIVES .....</b>	<b>39</b>
<b>5.0</b>	<b>APPROACH .....</b>	<b>40</b>
<b>5.1</b>	<b>MATERIAL PREPARATION.....</b>	<b>40</b>
<b>5.1.1</b>	<b>Hydroxyapatite Powder Preparation .....</b>	<b>40</b>
<b>5.1.2</b>	<b>High Calcium Content Pellets .....</b>	<b>40</b>
<b>5.1.3</b>	<b>High Calcium Phosphate Ratio Foam .....</b>	<b>41</b>
<b>5.2</b>	<b>CHARACTERIZATION .....</b>	<b>42</b>
<b>5.2.1</b>	<b>XRD .....</b>	<b>43</b>
<b>5.2.2</b>	<b>SEM Observation .....</b>	<b>45</b>
<b>5.3</b>	<b>SOLUBILITY EXPERIMENTS .....</b>	<b>46</b>
<b>5.3.1</b>	<b>Static Solubility Testing on Pellets.....</b>	<b>46</b>
<b>5.3.2</b>	<b>Static Solubility Testing on Scaffolds .....</b>	<b>47</b>
<b>5.4</b>	<b>BIOCOMPATIBILITY EXPERIMENT.....</b>	<b>48</b>
<b>5.4.1</b>	<b>Endothelial Cell Biocompatibility Testing.....</b>	<b>48</b>
<b>5.4.2</b>	<b>Hematopoietic Stem Cells / Osteoblasts Co-Culture Biocompatibility Testing .....</b>	<b>51</b>
<b>6.0</b>	<b>RESULTS AND DISCUSSION .....</b>	<b>55</b>

<b>6.1</b>	<b>INFILTRATION PROCESSING.....</b>	<b>55</b>
6.1.1	Effect of the Infiltration on the Phase Distribution in Pellets .....	55
6.1.2	Microstructural Analysis of Polished Surfaces on Pellets .....	57
6.1.3	Effect of the CaCO <sub>3</sub> Phase on Dissolution and Damage Accumulation on Polished Surface of Pellets.....	65
6.1.4	Effect of the Infiltration on the Phase Distribution of Foams.....	78
6.1.5	Infiltration of HA foams .....	79
<b>6.2</b>	<b>HUMAN UMBILICAL VEIN ENDOTHELIAL CELLS CULTURING ....</b>	<b>85</b>
6.2.1	Genomic DNA data and Medium Analysis during Culture.....	85
6.2.2	Real Time Polymerase Chain Reaction (RT-PCR) .....	90
6.2.3	Fluorescence Activated Cell Sorting (FACs) .....	93
6.2.4	Colony Unit Forming Assay .....	98
<b>6.3</b>	<b>HEMATOPOIETIC STEM CELLS AND OSTEOBLASTS CO-CULTURING.....</b>	<b>100</b>
6.3.1	Cell Population and Culturing Observations .....	100
6.3.2	Fluorescence Activated Cell Sorting.....	104
6.3.3	Colony Forming Unit Assay .....	111
<b>7.0</b>	<b>CONCLUSIONS .....</b>	<b>114</b>
<b>7.1</b>	<b>EFFECT OF THE INFILTRATION PROCESS ON HA AND CONSEQUENT EFFECT ON DISSOLUTION.....</b>	<b>114</b>
<b>7.2</b>	<b>PREPARATIONS OF A BIPHASIC CALCIUM PHOSPHATE SCAFFOLD AND THE CULTURING OF HUVECS .....</b>	<b>115</b>
<b>7.3</b>	<b>PREPARATIONS OF A BIPHASIC CALCIUM PHOSPHATE SCAFFOLD AND THE CULTURING OF HSC/OSTEOBLAST CO-CULTURE.....</b>	<b>116</b>
<b>8.0</b>	<b>SUGGESTED FUTURE WORK.....</b>	<b>117</b>

<b>8.1</b>	<b>BIOREACTOR CONSTRUCTION .....</b>	<b>117</b>
<b>8.2</b>	<b>THE BIOCOMPATABILITY OF THE HIGH CALCIUM CERAMICS WITH HSCS.....</b>	<b>117</b>
<b>8.3</b>	<b>THE DIFFERENTIATION PATHWAY OF HUVECS TOWARDS HEMATOPOIETIC LINEAGE.....</b>	<b>118</b>

## **LIST OF TABLES**

Table 1. Static solubility experiment time point.....	46
Table 2. Static solubility experiment time point for hydroxyapatite scaffolds.....	47
Table 3. Endothelial cell biocompatibility experiment controls and time points in each repeat ..	48
Table 4. HUVECs Medium formulation.....	49
Table 5. Hematopoietic stem cells / osteoblasts co-culture experiment controls and time points in each repeat.....	51
Table 6. HSCs Medium formulation.....	52
Table 7 CFU accounting for HUVECs .....	99

## LIST OF FIGURES

Figure 2.1 Stirred-tank bioreactor uses baffles and an agitator for optimal mixing, and recycles biomass.....	8
Figure 2.2 Fixed bed reactor model with hollow fiber membranes .....	9
Figure 2.3 Bone structure.....	13
Figure 2.4 Hematopoietic and stromal stem cell differentiation.....	16
Figure 2.5 HA unit cell structure .....	21
Figure 2.6 CaO-P2O5-H2O Phase Diagram.....	22
Figure 2.7 Calcium environments of Ca1 site (a), Ca2 site (b), Ca3 site (c), Ca4 site (d) and Ca5 site (e) in the $\beta$ -TCP structure .....	23
Figure 2.8. Disposition of constituent atoms in $\beta$ -TCP, $\alpha$ - TCP: Ca2+, green; P5+, magenta; O2 $^-$ has not been represented. a) Along the [001] direction b) along [010] direction.....	24
Figure 2.9 Solubility isothermal of Calcium Phosphates in water,.....	25
Figure 2.10 Scheme of possible processing routes used for the production of macroporous ceramics .....	29
Figure 2.11 Scheme of foams and mists that can be produced through the adsorption of colloidal particles at the gas–liquid interface. The drawings on the right hand side indicate the force balance at equilibrium for particles lyophobized to different extents.....	33
Figure 2.12 sintering stage model .....	35
Figure 5.1 X-ray diffraction standard pattern for (A) HA, (B) CaCO3 .....	44
Figure 6.1 X-ray diffraction patterns of infiltrate HA pellet surface (* stands for CaCO3 peak, green line stands for HA main peak).....	56

Figure 6.2. SEM for the surface of pellets. A) HA pellet surface; B) 0.5M calcium nitrate infiltrated HA pellet surface; C) 1M calcium nitrate infiltrated HA pellet surface; D) 2M calcium nitrate infiltrated HA pellet surface .....	58
Figure 6.3. Polished surface of Ca <sup>2+</sup> solution infiltrated HA pellet (A) BSE, (B) SEM, and (C) EDS.....	59
Figure 6.4. SEM on pellet surfaces: A) HA pellet surface; B) 0.5M calcium nitrate infiltrated HA pellet surface; C) 1M calcium nitrate infiltrated HA pellet surface; D) 2M calcium nitrate infiltrated HA pellet surface .....	60
Figure 6.5. Thermal-etched infiltrated HA pellet .....	61
Figure 6.6. Polished surface of infiltrated HA pellet (a) BSE, (B) SEM.....	61
Figure 6.7. A) section of infiltrated HA pellets and B) section of HA pelltes.....	62
Figure 6.8. The defect size distribution on the section of infiltrated HA pellets in Figure 6.7 ....	63
Figure 6.9. Polished HA pellet surface (A) with propanol, (B) with water .....	64
Figure 6.10. Polished surface of infiltrated HA pellet (A) with isopropanol, (B) with water .....	65
Figure 6.11. Ca <sup>2+</sup> ion concentrations in the Tris-buffered saline were plotted as a function of time for static experiment on pellet samples. ....	66
Figure 6.12. 0.5 hours microscopy for pellet surfaces (a) HA pellet, (b) 1M Ca <sup>2+</sup> solution infiltrated HA pellet, (c) 2M Ca <sup>2+</sup> solution infiltrated HA pellet.....	67
Figure 6.13. 1 hour microscopy for pellet surfaces (a) HA pellet, (B) 1M Ca <sup>2+</sup> solution infiltrated HA pellet, (c) 2M Ca <sup>2+</sup> solution infiltrated HA pellet.....	68
Figure 6.14. 1 day microscopy for pellet surfaces (a) HA pellet, (B) 1M Ca <sup>2+</sup> solution infiltrated HA pellet, (c) 2M Ca <sup>2+</sup> solution infiltrated HA pellet .....	69
Figure 6.15. 3 day microscopy for pellet surfaces (a) HA pellet, (B) 1M Ca <sup>2+</sup> solution infiltrated HA pellet, (c) 2M Ca <sup>2+</sup> solution infiltrated HA pellet .....	70
Figure 6.16. 7 day microscopy for pellet surfaces (a) HA pellet, (B) 1M Ca <sup>2+</sup> solution infiltrated HA pellet, (c) 2M Ca <sup>2+</sup> solution infiltrated HA pellet .....	71
Figure 6.17. 14 day microscopy for pellet surfaces (a) HA pellet, (B) 1M Ca <sup>2+</sup> solution infiltrated HA pellet, (c) 2M Ca <sup>2+</sup> solution infiltrated HA pellet.....	72
Figure 6.18. 28 day microscopy for pellet surfaces (a) HA pellet, (B) 1M Ca <sup>2+</sup> solution infiltrated HA pellet, (c) 2M Ca <sup>2+</sup> solution infiltrated HA pellet.....	73

Figure 6.19. The defect distribution on HA pellet surface .....	74
Figure 6.20. The defect distribution on 1M infiltrated HA pellets .....	75
Figure 6.21. The defect distribution on 2M infiltrated HA pellets .....	76
Figure 6.22. Number of defects/ unit area on the pellet surface .....	77
Figure 6.23 X-ray diffraction patterns of (A) (B) ground foam .....	79
Figure 6.24 Ca <sup>2+</sup> ion concentration in the tris-buffered saline plotted as a function of time for static experiment.....	81
Figure 6.25 0.5 hour exposure for scaffold surfaces (A) HA, (B) 2M Ca <sup>2+</sup> solution infiltrated HA .....	82
Figure 6.26 1 hour exposure for scaffold surfaces (A) HA, (B) 2M Ca <sup>2+</sup> solution infiltrated HA .....	82
Figure 6.27 1 day exposure for scaffold surfaces (A) HA, (B) 2M Ca <sup>2+</sup> solution infiltrated HA	82
Figure 6.28 3 days exposure for scaffold surfaces (A) HA, (B) 2M Ca <sup>2+</sup> solution infiltrated HA .....	83
Figure 6.29 7 days exposure for scaffold surfaces (A) HA, (B) 2M Ca <sup>2+</sup> solution infiltrated HA .....	83
Figure 6.30 14 days exposure for scaffold surfaces (A) HA, (B) 2M Ca <sup>2+</sup> solution infiltrated HA .....	84
Figure 6.31 28 days exposure for scaffold surfaces (A) HA, (B) 2M Ca <sup>2+</sup> solution infiltrated HA .....	84
Figure 6.32 DNA amounts of samples in 42 days .....	88
Figure 6.33 Cumulated secretions and Ca <sup>2+</sup> concentration in culture medium (A) accumulated glucose consumption (B) accumulated lactate consumption (C) accumulated Ca <sup>2+</sup> concentration .....	89
Figure 6.34 Gene expression data for HUVECs normalized to day 0 cells (**p<0.001, **p < 0.01, *p < 0.05).....	92
Figure 6.35 (A) more mature endothelial cell percentages, (B) hematopoietic progenitor cell percentages, and (C) endothelial progenitor cell percentages for three conditions at Day 15 and Day 42 (**p<0.001, **p < 0.01, *p < 0.05) .....	94

Figure 6.36 Hematopoietic stem cell percentages for three conditions at (A) Day 15, and (B) Day 42 Significant differences were showed (*p < 0.05) .....	96
Figure 6.37. CD45, CD235a and Lin positive cell percentages for three conditions at (A) Day 15 and (B) Day 42. Significant differences were showed (**p < 0.01,*p < 0.05) .....	97
Figure 6.38 Total cell number in the samples over a 42 day period samples in 42 days.....	101
Figure 6.39 (A) accumulated glucose consumption (B) accumulated lactate secretion, and (C) Ca <sup>2+</sup> concentration over a 42 day period.....	102
Figure 6.40 FACs results for HSC/Saos-2 for (A) CD235a, (B) Linage, (C) ALP, and (D) HSCs cell for all the conditions during 42 days of culture .....	106
Figure 6.41 Normalized FACs results for HSC/Saos-2 for (A) CD235a, (B) Linage, (C) ALP, and (D) HSCs cell for all the conditions during culture .....	109
Figure 6.42 CFU colonies accounting of HSC/Saos-2 in (A) CFU-E and (B) CFU-GM for all the conditions at harvest time points .....	112
Figure 6.43 CFU-GM colonies accounting of HSC/Saos-2 of each repeat .....	113

## **PREFACE**

I would like to acknowledge first my advisor Dr. Nettleship for all of his guidance over the last 4 years. I would also like to thank Dr. Gerlach and Dr. Schmelzer for guidance with all things related to biology and biological experiments, as well as Matthew Young for this help with cell culturing testing and Roger Esteban for biostatistics analysis. This work is funded by National Institutes of Health (1R01HL108631-01).

## **1.0 INTRODUCTION**

Tissue engineering is one of the most important approaches to tissue replacement and organ repair including bone repair<sup>1,2</sup>, eye transplantation<sup>3</sup> and heart transplantation<sup>4</sup>. This thesis is focused on materials engineering for bone marrow cell transplantation and Hematopoietic stem cell transplantation (HSCT). The latter is the transplantation of multipotent hematopoietic stem cells, usually derived from bone marrow, peripheral blood, or umbilical cord blood. HSCT was first developed in the 1950s and has been the leading therapy for leukemia<sup>5</sup>, but it is also used in therapies for cancers of the blood, bone marrow and multiple myeloma. Since the first successful bone marrow transplantation was performed in 1968<sup>6</sup>, more and more patients have undergone this therapy and the total number of bone marrow transplant procedures reached 25,000 by the end of the 1988<sup>7</sup>. In 2008 alone, 51,536 hematopoietic stem cell transplants were reported to have occurred in 72 countries in a globalize survey conducted by the Worldwide Network for Blood and Marrow Transplantation<sup>8</sup>.

However, bone marrow transplantation still exposes patients to significant life threatening risks. One important risk factor in this therapy is graft-versus-host disease following an allogeneic HSCT, because the white blood cells in the graft may target and attack cells in the host's body. This risk persists even when there is more than 25 to 30 percentage of the same human leukocyte antigens (HLA) shared between the between the donor and the recipient.

Although this level is considered a perfect match there is still a chance of graft-versus-host disease<sup>9</sup>.

Autologous HSCT is an alternative that would avoid such patient risk but unfortunately, the low availability of the patients own hematopoietic stem cells (HSCs) for re-implantation can inhibit this option. In autologous HSCT, it is necessary to collect the stem cells from the patient, treat them to separate the healthy hematopoietic stem cells and re-culture the stem cells in vitro to expand their number. During the consequent treatment to kill the cancer cells or because of infection factors, the patients remaining population of health hematopoietic stem cells decrease sharply. At present it is difficult to obtain an appropriate number of healthy stem cells after the patients undergoes a painful partial or complete bone marrow ablation<sup>10</sup>. This proposal, aims to provide a new material system that will increase the population of hematopoietic stem cells resulting from the vitro culture for subsequent repopulation of the bone marrow and thereby reduce the risk of HSC transplantation failure.

Hematopoietic stem cells mostly exist in the bone marrow, which is the main hematopoiesis soft tissue and lies at the interior of long bones. When HSCs are harvested as bone marrow and cultured in-vitro environment, there will be other cells from the bone marrow tissue in the HSC microenvironments. For example, osteoblast cells play an essential role in controlling the fate of HSCs in the endosteal microenvironment because they could localize human hematopoietic progenitor cells in the bone marrow. The endosteal microenvironment exists in the bone marrow at the inner bone surface while the central part of the trabecular zone contains the vascular microenvironment<sup>11</sup> which is occupied by vasculature and capillaries by which the HSCs enter the blood stream.

Therefore, the core aim of this work is to develop a composite biodegradable 3D scaffold that would simulate key aspects of the in-vivo microenvironment in which expansion of the hematopoietic stem cells takes place in the human body.

In tissue engineering, hydroxyapatite (HA) has been widely used as artificial bone and bone substrate since it has a similar chemical formula as the main mineral component of human bone. It has excellent bioactivity, biocompatibility and osteoconduction<sup>12</sup> that are the desired biological properties for bone grafts. With the development of the 3D cell culturing for tissue engineering, there has been more interest in culturing cells on porous hydroxyapatite scaffolds with suitable pores diameters and morphology. Indeed, studies<sup>13,14,15,16</sup> have reported success on hydroxyapatite as the scaffold for the bone marrow cell niche, which refers to a specific anatomic location which regulates bone marrow cell participation in tissue generation, maintenance and repair<sup>17</sup>. In those studies, bone marrow cells were cultured in an in-vivo animal model.

Among 3D cell culture studies, several reports have been published concerning the effect of calcium concentration on the hematopoietic stem cell proliferation and the differentiation in cell niche. Scadden reported that high ionic calcium concentrations that exist near active osteoclasts might influence stem-cell function<sup>17</sup>. At the site of active bone remodeling, ionic concentrations have been observed that dramatically exceed serum levels and vary with osteoclast activity. Shinya Nakamura et al<sup>18</sup> also reported that the calcium ions will affect the osteogenic differentiation, in which pre-osteoblasts would differentiate to osteoblasts.

In general, tissue engineering scaffolds must contain interconnected pores with a mean gate size between neighboring pores of 100  $\mu\text{m}$  or greater, and open porosity of >50% to permit tissue ingrowth and function in porous scaffolds<sup>19</sup>. The hydroxyapatite would be formed into

tiles which are high porous and meets the requirement of the tissue function scaffold. According to the HA ceramic manufacturing process, small connecting pores between the ceramic particles would disappear during full sintering while the large pores on macro-scale should not be effected. Such structural changes should allow another phase, such as Ca-rich phase, to be introduced into HA scaffolds without affecting the macro-pore structure

In this study it was hypothesized that hydroxyapatite scaffolds containing soluble phases with relatively high calcium content could be used to effect hematopoietic stem cell expansion during in-vitro culture. In such case, over a period of 4 weeks, the steady release of calcium from an hydroxyapatite scaffold could promote the stem cell population expansion, or stimulate the HSCs differentiate down to the hematopoietic lineage towards blood cells and cells for the immune system..

In a final application the in-vitro culturing materials developed in this study would be used to expand the population of HSCs harvested from a patient prior to bone marrow ablation after which the expanded population would be re-transplanted into the same patient. Also, the scaffolds might guide the HSCs differentiation into useful cell types, such as blood cells to augment the blood supply for rare blood types or lymphocytes, for cell therapies involving the immune system.

## **2.0 BACKGROUND**

### **2.1 REGENERATIVE MEDICINE**

Regenerative medicine involves replacing or regenerating cells, tissues or organs in the human body, in order to restore or establish normal function<sup>20</sup>. It includes cell therapy, gene therapy, tissue engineering and other methods, and it has enormous potential to treat and cure diseases<sup>21</sup>.

#### **2.1.1 Cell therapy**

As one of the main application of regenerative medicine, cell therapy is defined as the administration of cells to the body to the benefit of the recipient<sup>22</sup>. In cell therapy, cellular materials are injected into the patient's body to cure cell level tissue damage. Cell therapy has two branches, one is the use of human cells transplanted from a human donor to a patient and has been used with some success in clinical application, the other, and rather more dangerous alternative is the use of animal cells to treat human illness, which needs much more research before moving to clinical application<sup>23</sup>.

Stem cells, which have genomic plasticity with unlimited ability for self-renewal, are highly desirable for cell therapy and have successfully been used in some clinic applications. One of these applications is hematopoietic stem cell transplantation, which helps patients to rebuild their blood and immune systems. In this transplantation, hematopoietic stem cells (HSCs)

are used by themselves or as part of a sample of bone marrow cells, which also include endothelial cells, osteoblast cells and other cell types. The field of cell therapy continues to advance towards new therapies for treating human disease<sup>24</sup>. Notable examples include cell therapies for Lysosomal Storage Diseases, Parkinson's disease, Huntington's disease and brain tumors<sup>25</sup>. However stem cell science still needs more understanding of the behavior of implanted cells. Nevertheless it is clear that cell therapies will contribute to growth of regenerative medicine and increase the demand for in-vitro expansion of stem cell supplies derived from human donors.

### **2.1.2 Tissue engineering**

The field of tissue engineering is driven by the need to provide functional equivalents of native tissues that can be used for implantation. Modern society desires life-time enhancement, and so the need for tissue repair continues to grow. However, the field of tissue engineering is responding to it relatively slowly because of the issues which include: biological complexity, regulatory issues, and the high cost of new cell-based devices. At the same time, engineered tissues are finding new roles as models for fundamental research on disease, testing of drugs, and many other applications. In all cases, the requirements are to provide the cells with the appropriate cues, to control the conditions in the cell microenvironment, and to monitor cellular responses on multiple hierarchical levels. In order to develop a whole organism tissue, there are coordinated sequences that need to be followed including: cell renewal, differentiation, and assembly, within an ever-changing environment characterized by spatial and temporal gradients of multiple factors<sup>26</sup>.

In the general context of technologies for culturing cells and stem cells in particular, the environments for guiding stem cell function will be discussed, with a particular focus on two key components—biomaterial scaffolds and bioreactors. For both components, the interplay between molecular and physical regulatory factors will be considered while highlighting some of the important findings pertinent to the design of cell scaffold–bioreactor systems for applications in tissue engineering and biological and medical research<sup>13</sup>.

### **2.1.3 Bioreactor**

Bioreactors are generally defined as devices in which biological processes (such as cell expansion, differentiation, or tissue formation on 3D scaffolds) occur under tightly controlled environmental conditions such as exchange of oxygen, nutrients, and metabolites, and application of molecular and physical regulatory factors<sup>26</sup>. Tissue-engineering bioreactors are designed to precisely regulate the cellular microenvironment needed to support cell viability, 3D organization and provide spatial and temporal control of cell signaling. These requirements translate into a set of practical design objectives: (i) rapid and controllable expansion of cells; (ii) enhanced cell seeding of 3D scaffolds (at a desired cell density, high yield, high kinetic rate, and spatial uniformity); (iii) efficient local exchange of oxygen, nutrients, and metabolites; and (iv) provision of physiological stimuli.<sup>13</sup>

Bioreactor can be separated into two basic categories, stir tank and fixed bed. The stir tank consists of a vessel in which cells float freely in cell culture medium, and fresh culture medium can be continuously added while culture liquid is removed to keep the culture volume constant. A typical stirred-tank is shown in Figure 2.1. The culture medium contains components

such as nutrients, growth factors to support the culture of cells and antimicrobials<sup>27</sup>. The stir tank could provide a physiological steady-state and is ideal for non-adherent cells.

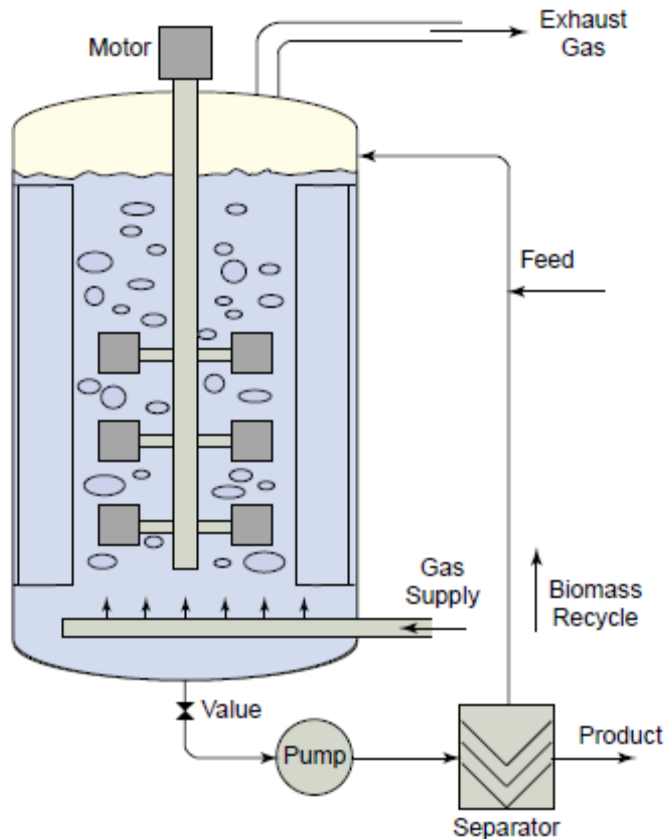


**Figure 2.1** Stirred-tank bioreactor uses baffles and an agitator for optimal mixing, and recycles biomass<sup>28</sup>.

Carriers made from biocompatible polymers and ceramics can be used for culturing cells that usually grow on a surface<sup>29</sup>. The cells can attach to the carriers which are then suspended in the stirred tank reactor.

The other type of bioreactor is the perfusion reactor, such as packed bed reactors<sup>29,30</sup>, fibrous bed bioreactor<sup>31</sup> and the hollow fiber membrane reactors<sup>32</sup> such as that shown in Figure 2.2. In this type of reactor, cells are immobilized in a fixed chamber or core in the bioreactor and

the culture medium is perfused through the container. The architecture of the core is used to control the perfusion of culture medium and gases.

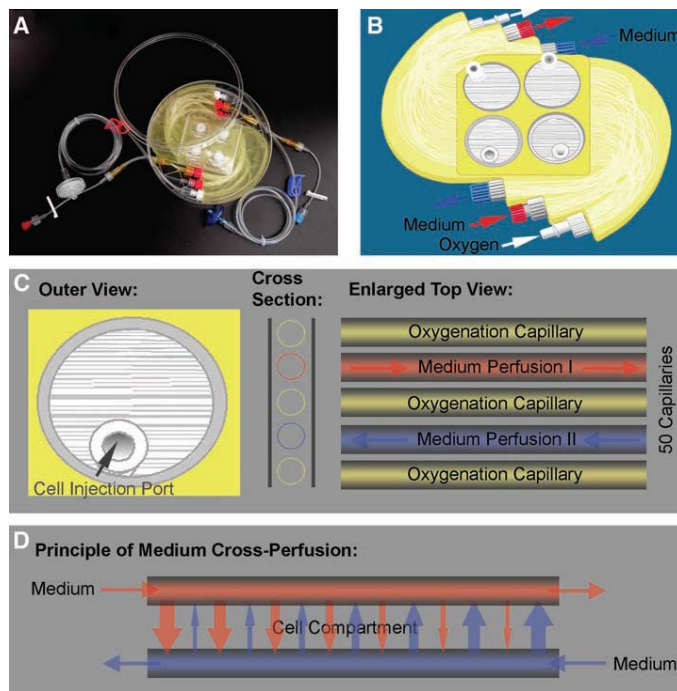


**Figure 2.2** Fixed bed reactor model with hollow fiber membranes<sup>33</sup>

In all bioreactors, it is found that mechanical cues are important for both in-vivo and in-vitro culture, including musculoskeletal and cardiovascular tissues<sup>34</sup>, such as osteoblasts and endothelial cells<sup>35,36</sup>. Mechanical forces could regulate cell fate, cell morphology cell physiology and the organization of the extracellular matrix, signaling, and biomechanics of the cellular microenvironment<sup>25</sup>. During in- vitro culture, it is important to create or provide similar mechanical conditions to those that govern in-vivo tissue development<sup>25</sup>. Perfusion bioreactor can control medium flow and shear forces as physiological stimuli and the effects have been reported on application to tissue engineering and cell culturing<sup>37,38</sup>. For example, Sikavitsas et al<sup>39</sup> reported that there were more osteogenic genes expressed in osteoblasts under the shear

stresses were associated with medium flow. Other groups also reported a similar effect of flow on genes<sup>40</sup> and enhanced mineralization under mechanical forces<sup>41</sup>.

#### **2.1.4 Biomaterial scaffold**

In tissue engineering, the biomaterials used in implantations, known as the scaffold, can be made in a variety of shapes using different fabrication techniques<sup>42</sup>. During service, the scaffolds should meet the requirements of architecture and properties needed to provide a short term support for cell growth and new tissue formation.

The ideal scaffold should<sup>43</sup>: (i) have a biocompatible (non-toxic) surface that promotes cell adhesion and proliferation; (ii) after in-vitro tissue culture, exhibit mechanical properties that are comparable to those of the tissue to be replaced; (iii) have a porous three dimensional (3-D) architecture to allow vascularization and diffusion of nutrients between the cells seeded within the matrix; (iv) degrade at a rate that matches the production of new tissue, into nontoxic products that can be easily resorbed or excreted by the body; (v) be capable of being processed economically into anatomically relevant shapes and dimensions, and sterilized for clinical use. In modern tissue engineering, biomaterial scaffold should also play an important role in biomimetic simulation of the microenvironment, or niche, in which stem cells reside in the body. It should allow the cells to attain their natural morphology and also mimic the chemical environment that controls stem cell fate. Most of the ceramic biomaterial scaffolds used in perfusion bioreactors are calcium phosphate with a chemical formula similar to that of natural human bone .Synthetic calcium phosphate scaffolds have also been used to host a variety of orthopedic cells, such as osteoblasts, endothelial cells and mesenchymal stem cells (MSC) in in-vivo bone implants<sup>44,45,46</sup>. Hydroxyapatite (HA) and β- tricalcium phosphate (TCP) are the main phases that have been used

to culture human mesenchymal stem cells and shown to induce bone formation<sup>47,48,49</sup>. Also, in the vivo models, calcium phosphates are reported for bone repair and bone graft substitutes. HA has been found to exhibit excellent biocompatibility with osteoblasts, which forms bone tissue. HA can also: induce the osteoblast cells and react with osteoclast cells, resulting in the secretion of new apatite on the surface after implantation into body<sup>50</sup>. Researchers also found that HA could be used as an excellent carrier for osteo-inductive growth factors and osteogenic cell populations<sup>51</sup>. HA could also be used as a DNA carrier and suggests utility as a bioactive delivery vehicle. Another commonly reported calcium phosphate used for bone hard tissue regeneration is TCP. Jarcho<sup>52</sup> reported an in-vivo experiment in which TCP completely resorbed in six weeks. Other groups<sup>53,54</sup> reported that biphasic calcium phosphate, containing HA and TCP, achieved a desirable degradation rate and mechanical properties while bone tissue was regenerated during the resorption of scaffold. The ratio of HA to TCP in these studies varies a lot with 60% HA / 40%  $\beta$ -TCP being the ratio most commonly reported<sup>55, 56</sup>.

Calcium phosphate scaffolds have also been used in tissue engineering of bone marrow. For example, an HA scaffold was used for loading regenerated bone marrow and was tested in a mouse model in terms of its ability to reconstitute the functionality of bone marrow niche<sup>57</sup>. In the mouse model, the results suggested that the functional niche was reconstituted at least partly from regenerated bone marrow on the scaffold. Those studies demonstrate the possibility of culturing hematopoietic stem cells (HSCs), an important bone marrow stem cell population, on calcium phosphate ceramics. In this proposal, HSCs will be cultured in-vitro, on calcium phosphate ceramics with different bone marrow cells such as endothelial cells and osteoblast cells in an attempt to co-culture the bone marrow stem cell niche.

## **2.2 BONE MARROW**

As one of the most important part of body, bones support and protect the various organs of the body and store minerals. The large bones also house the bone marrow cavities in which blood cells and the cells for the immune system are produced. Bone marrow has two extracellular components, organic and inorganic. The organic part of bone tissue is mainly collagen, with various growth factors. The composition of the inorganic mineral component can be approximated as hydroxyapatite (HA), with the chemical formula  $\text{Ca}_{10}(\text{PO}_4)_6(\text{OH})_2$  with a Ca/P ratio of 1.67<sup>58</sup>. However the Ca/P ratio in the mineral phase of bone varies from 1.37 to 1.87. This phase is secreted by osteoblasts during biominerization and contains additional ions such as silicon, carbonate and zinc in solid solution<sup>59</sup>. The remodeling of the bone structure continues over the whole lifetime of a human by the bio reactions in which osteoclast cells resorb bone and the osteoblasts secret new bone mineral<sup>60</sup>.

### **Compact Bone & Spongy (Cancellous Bone)**

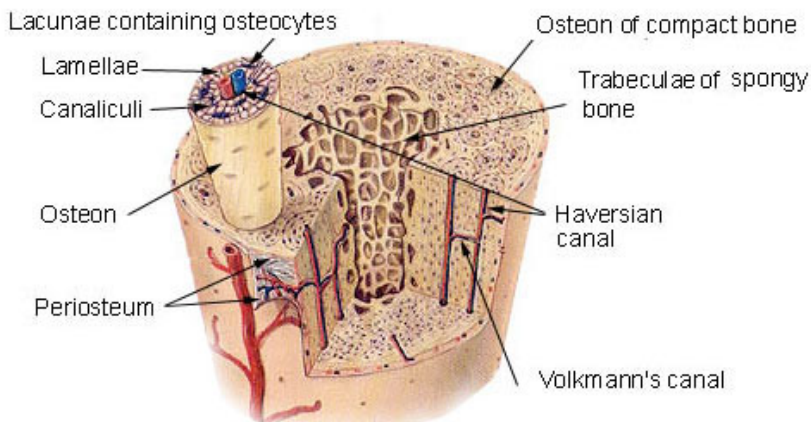


**Figure 2.3** Bone structure<sup>61</sup>

As depicted in Figure 2.3, bone is not an uniform solid material, in fact, bones are quite porous, and can be separated into two types of structure:, compact bone and the trabecular bone. The compact or cortical bone that surrounds the central marrow, forms a hard outer layer and provide 80% of the bone mass in adult humans due to its relatively low porosity ( 5 -30%)<sup>62</sup>.The cortical bone tissue provides the high strength and high stiffness required to protect the central bone marrow cavity and provide suitable skeletal properties.

The other major bone structure is trabecular bone, which fills the interior of the large bones and is characterized by its open cell porous network structure. The open honeycomb structure of trabecular bone tissue houses the bone marrow and the blood vessels that perfuse the bone marrow with blood. The porosity of trabecular bone is in the range 30–90% and the surface area is ten times that of compact bone while the mass is only one fourth. Bone marrow is the soft tissue in the trabecular bone and constitutes 4% of the total body mass of humans<sup>63</sup>. It has an important function in the formation the blood cellular component by a process known as hematopoiesis. Bone marrow is also regarded as an important part of the lymphatic system,

producing the lymphocytes that support the body's immune system<sup>64</sup>. The bone marrow can be separated into two types, red marrow or *medulla ossium rubra*, which mainly consists of hematopoietic tissue; and yellow marrow or *medulla ossium flava*, which mainly contains fat cells. All the bone marrow is traversed by a blood vessel and a capillary network.

### 2.2.1 Hematopoietic Stem Cell

Of the two types of marrow, the red marrow is the one that controls and contributes cells to the blood and lymphatic system. In the red marrow, hematopoiesis occurs continuously throughout life. Hematopoietic stem cells (HSCs) are the cells that are of central importance to hematopoiesis and the formation of hematopoietic tissue in red marrow. HSCs have ability to replenish all cellular components of blood and self-renew. In order to maintain steady-state levels in the peripheral circulation, the HSCs produce  $10^{11}$ – $10^{12}$  blood cells per day in a healthy human adult and use the bone marrow vasculature as a conduit to the body's systemic circulation<sup>65</sup>. In bone marrow, the blood vessel network, lined by endothelial cells, plays an important role in supporting the nutrition and renewal of differentiated mature blood cells. Those blood cells includes: erythroid cells for carrying oxygen, myelocytes such as monocytes and macrophages, and lymphocytes lineages for the adaptive immune system, such as T-cells, B-cells<sup>66</sup>.

In the first step of the HSCs differentiation process, which is shown in Figure 2.4, the specific progenitors are induced from the HSC population. In asymmetric division, small numbers of the self-renewable HSCs can divides into a large number of cells while a part of the population remain as HSCs keeping the pool of stem cells available. The other daughter HSCs will be induced into myeloid or lymphoid progenitor cells in alternative pathways<sup>67</sup>. Those

progenitors don't have the ability of self-renew but could lead to the specific types of mature blood cells, which will be released to the body's circulation through blood vessels in bone marrow.

Additionally, the pool of HSCs itself is heterogeneous and can be classified as long-term self-renewing HSC and short-term self-renewing HSC<sup>68</sup>, which depends on the long-terms or short-terms regeneration capacities. Self-renewal is one of the most vital processes in the body and is also a cornerstone for hematopoietic stem cell transplantation in which a small amount of HSCs is used to reconstruct a new functional hematopoietic tissue system. The two types of HSCs with different regeneration capacities reside in the endosteal niche and the vascular niche. The endosteal niche is next to the trabecular bone surface, where the HSCs renew and also remain dormant. In this niche, HSCs are thought to favor long-term self-renewal and their multipotent capacity remains to give a HSC reservoir. The other type of niche, the vascular niche, exists near blood vessels in which HSCs would differentiate and recover blood cells in a relative short time when needed. After the differentiation, the blood cells would go through the vascular wall and released into the body's blood stream.

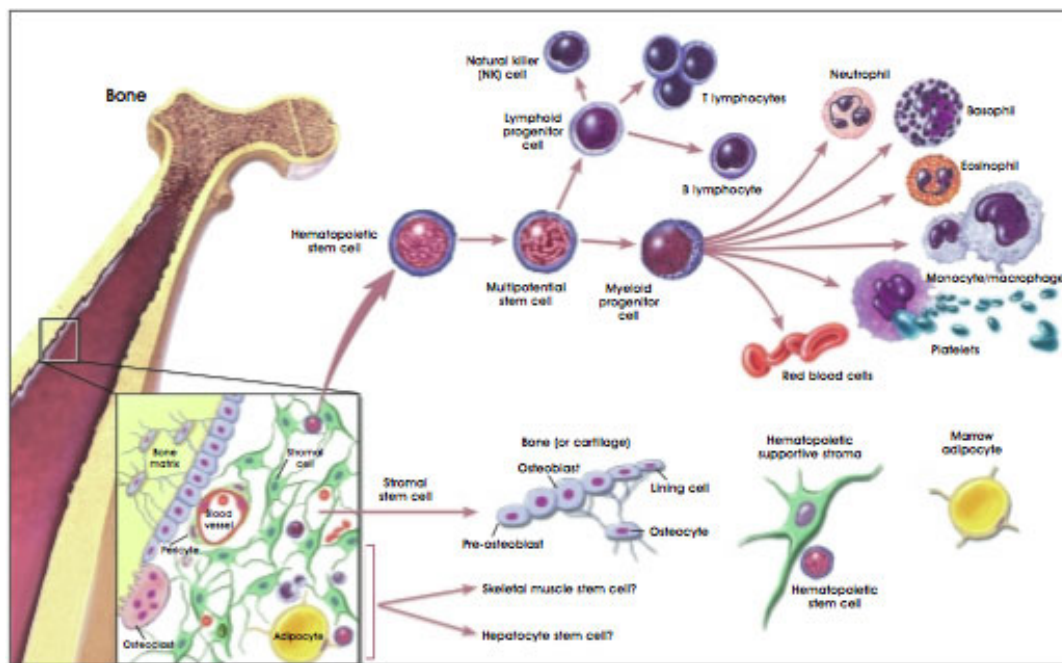


**Figure 2.4** Hematopoietic and stromal stem cell differentiation<sup>69</sup>.

## 2.2.2 Hematopoietic Stem Cell Applications

As a component of the first stem cell therapy, bone marrow stem cells have been used for the treatment of blood and immune system disorders for more than 50 years. Since then, more than half a million people have undergone routine HSC stem cell transplantation<sup>70</sup>. These HSC transplantation therapies have been used to treat: multiple myeloma or leukemia patients<sup>71, 72</sup>, including those with severe combined immunodeficiency or congenital neutropenia with defective stem cells, aplastic anemia<sup>73</sup>, sickle-cell disease, myelodysplastic syndrome, neuroblastoma, lymphoma, Ewing's sarcoma, desmoplastic small round cell tumors, chronic granulomatous disease and Hodgkin's disease.

HSC transplantation can be split into two types, autologous and allogeneic. Both types of therapies have been used for numerous patients all around the world. Autologous HSCT requires

the HSC source from the patients themselves. After being extracted from the patient, the cells are sorted and the HSCs are frozen and stored. After the disease is treated with high-dose chemotherapy or radiation treatment, the patient's immune system will be compromised by either the partial or the complete bone marrow ablation required to kill the aberrant disease-causing immune cells. Then the stored stem cells are unfrozen and transplanted back into the patient in order to replace the destroyed hematopoiesis tissue. The transplanted HSCs are required to regenerate a new and antigen-naive immune system and resume the patient's normal blood cell production<sup>74</sup>. Autologous transplants have the advantage that the patients rarely experience rejection and the risk of infection during the chemotherapy treatment process is lower<sup>75</sup>.

Allogeneic HSCT involves donated cells and the donor and the recipient must be matched by gene typing. Special blood tests are done to test the human leukocyte antigen (HLA) gene type match. HLAs are the major cause of organ transplant rejections<sup>76</sup> so that allogeneic HSCT prefers a perfect match at the loci of HLA gene between the donor and the recipient. Even if these critical alleles are matched well between the donor and the recipient, there is still a risk of graft-versus-host disease and immunosuppressive medications are required for the recipient.

Allogeneic HSCTs could have improved likelihood of a cure and long term remission since healthy stem cells are transferred to reform the immune system; however, the immediate transplant-related complications are the main obstacle of concern<sup>77</sup>. This roadblock could be addressed if the HSC population could be proliferated in bioreactors since the cell population growth could enrich the HSCs in transplantation and shorten the time that is required to recover of immune system. In one study conducted by the European Group for Blood and Marrow Transplantation from 1993 to 2003, the patients who received autologous hematopoietic stem cell transplantation, 420 patients (89%) were alive and 53 patients (11%) had died: 31 (58% of

deceased patients) due to transplant-related causes and 22 (42% of deceased patients) due to disease progression. Amongst all of these the highest mortality was caused by infections (N=16; 50%)<sup>78</sup>.

According to the hypothesis of this proposal a new type of hydroxyapatite foam could enhance the HSCs proliferation and expand the population in bioreactors, the HSCs read ministered to patients in transplantation could thereby be enriched and shorten the time of immune system recovery, leading to decreased risk of infection and higher survival rates.

Besides the traditional hematopoietic stem cells application, such as HSC transplantation, researchers are also showing great interest in in-vitro culture of hematopoietic stem cells for other reasons Recent reports have suggested that hematopoietic stem cells could form other kinds of cells, such as muscle<sup>79</sup>, blood vessels<sup>80</sup> and hepatocyte tissue<sup>81</sup> in in-vivo models. The results lead to another possible direction for the use of HSCs in regenerative medicine, namely the use of hematopoietic stem cells to replace specific tissue and organ<sup>82</sup>.

### **2.2.3 In vitro Hematopoietic Stem Cell Culture**

The Hematopoietic stem cells (HSC) have been unquestionably important to therapies that involve blood and immune system replacement. However, the in-vitro culture and the expansion of HSCs are still roadblocks on expand the application of HSCs. The proliferation of HSCs is being researched for suitable conditions. There is a report by Lagasse and Weissman<sup>83</sup> concerning the failure and difficulty in culturing HSCs alone by in-vitro culture. Most of the stromal cell lines that were shown to maintain HSCs in vitro, contained osteoblasts<sup>84, 85</sup>, and would be relevant to the endosteal bone-marrow niche. Recently, a research group also proposed the successful co-culture of mice HSCs with stromal cells and cytokines<sup>86</sup>. Even though there is

a hypothesis that osteoblasts are necessary and rate-limiting for the niche function<sup>87,88</sup>, other cell types, such as endothelial cells, stromal fibroblasts, are also attributed to HSC niche and might be important to HSCs in-vitro culture<sup>89</sup>. Another important consideration is the vascular bone-marrow niche, mentioned above. In this niche model, there is also success on HSC in-vitro culture. Embryonic precursor endothelial cells or purified primary endothelial cells from the yolk sac or aorta-gonad-mesonephros were reported to promote the maintenance or expansion of HSCs in vitro<sup>90,91,92</sup>. However, there is no capability for vascular endothelial cells from adult non-hematopoietic organs to maintain HSCs in vitro culture<sup>93</sup>.

In this proposal, therefore,, it is important to determine the effects of the new scaffold material on different cell types that are known to reside in bone marrow, and consider co-cultures with HSCs on the scaffold material.

## **2.3 CALCIUM PHOSPHATE**

### **2.3.1 Calcium Phosphate**

Calcium orthophosphates are of interest in many scientific fields, such as geology, chemistry, biology and medicine. They form a large family of phases which shares the same constituent elements of calcium, phosphorous and oxygen. Calcium phosphates can also incorporate hydrogen as acidic orthophosphate anion or water<sup>94</sup>.

We can distinguish the calcium phosphates by the type of the phosphate anion: ortho- ( $\text{PO}_4^{3-}$ ), meta- ( $\text{PO}_3^-$ ), pyro- ( $\text{P}_2\text{O}_7^{4-}$ ), and poly- ( $(\text{PO}_3)^{n-}$ ). Meanwhile, the calcium phosphates with multi-charged anions (orthophosphates and pyrophosphates) can be differentiated by the

number of hydrogen ions attached to the anion<sup>94</sup>. For example, there are several calcium phosphates used in bioceramics, including: mono- ( $\text{Ca}(\text{H}_2\text{PO}_4)_2$ ), di- ( $\text{CaHPO}_4$ ), tri- ( $\text{Ca}_3(\text{PO}_4)_2$ ), and tetra- ( $\text{Ca}_2\text{P}_2\text{O}_7$ ) calcium phosphates<sup>95,96,97</sup>.

In these examples, it is clear that the atomic arrangement of calcium orthophosphates is based on a network of orthophosphate ( $\text{PO}_4$ ) groups that leads to structure stability. The vast majority of calcium orthophosphates are sparingly soluble in water; however, all of them are easily soluble in acids and relatively insoluble in alkaline solutions. In all mammalian calcified tissues, biological formed calcium phosphates play an important role in bones, teeth and antlers and also pathological (i.e. those appearing due to various diseases) calcified tissues of mammals<sup>98</sup>.

Bones in the human body could be separated into organic and inorganic as mentioned before. Calcium orthophosphate has a similar chemical make up as inorganic bone tissue. In orthopedics and related areas of medicine, the calcium phosphates are widely used because of the good compatibility, non-toxicity and bioactivity<sup>99</sup>. Also, as mentioned earlier, synthetic calcium phosphates can be fabricated as a scaffold for bone regeneration that support the adhesion and proliferation of osteoblasts<sup>100,101</sup>. In such cases, osteo-integration, a bone remodeling process, can occur on the surface of calcium phosphates which facilitates bonding between implants and bone<sup>102,103</sup>.

Also, in the processes of demineralization and biominerization, calcium phosphates with other Ca/P ratio are reported, including: octacalcium phosphate (OCP), brushite and whitlockite ( $\beta$ -TCP).

### 2.3.2 Hydroxyapatite

The chemical formula for hydroxyapatite is  $\text{Ca}_5(\text{PO}_4)_3(\text{OH})$ , but it is usually written  $\text{Ca}_{10}(\text{PO}_4)_6(\text{OH})_2$  to emphasize the fact that the crystal unit cell comprises two formula units<sup>104</sup>. Hydroxyapatite is a hexagonal material, with space group P63/m, and a total of 44 atoms per unit cell<sup>105</sup>. HA has a calcium-to-phosphate ratio of 1.67 while the unit cell dimensions are  $a=b=9.432\text{\AA}$  and  $c=6.881\text{\AA}$ . The structure of an HA unit cell is shown in Figure 2.5.

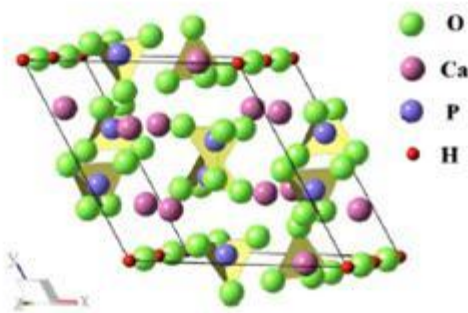


**Figure 2.5** HA unit cell structure

The OH<sup>-</sup> ion can be replaced by fluoride, chloride or carbonate ions producing fluorapatite or chlorapatite<sup>106</sup>. Pure hydroxyapatite powder is white but naturally occurring apatites can, also have brown, yellow, or green colorations, comparable to the discolorations of dental fluorosis. Hydroxyapatite is a member of CaO-P<sub>2</sub>O<sub>5</sub>-H<sub>2</sub>O system. The ternary compositional diagram for this system is shown in Figure 2.6. It can be seen that hydroxyapatite (HA) lies on a tie line between calcium hydroxide ( $\text{Ca(OH)}_2$ ) and tricalcium phosphate ( $(3\text{CaO}\cdot\text{P}_2\text{O}_5)$ )<sup>107</sup>.

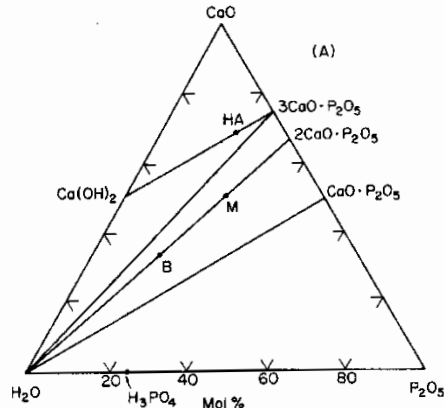


**Figure 2.6** CaO-P<sub>2</sub>O<sub>5</sub>-H<sub>2</sub>O Phase Diagram

### 2.3.3 Tri-calcium phosphate

Tri-calcium phosphate (TCP) has three polymorphs,  $\beta$ -TCP,  $\alpha$ - TCP and  $\alpha'$ -TCP.  $\alpha'$ -TCP only exists in equilibrium at temperatures higher than 1430 °C and converts back to  $\alpha$ -TCP on cooling below the transition temperature.  $\beta$ -TCP and  $\alpha$ - TCP can exist at room temperature although the equilibrium phase transition between  $\beta$ -TCP and  $\alpha$ - TCP occurs at  $\sim 1125^\circ\text{C}^{108}$ .

$\beta$ -TCP,  $\beta\text{-Ca}_3(\text{PO}_4)_2$ , has the rhombohedral space group R3 c, Z=21, with unit cell  $a=b=10.4352(2)$  Å,  $c=37.4029(5)$  Å,  $\gamma=120^\circ$  in the hexagonal setting. There are 21 formula units per hexagonal unit cell and 5  $\text{Ca}^{2+}$  sites with three types of crystal graphically non-equivalent  $\text{PO}_4^{3-}$  groups located at general points of the crystal in the unit cell. The 5 types of calcium environment are shown in Figure 2.7.

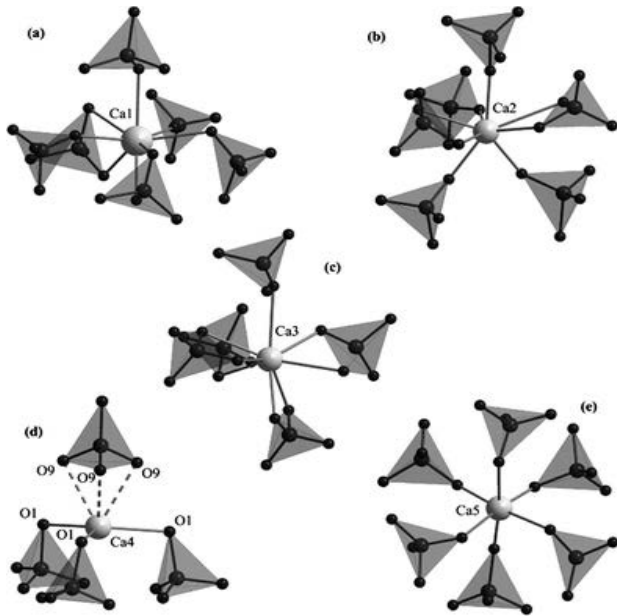


**Figure 2.7** Calcium environments of Ca1 site (a), Ca2 site (b), Ca3 site (c), Ca4 site (d) and Ca5 site (e) in the  $\beta$ -TCP structure<sup>109</sup>

$\beta$ -TCP has a higher solubility than HA and can be degraded more rapidly in the body<sup>110</sup>. Hence,  $\beta$ -TCP is applied as a bone tissue scaffold and shows outstanding biological responses to physiological environments<sup>111</sup>. Amongst others Gibson et al proved that implanted  $\beta$ -TCP could be resorbed in vivo with new bone growth<sup>112</sup>.  $\beta$ -TCP also showed excellent bioactivity and biocompatibility in in-vitro culture of bone marrow stromal cells culture towards osteogenic differentiation<sup>113</sup>.

$\alpha$  -TCP,  $\alpha$  - $\text{Ca}_3(\text{PO}_4)_2$ , has the same chemical formula as  $\beta$ -TCP but a monoclinic space group ,  $\text{P}2_1/a$  .There is 24 formula unit in the unit cell, which  $a= 1.2859(2)$  Å  $b= 2.7354(2)$  Å,  $c= 1.5222(3)$  Å,  $\beta=126.35(1)^\circ$ ,  $\alpha=\gamma=90^\circ$ .Compare with  $\beta$ -TCP,  $\alpha$ -TCP is a less densely packed structure and accordingly is expected to have a higher solubility and degradation rate during in vitro and vivo culture , which are consisted with the experiments. In Figure 2.8,  $\beta$ -TCP and  $\alpha$ -TCP structure were shown in  $\text{Ca}^{2+}$  and  $\text{P}^{5+}$  type.

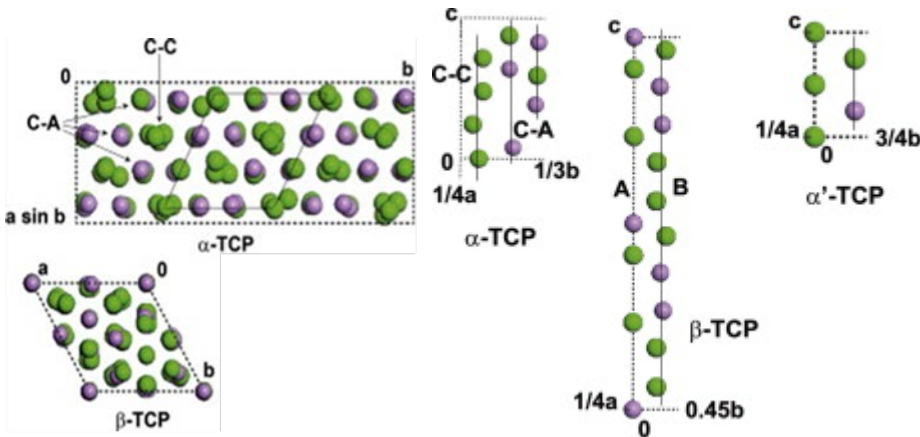


**Figure 2.8.** Disposition of constituent atoms in  $\beta$ -TCP,  $\alpha$ -TCP:  $\text{Ca}^{2+}$ , green;  $\text{P}^{5+}$ , magenta;  $\text{O}^{2-}$  has not been represented. a) Along the [001] direction b) along [010] direction<sup>114</sup>

In clinical applications,  $\beta$ -TCP is used as macro-porous granules or blocks and plays an important role in mono-phasic or biphasic bio-ceramics and composites<sup>114</sup>, while  $\alpha$ -TCP is generally used only as a fine powder for calcium phosphate cements, such as hydraulic bone cements<sup>115,116</sup>, because of its higher solubility.

Tri-calcium phosphate has been provided to have excellent properties in clinic application, such as dentistry, orthopedic surgery, and bone regeneration and repair.

### 2.3.4 Solubility of Calcium Phosphate Phases

Calcium phosphate can be remodeling by the osteoblast and osteocytes in biological process. However, these materials will dissolve chemically in aqueous solution. Indeed, the rate at which calcium phosphate scaffold materials will degrade is often measured, to a first approximation, in terms of their chemical solubility. In the dissolution process, calcium ions and phosphate ions are released from the ceramic scaffold into the solutions and influence the cell culture environment. Calcium in particular is known to effect cells that reside in the bone marrow niche cells, such as

osteoblasts<sup>117</sup> and endothelial cells. Therefore calcium released by a calcium phosphate scaffold should affect the HSC niche and HSC fate. Thus the solubility of calcium phosphates will be important to culturing HSCs on calcium phosphate scaffolds in bioreactors.

Several studies have been performed on calcium phosphates in different solutions<sup>84,85, 118</sup>, which compared calcium phosphate solubility in different environment conditions. A study by M.Bohner showed most of the calcium phosphates and calcium phases, which provided an important foundation for this proposal. In Figure 2.9, the solubility of those calcium phases, which might infect the proposal, is compiled in one graph except Ca(OH)<sub>2</sub>. Calcium hydroxide has solubility as high as 1.25E-2mol/L in pure water. And in tris-buffer, calcium hydroxide has solubility larger than 1 mol/L, which is too high to be easily compared with other calcium phases.

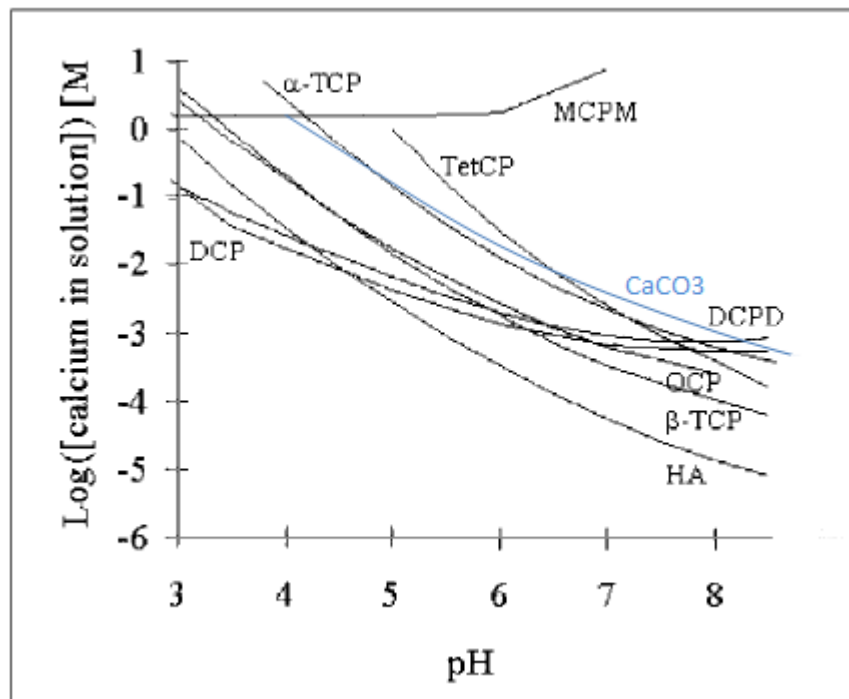


**Figure 2.9** Solubility isothermal of Calcium Phosphates in water<sup>119,120</sup>

In Figure 2.9, solubility of calcium phosphates with different Ca/P ratio has been shown as a function of pH. As Figure 2.9 showed, calcium phosphates have a wide range of solubility that range from  $10^{-1}$  to  $10^{-5}$  at PH=7~8 in water. MCPM, Mono-calcium phosphate monohydrate, has a Ca/P =0.5 has the largest solubility, which is too high for in-vitro bone tissue culture. Besides MCPM, other Calcium phosphates and the Calcium carbonate have more suitable solubility for scaffold degradation. At pH=7.35 to 7.45 range, which is general bone marrow culture pH condition, calcium carbonate had a solubility range at around  $10^{-2.5}$  and would release the most amount of  $\text{Ca}^{+2}$  ions into the solution. Then it was followed by Tetracalcium phosphate (TeCP) and one phase of the tricalcium phosphate,  $\alpha$ -TCP. The solubilities of these two phases are about the same at pH=7.4. The solubility of the CaP phases decreases in the order: Dicalcium phosphate dehydrate (DCPD) > Dicalcium phosphate (DCP)> Octocalcium phosphate (OCP)> low temperature phase of tricalcium phosphate,  $\beta$ -TCP, and finally HA.

According to the graph, HA has the solubility which is around  $10^{-5}$  and is not considered to resorb fast enough in vitro or in-vivo conditions with little  $\text{Ca}^{2+}$  released, it dissolves slower than the mineral part of bone<sup>83</sup>.HA has good biocompatibility and bioactivity for tissue remodeling but the  $\text{Ca}^{2+}$  release is very low. In the studies, researches have successfully increased HA dissolution by different techniques<sup>121,122</sup>. However, those techniques decreased the Ca/P ratio.

### 2.3.5 Effect of Calcium on the Bone Marrow Niche

In bone marrow in-vitro culture, the activity and the bone remodeling by osteoblasts is considered to be of particular importance. However, angiogenesis and vascularization with endothelial cells will also play a vital role. Angiogenesis, which is not much different with

vascularization, is the physiological process through which new blood vessels form from pre-existing vessels<sup>123</sup>. In wound healing, functional tissue recovery, and granulation tissue formation, angiogenesis is a normal and vital process in tissue growth and development<sup>124</sup>. After the angiogenesis process, the vasculature becomes mature and functional, leading to the vascularization process finishing.

As mentioned, vascularization plays a crucial role in 3D cell cultures. The capillary vessels, lined by endothelial cells, allow vascular transportation of nutrients to the cells and takes cell waste to external environment. Endothelial cells are expected to reside in the HSCs niche for their vascularization potential and vascular niche model has been used to successfully co-culture with HSCs<sup>125,126</sup>. As common cell type in the bone marrow, osteoblast cells are also considered to be essential for controlling the fate of HSCs. It has been found that osteoblast cells could secrete proteins that help in HSCs localization at the endosteal surface<sup>127,128,129</sup> and help adhesion to the matrix<sup>130</sup>. Notably, Nakamura et al<sup>131</sup> showed that calcium ion concentrations effect osteogenic differentiation and protein expression of osteoblast cells. And the Ang protein expressed by osteoblasts was found to play a pivotal role in controlling HSCs' fate. The result suggests that Ca concentrations released from scaffold materials might be used to control HSC fate in bone marrow in-vitro culture.

In the present work, it is proposed that ceramic foam will be used to elevate the release Ca ions in the in-vitro bone marrow niche and induce HSCs proliferation.

## **2.4 CERAMIC FOAM**

In order to mimic the microenvironment of the HSCs endosteal niche in the body, this study will process scaffold material with a similar structure and chemistry to trabecular bone but with higher Ca concentration than existing in pure synthetic hydroxyapatite. The scaffold should provide a temporary support for the cells, allowing them to attach to the scaffold surface and should provide a chemical environment similar to trabecular bone .The open foam structure will allow for the nutrients in culture to be transferred to the cells and the waste to be removed. The most suitable structures are macroporous calcium phosphate foams with high pore fractions (greater than 80%) and large open pore architectures. The methods used to process macroporous ceramics will now be reviewed.

Foam is one type of the cellular ceramics, which are comprised of various arrangements of a space-filling polygon (cells) <sup>132</sup>and could satisfy the requirement of three-dimensional cell culture.

Porous ceramics can be produced by numerous processing methods, commonly separated into three main categories by the principle used in their preparations<sup>133</sup>. They include replication, templating and direct foaming, as it is shown Figure 2.10.

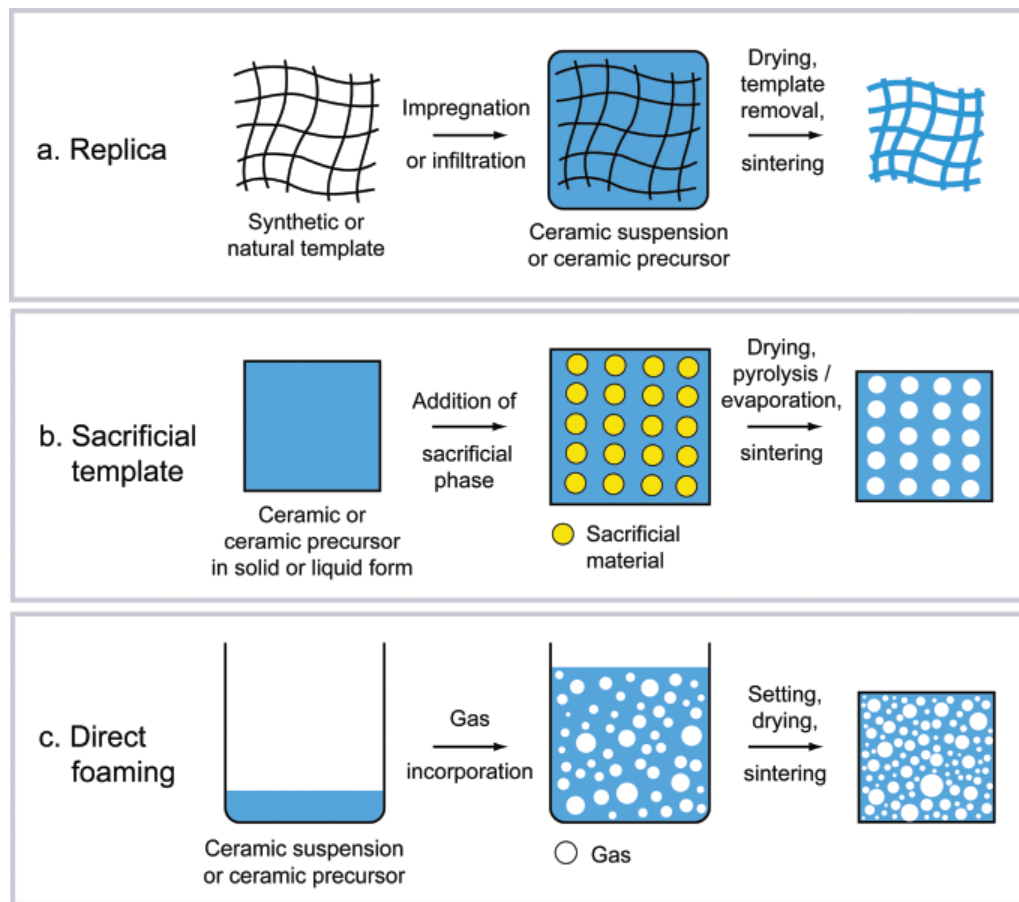


**Figure 2.10** Scheme of possible processing routes used for the production of macroporous ceramics<sup>134</sup>

#### 2.4.1 Replication

Replication is a method that coats a polymeric sponge with a ceramic particulate suspension and removes the polymer foam during controlled heating, the particles then sinter into a rigid copy of the polymer foam<sup>135, 136</sup>. In this replication method, a variety of ceramic cell types could be processed, including open-cell, semi-closed cell and closed-cell<sup>123</sup>. The ceramic pore or cell sizes are determined by the polymer sponge pore size and to a limited extent by the shrinkage in the sintering step.

As one of the most commonly used processing method since 1963, replication could be used on many polymer materials. The desirable properties of the polymer foam for the replication process include: (i) volatilization at low temperature without yielding noxious by-products, (ii) softness at the coating temperature, (iii) burning off of the polymer without inducing significant residual stresses and disrupting the unsintered ceramic, (iv) hydrophobic behavior, and its ability to be uniformly covered network<sup>123</sup>. Many polymers have been found to be suitable for replication including polyurethane, cellulose, polystyrene, etc. Perhaps the most commonly used polymer is polyurethane which has been shown to be capable of controlled pore size and morphology<sup>137</sup>.

In replication, the slurry is formed by a ceramic powder with a dispersion medium, which can be aqueous or non-aqueous. Commonly, some additives are added to the slurry to enhance stability and uniformity of coating. Replicated ceramic foams are distinctive in that the core of the foam struts is hollow due to the original polymer foam. The walls of the foam can also be cracked by the burn out process. Both of these features tend to compromise the strength and of the foam and render them fragile at high porosities

#### **2.4.2 Templating**

In the templating, or sacrificial template method, the initial biphasic mixture consists of a continuous matrix of ceramic precursors and a dispersed sacrificial phase, which should be homogeneously distributed in the matrix<sup>125</sup>. In this template method, the sacrificial phase aims to generate pores as a negative replica, as shown in Figure 2.10.

There are generally three methods to prepare the biphasic mixtures in templating ceramics<sup>138</sup>: the first one is mixing the two component powders and the compaction by pressing<sup>139</sup>; the second method creates a two phase suspension that is subsequently processed by wet colloidal routes such as slip, tape or direct casting<sup>140</sup>; and the third method is impregnating previously consolidated preforms of the sacrificial material with a pre-ceramic polymer or ceramic suspension<sup>141</sup>.

The sacrificial material plays an important role as a pore former and controls the pore size, connectivity, pore distribution and other properties. There are many suitable particulate sacrificial materials including organics, salts, metals, ceramics and even some types of liquids<sup>129</sup>.

#### **2.4.3 Direct Foaming**

The third route for processing macro-porous ceramics is direct foaming, in which air or another gas is dispersed into a suspension to create bubbles while the liquid phase, commonly a suspension of ceramic particulates, is used to keep the structure and form of the material<sup>129</sup>. As Figure.2.10 (c) shown, the mixing between the gas phase and the liquid suspension determine the resultant porosity. The stability of the bubbles is the most important factor. After setting, the foam is generally dried at room temperature and then sintered.

The critical issue in direct foaming is the stability of bubbles during drying due to drainage of the liquid through the liquid strut network under gravity. It is known that liquid foams are thermodynamically unstable systems and there is several physical processes taking place at their high gas–liquid interfacial area to decrease the high free energy<sup>129</sup>. Those physical processes can be of benefit to increasing the pore size, but rapid Ostwald ripening can remove many of the struts and collapse the foam<sup>129</sup>.

In order prevent coarsening and stabilize the foams, surfactant and biomolecules can be added to the liquid and have been found to slow down this coarsening process by decreasing the interfacial energy. Pugh<sup>142</sup> proved that foam bubbles coated with long-chain surfactant by adsorption could survive for several hours longer than without surfactant.

There are two methods that can be successfully used to achieve foaming stabilization<sup>129</sup>; one is stabilization with surfactants while the other is stabilization with particles.

In the surfactant stabilization, long-chain molecules with amphiphilic property and biomolecules such as lipids and proteins are used to make the wet foam stable. Those molecules, can act as surface-active agents to decrease the free energy between the hydrophilic phase and hydrophobic phase and preserve the interfacial area. In effect the molecules are adsorbed at the gas bubble surface, reduce the interfacial energy, and slow down the coalescence. However, the surfactant could not prevent the long-term destabilization and it is hard to increase the wet foaming time beyond several hours.

In the other stabilization method, solid particles are used to impede the destabilization and enhance the wet foaming time significantly, which could be several days<sup>143</sup>. In this method, the colloidal particles are used in Pickering emulsions to stabilize high energy interfaces<sup>144</sup> and have been applied to ultra-stable wet foams preparation<sup>145,146</sup>.

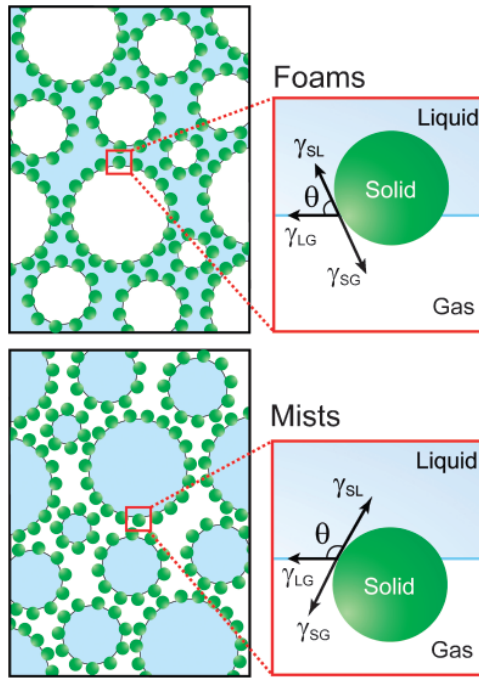


**Figure 2.11** Scheme of foams and mists that can be produced through the adsorption of colloidal particles at the gas–liquid interface. The drawings on the right hand side indicate the force balance at equilibrium for particles lyophobized to different extents<sup>129</sup>

As it is shown in Figure 2.11, the particles attach to both gas and liquid phases if they are partially hydrophobic. In this case, the high energy interface between gas and liquid is replaced by the lower energy boundaries of solid-gas and solid-liquid interfaces. With the particles added, the contact angle between solid and liquid phase is  $> 90^\circ$ , while the gas and solid phases have a contact angle  $< 90^\circ$ .

The contact angle of the particles could determine the dispersion of the phases<sup>147</sup> and act as one of the free energy determine factors. In this condition, the energy of attachment or free energy gained (G) by the adsorption of a particle of radius r at the interface can thus be calculated using simple geometrical arguments, which lead to the equation 2.1 and 2.2<sup>138</sup>:

$$G = \pi r^2 \gamma_{LG} (1 - \cos \theta) \text{ for } \theta < 90^\circ \quad \text{eqn 2.1}$$

$$G = \pi r^2 \gamma_{LG} (1 + \cos \theta) \text{ for } \theta > 90^\circ \quad \text{eqn 2.2}$$

Where  $\theta$  is the contact angle and  $\gamma_{LG}$  is the gas-liquid interfacial tension.

In the particle stabilization method, foam with smaller pores and higher pore fractions can be made. The typical porosity of these macro-porous structures range from 40% to 93% while the average pore sizes are much lower than those formed by the surfactant method formed pore sizes, in the range 10 to 300  $\mu\text{m}$ .

#### 2.4.4 Emulsion Foaming

An open porous ceramic, which has porosity as high as 97%, was created by Barg et al<sup>148</sup> using emulsifying aqueous suspensions of heptane containing ceramic powders and cationic or anionic surfactant. These ionic surfactants help to stabilize the bubbles in the emulsion using repulsive force between lyophilic end of molecule and the bulk liquid. This repulsive force helps to control the bubble development during the evaporation of volatile alkane and create porosity ceramic foam.

In this proposal, the foams are made in a similar method as Barg et al, and porosity is approximately 90% with the average pore size 500 $\mu\text{m}$ . This structure is suitable for cell seeding, cell growth, and nutrient transportation in the bioreactor application.

### 2.5 SINTERING

Sintering is an important thermal treatment step for ceramic fabrication. Ceramics commonly require sintering at temperature lower than the melting point, which allows mass

transport to eliminate by solid state sintering in response to the thermodynamic driving force provided by the elimination of pore surface.

There are three stages of microstructural evolution during the sintering process<sup>149</sup>: In the initial stage of sintering necks form to connect neighboring particle and the necks will grow but remain discrete. The growth of the necks causes center to center approach of the particles. This stage will result in some shrinkage (Figure 2.12) but ends at the relative density of about 65% of the “theoretical when the necks begin to overlap<sup>150</sup>. Initial stage sintering usually occurs during heating to the sintering temperature.

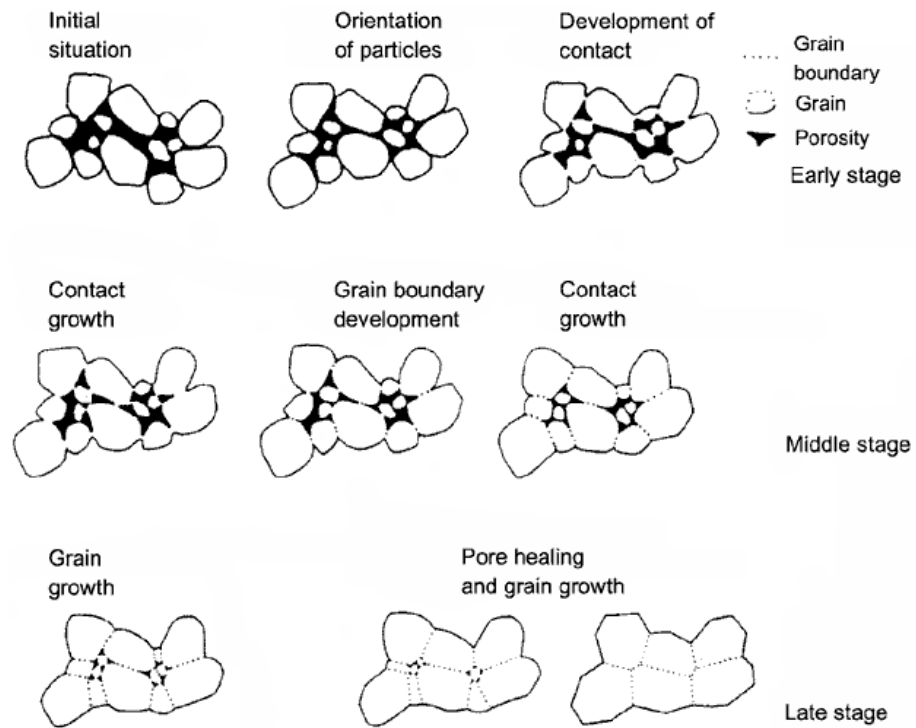


**Figure 2.12** sintering stage model<sup>151</sup>

In the second or intermediate stage, the microstructure is a network of connected grains and pores. During this stage, the stage the pores continue to shrink but remain open to the environment as shrinkage continues by neck growth. The intermediate stage is the stage in which

most of the sintering shrinkage takes place. Again much of this stage will occur during heating to the sintering temperature.

The final stage of sintering is characterized by the pore channels pinching off to give isolated pores. It begins at a relative density of approximately 90%. The sintering rate is now quite slow and full density is only achieved by the elimination of all the isolated pores.

### 2.5.1 Infiltration

Porous ceramics can be successfully infiltrated by a second phase through pores that are connected to the exterior surface if they are first sintered into the initial stage or intermediate stage sintering. These phases can be introduced as liquids, resins or particles in suspensions<sup>152</sup>. In all cases the infiltration processes are characterized by flow of a fluid through a porous ceramic that has been sintered into the initial stage or the intermediate stage of sintering. During the infiltration process, the pores and the voids of the solid-phase powder compact are filled by a wetting liquid that displaces gas that is residing in the pores. The force and the energy that draw the fluid inward are the capillary force and the reduction of the surface-free energy.

In the infiltration process, the ceramic should provide a system of interconnected pores and channels that allow the infiltrant penetration. The infiltration process can provide unique microstructures, with relatively broad control of both the depth and the composition of the infiltration modified zone<sup>55</sup>. Infiltrations have been used for preparing multiphase ceramics in several studies. Marple and Green<sup>153</sup> fabricated alumina / mullite ceramic and pointed out that infiltration approaches could control the phase distribution and the microstructure development. After partial sintered at 1300°C, the alumina cylinder compacts were immersed in prehydrolysed ethyl silicate solution for different times, dried and heated at 1200°C to allow decomposition of

the ethyl silicate. Finally, mullite was formed and the compacts were densified during a final heating step at 1650°C. Similarly, Lin et al<sup>154</sup> cyclically infiltrated porous zirconia with a mullite precursor liquid solution. In the cyclic process, the maximum amount of mullite precursor infiltrated depended on the initial open porosity of the matrix. The distribution was non-uniform, with higher mullite concentration near the surface external surface. After the infiltration and sintering, the gradient in second phase created residual stresses and cracking on cooling. This residual stress is thought to arise because of differential thermal expansion<sup>155</sup>.

In the preliminary work for this proposal, calcium nitrate solution was infiltrated into porous HA foam. Then the foam was immersed in ammonium hydroxide to give in-situ formation of CaO particles in the HA foam before final sintering.

### **3.0 HYPOTHESIS**

In the past decades, synthetic calcium phosphate has become an important biomaterial for hard tissue growth in-vivo. The ratio of Ca/P varies with the different phases and this has been reported to affect bioactivity and biocompatibility. Hydroxyapatite with Ca/P=1.67 is reported to enhance bone marrow cell culturing. Recent studies have shown that high calcium content in the media can enhance osteogenesis (growth of new bone) and angiogenesis (growth of new blood vessels). The hypothesis of this work is that composites of HA and CaO can increase the release of Ca into the media surrounding bone marrow cells and thereby promote HSC expansion and endothelial cell growth. If this can be achieved it would show, for the first time, that a scaffold could be manipulated to control stem cell fate during in-vitro culture that seeks to recreate the endosteal niche in which a population of HSCs could be expanded over the course of 4 weeks of culture.

## **4.0     OBJECTIVES**

1. Partially sintered HA foams were infiltrated with calcium nitrate precursors to produce CaO or CaCO<sub>3</sub> phase in-situ. The effect of the calcium nitrate concentration on infiltration, CaO or CaCO<sub>3</sub> phase fraction and the spatial distribution of the phases will be studied in pellets and foams.
2. Determine the time frame over which calcium is released into the media from the infiltrated ceramics. The solubility of infiltrated foam will be measured in static conditions.
3. Determine the effect of Ca content on endothelial cell and osteoblast / HSC population in static cell culture. After the examination of the infiltrated foam biocompatibility on endothelial cells and osteoblasts, it is necessary to determine the effect on HSCs, which was co-cultured with osteoblasts.
4. Examine the microstructural mechanism by which the dissolution of the Ca rich phase controls the fragmentation of the microstructure and the possible loss of structural integrity of the scaffold.

## **5.0 APPROACH**

### **5.1 MATERIAL PREPARATION**

#### **5.1.1 Hydroxyapatite Powder Preparation**

In order to ensure the phase purity, hydroxyapatite powder was calcined at 900°C for 1 hour. After calcination, the powder was milled in water for 24 hours and was dried and granulated again by pestle and mortar.

#### **5.1.2 High Calcium Content Pellets**

After the powder preparation, the hydroxyapatite powder was pressed into 13mm diameter pellets at a pressure of 26 MPa pressure. The resulting green density was 49.5%. After pressing, the pellets were sintered in air at 1100°C for 1 hour, using a heating rate is 5 °C/min and a cooling rate at 10 °C/min. After partial sintering, the relative density was 67%.

The infiltrant was prepared from calcium nitrate tetrahydrate ( $\text{Ca}(\text{NO}_3)_2 \cdot 4\text{H}_2\text{O}$ , Alfa Aesar, England) with water. The solution concentrations were prepared with  $\text{Ca}^{2+}$  concentrations of 0.5 mol/L, 1 mol/L and 2 mol/L. The pellets were then evacuated to remove the air from the pores and immersed in the calcium nitrate solution. After 24 hours the pellets were removed from the calcium nitrate solution and drops of ammonia hydroxide solution with pH=12-13 were

placed on to the surface of the pellets followed by immersion in ammonium hydroxide solution for 30 minutes before drying in air at room temperature for 24 hours. The pellets were heat treated at 900 °C to achieve crystallization of CaO in the infiltrated pellet<sup>156</sup>. The average calcium to phosphate ratio in the hydroxyapatite pellets was higher than that of HA (1.67). Then the hydroxyapatite pellets were sintered to high density at 1300 °C for 1 hour to remove the pore space and to make sure the porosity that remains was closed. The heat rate was 5 °C /min while cooling rate is 10 °C/min. The mass changes were recorded after each step of process. During the whole process, control samples were made in the same processing steps except for infiltration

### **5.1.3 High Calcium Phosphate Ratio Foam**

In order to create a high calcium content ceramic foam, a HA ceramic foam was created by emulsion method and infiltrated with Ca<sup>2+</sup> solution in the following process.

The HA foam was prepared by an emulsion process. A suspension was made by mixing deionized water with HA powder prepared as described above with 30 vol% solids. Ammonium polymethacrylate polyelectrolyte dispersant (Darvan C, RT Vanderbilt Co.) was then added to DI water and adjust pH to 5.5 by HCl solution. In this pH condition, a cationic surfactant (benzethonium chloride, Sigma) was active and could stabilize the alkane droplets by forming critical micelle concentration layers. After adding the HA powder the suspension was mixed at 2500 RPM for 20 minutes, in order to get proper dispersion. After the high speed mixing, the cationic surfactant (benzethonium chloride, Sigma) was added to the emulsion and mixed at 2500 RPM speed for 2 minutes. The final step was the addition of 10% volume of heptane to create bubbles and then mixed at high speed for 2 minutes.

In order to make the foam expand and form connected pores, the emulsion was poured into a paper mold in an incubator with 60% humidity for 1 hour and then the humidity was decreased to 40% until the foam had fully dried. The mold was then fired in furnace to 900 °C using 2 °C/min heating rate and a 10 °C/min cooling rate.

The foams were sintered in air at 1000 °C for 1 hour, using a heating rate is 5 °C/min with cooling rate at 10 °C/min. Then the infiltration procedure is similar to the pellets infiltration process as described before. After being infiltrated with Ca<sup>2+</sup> solution at 0.5, 1 or 2 mol/L, the foams was immersed in ammonia hydroxide solution at pH=12-13 to precipitate Ca(OH)<sub>2</sub>. After drying the foam was fired at 900 °C to achieve in situ-crystallization of CaO in the pores, and then sintered to high density at 1300 °C for 1 hour. In this process, the pores between the HA particles are closed leaving the CaO inside the foam walls. The heat rate for sintering was 5 °C/min while the cooling rate was 10 °C/min.

## 5.2 CHARACTERIZATION

Previous impregnation studies produced gradients in the infiltrated phase from the external surface<sup>155</sup>. It is therefore necessary to identify the second phase(s) attributable to the impregnation process and their distribution in the microstructure. X-ray diffraction was used to identify the crystalline phases present and qualitatively determine the phase fraction. In the determination of CaO or CaCO<sub>3</sub> phases, XRD and SEM were the main methods used.

### **5.2.1 XRD**

In XRD analysis, the phases on the as-sintered pellet surfaces and machined cross-section surfaces were determined. Additionally, the pellet was ground into powder and analyzed.

As the HA main characterize peak (221) is at the range of 30 to 33° for  $2\theta$ , and the  $\text{CaCO}_3$  main peak is at 33.909° as seen in Figure 5.1(b).The XRD scanning  $2\theta$  range was 20° to 80°.

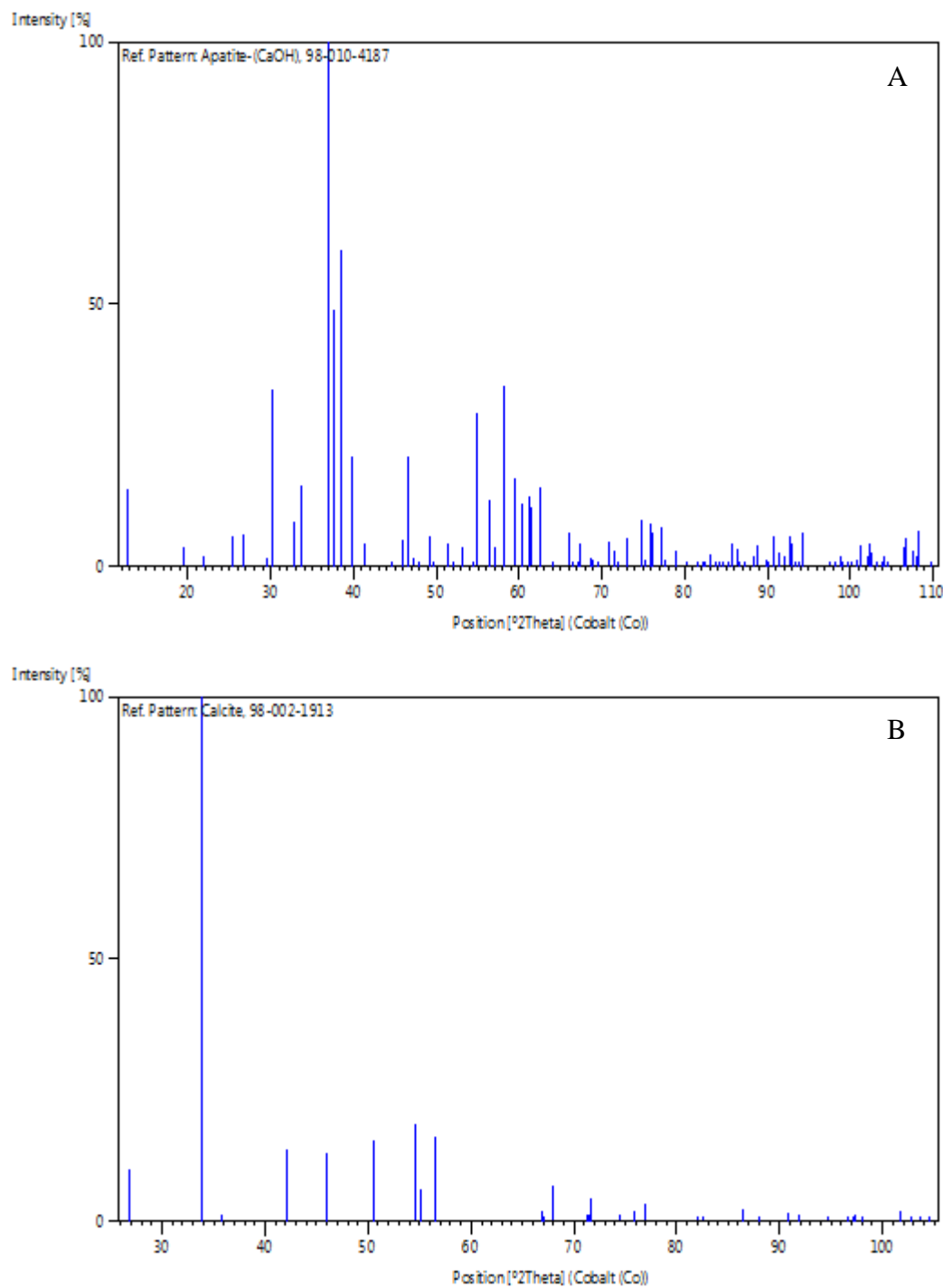


**Figure 5.1** X-ray diffraction standard pattern for (A) HA, (B)  $\text{CaCO}_3$

### **5.2.2 SEM Observation**

Scanning electron microscopy analysis was done on the sintered surface of the infiltrated sample pellets and the uninfiltrated control pellets. In order to compare the differences in microstructure and the dissolution behavior with/without infiltration, the samples were impregnated with a low viscosity resin and ground to a planar surface by EcoMet 250 Grinder-Polisher (Buehler, Lake Bluff, IL). In this procedure, both external surface and cross-section of one sample should be mounted in resin. The samples were grounded with 45  $\mu\text{m}$  and 30  $\mu\text{m}$  diamonds in water loaded with 18 lbs. at 60 RPM. Then, the samples were pre-polished with 15  $\mu\text{m}$  diamond with polishing oil AT 17 lbs. at 70 RPM. Finally, the polishing was completed with 6  $\mu\text{m}$  diamond and 1  $\mu\text{m}$  diamond with oil loading 16 lbs. at 50 RPM.

After polishing the samples were coated with palladium using a sputter coater and examined in a Phillips XL30 scanning electron microscope. Besides secondary electron images, backscattered images were also taken for the second phase detection ( $\text{CaO}$  or  $\text{CaCO}_3$ ) by contrast. In order to assist the Ca-rich phase detection, EDS was combined with back-scattered imaging. As  $\text{CaO}$  and  $\text{CaCO}_3$  has no phosphorous, EDS result confirmed the presence of a high calcium phase.

### 5.3 SOLUBILITY EXPERIMENTS

#### 5.3.1 Static Solubility Testing on Pellets

Pressed hydroxyapatite pellets were infiltrated with 1M Ca<sup>2+</sup> solution as described above. The negative control group was processed similarly but not infiltrated. All the samples were impregnated with a low viscosity resin and ground to a planar surface. After grinding with 45 µm and 30 µm diamonds in water the samples were pre-polished with 15 µm diamonds and 6 µm diamonds with polishing oil and finally with 1 µm diamonds in polishing oil.

After polishing the pellets were removed from the mounting resin and placed in sealed tube containing 50 ml Tris-buffer Saline (TBS). At each time point, listed in Table 1, two pellets were removed from the TBS, one for the infiltrated group and the other from negative control group.

**Table 1.** Static solubility experiment time point

Time pellet	0.5 hr	1 hr	12hrs	24 hrs	72hrs	1 week	2 week	4 week
HA pellet								
1 M infiltrated HA pellet								
2M infiltrated HA pellet								

After immersion the pellets were dried with Kimtech Wipes and stored in a desiccator while the Ca<sup>2+</sup> concentration in the TBS was measured using Ca<sup>2+</sup> probe (Roche, detection limit 0.001mmol/L). The exposed polished surfaces were then examined in SEM.

### 5.3.2 Static Solubility Testing on Scaffolds

Hydroxyapatite scaffolds were infiltrated with 2M Ca<sup>2+</sup> solution as described above. The negative control group was processed similarly but not infiltrated. All the samples were prepared as 0.0300 (+/- 0.001) g / sample and placed in sealed tube containing 1.5 ml Tris-buffer Saline (TBS). At each time point, listed in Table 2, two scaffolds were removed from the TBS, one for the infiltrated group and the other from negative control group.

**Table 2.** Static solubility experiment time point for hydroxyapatite scaffolds

Time scaffold \	0.5 hr	1 hr	12 hrs	24 hrs	72hrs	1 week	2 week	4 week
HA scaffold								
2M infiltrated								
HA scaffold								

After the scaffolds were dried with Kimtech Wiper they were stored in a dessicator while the Ca<sup>2+</sup> concentration in the TBS was measured using a Ca<sup>2+</sup> probe (Fisher Scientific™ Accumet™ Polymer Membrane Combination ISEs, Pittsburgh, USA, detection limit 0.001ppm) The scaffolds were then examined in SEM.

## 5.4 BIOCOMPATIBILITY EXPERIMENT

### 5.4.1 Endothelial Cell Biocompatibility Testing

For the endothelial cell biocompatibility testing, the cell type used was Human Umbilical Vein Endothelial cells, (HUVEC) passage 5. Hydroxyapatite foam was used for a control condition and hydroxyapatite foam, infiltrated with 2M Ca<sup>2+</sup>, was tested for biocompatibility.

In this experiment, three parallel repeats are applied for biological variability. In each repeat, there were three controls as listed in Table 3.

**Table 3.** Endothelial cell biocompatibility experiment controls and time points in each repeat

Time variables	5 days	15 days	42 days
Medium + Cells			
Medium+ cells + HA			
Medium+ cells + Infiltrated HA (2M)			

In Table 3, the Medium with cells condition was used as a positive control and there were three time point for all conditions. In each condition, three wells were applied for the different testing conditions.

Also, another two controls, medium and medium with HA foam, were designed for negative controls. In those two controls, there was no need to repeat three times because there was no cells and the only time point was 42 days. For these two conditions there were also three wells.

In the experiment process, the endothelial cell-line was taken from freezer and cultured. Meanwhile, scaffolds were put into labeled plates and sterilized with ethylene oxide. The cell culture medium formulation is given in Table 4. The Ca concentration in medium is 0.700 (+/- 0.005) mmol/L.

**Table 4.** HUVECs Medium formulation

Supplement	Amount	Supplier
Heparin	0.1 mg/mL	Sigma Aldrich
Endothelial cell growth supplement	0.05 mg/mL	Sigma Aldrich
Fetal bovine serum	10%	PAA
Anti-anti	1%	Invitrogen
F12-K	Basal medium	Invitrogen

Cells were suspended in cell culture medium and added at a concentration of 2E4/ml. In each well, 0.5 ml EC suspension was added to the center of scaffold or well bottom with 1E4 cells in each well. After plating, the ECs were cultured in an incubator at 37°C and 5% CO<sub>2</sub> for 42 days. The cell culture medium was replaced every 2-3 days to replenish nutrients and remove waste products. Aspirated medium was saved for future analysis. At each time point (5, 15, and 42 days), wells were harvested for gene expression.

In the endothelial cell biocompatibility experiment, three characterization methods were used to analyze the cell cultures. The first was glucose and lactate measurement, to determine the cell activity to give some indication of relative cell numbers. When the medium was changed at each time schedule, some was saved for future analyses while some it was used to measure glucose, lactate and  $\text{Ca}^{2+}$  ion concentrations.

RNA was extracted from the cell lysate using a kit from Qiagen. Reverse transcription polymerase chain reaction (PCR) was subsequently performed on the RNA, resulting in c-DNA samples. Real-time PCR (RT-PCR) was used to examine the cell types in the culture through gene expression. 25 ng of c-DNA from each sample was used and tagged with fluorescent TaqMan probes (Invitrogen), which bind to the specific gene sequences of interest. The following list shows the 5 markers used and their significance:

1.  $\beta$ -actin – one of six actin isoforms found in all human cells. This is used as a control gene to normalize the gene expression data.
2. CD 31 and CD144 – both of the markers are the endothelial progenitor markers which will participate in vascularization
3. von Willebrand Factor (vWF) – a marker of mature vascular endothelial cell
4. Antigen KI67 – a marker for cells in the proliferation stage

For the 3 repeats using the cell-line, prior to RNA isolation, the lysates were passed through a column to isolate genomic DNA from the samples. This was then quantified using a Qubit fluorometer (Invitrogen) and a double stranded-DNA assay kit and compared to the DNA –cell amount standard curve, which was draw by measuring DNA amount of different cell amounts.

#### **5.4.2 Hematopoietic Stem Cells / Osteoblasts Co-Culture Biocompatibility Testing**

In the hematopoietic stem cells/ osteoblasts co-culture testing, the HSCs and osteoblasts were mixed in the ratio of 9:1. This ratio is about an order of magnitude higher than the fraction of HSCs in the human bone marrow cell fraction. The HSCs are primary cells from healthy donors and the osteoblasts are the Saos-2 cell line. Hydroxyapatite foam was used as the control condition and hydroxyapatite foam conditions, infiltrated with 1M and 2M  $\text{Ca}^{2+}$ , were tested for biocompatibility.

In this experiment, three parallel repeats are applied to account for biological variability between different HSC donors. In each repeat, there were three controls as listed in Table 5.

**Table 5.** Hematopoietic stem cells / osteoblasts co-culture experiment controls and time points in each repeat.

Time variables	5 days	14 days	28 days	42 days
Medium + Cells				
Medium+ cells + HA				
Medium+ cells + Infiltrated HA (1M)				
Medium+ cells + Infiltrated HA (2M)				

In Table.5, the Medium + Cells condition was used as a positive control and there were four time point for all conditions. In each condition, three wells were applied for the different testing conditions.

Also, another two controls, Medium and Medium with HA foam, were designed for negative controls. In those two controls, there was no need to repeat three times because there was no cells and the only time point was 42 days. For these two conditions there were also three wells.

In the experiment process, the HSCs were mixed with pre-cultured osteoblasts as soon as delivered with fixed ratio of 9:1. Meanwhile, scaffolds were put into labeled plates and sterilized with ethylene oxide. The cell culture medium formulation is given in Table 6.

**Table 6.** HSCs Medium formulation

Supplement	Amount	Supplier
Human-specific Mesencult supplement	0.01 ml/mL	StemCell Technologies
AB Human serum	5%	Sigma-Aldrich
Anti-anti	1%	Invitrogen
Human-specific Mesencult Medium	Basal medium	StemCell Technologies

Cells were suspended in cell culture medium and seeded as 5000 cells/ cm<sup>2</sup> into the culture plates. In each well, 4 ml cell suspension was added to the center of scaffold or well bottom. After plating, the cells were cultured in an incubator at 37 °C and 5% CO<sub>2</sub> for 42 days.

The cell culture medium was replaced every 2-3 days to replenish nutrients and remove waste products. Aspirated medium was saved for future analysis. At each time point (5, 14, 28 and 42 days), wells were harvested for fluorescence activated cell sorting (FACS) and the CFU assay.

In the HSC/osteoblasts cell biocompatibility experiment, three characterization methods were used to analyze the cell cultures. The first was glucose and lactate measurement, to determine the cell activity and gives some indication of relative cell numbers. When the medium was changed at each time point, some was saved for future analyses while some it was used to measure glucose, lactate and  $\text{Ca}^{2+}$  ion concentrations.

Fluorescence Activated cell Sorting (FACS) was applied to the experiment for the cell type and to study differentiation. In FACS, cells could be identified and counted by the special protein expression on the cell membrane. Based upon the specific light scattering and fluorescent characteristics of each cell, the cells could be sorted and separated individually<sup>157</sup>.

For surface marker staining, cells were incubated with fluorochrome conjugated antibodies: FITC-Linage cocktail (Lin), PerCP Cy-CD34, BV421-CD31, PE-CD235a, APC-H7-CD45, AF700-CD38 (all Becton Dickinson). Compensation beads (Becton Dickinson) were used to compensate potential spectral fluorochrome overlap when cells were analyzed with a FACS Aria II. In data analysis used FlowJo software version 9.5.2 (Tree Star, Ashland, OR), a forward versus side scatter gate was applied to excluded cell debris and cell doublets

The Colony Forming Unit Assay (CFU) is a method to investigate the potential of hematopoietic progenitors to form colonies of differentiated cells in the hematopoietic lineage. Fresh mixed cells and the co-cultured cells from the four scaffold conditions were assayed using 5000 cells, and the cells were cultured in conventional Petri dish with counting after 14 days of culture by phase microscopy (Zeiss Invertoskop C, Carl Zeiss, Jena, Germany). A complete

MethoCult methylcellulose-based assay was used according to manufacturer's instructions (StemCell Technologies). Four different types of colonies were identified and their frequencies compared to expected numbers as given by the manufacturer: CFU-E (Colony Forming Unit – Erythrocyte), BFU-E (Burst Forming Unit – Erythrocyte), CFU-GM (Colony Forming Unit – Granulocytes, Macrophage), CFU-GEMM (Colony Forming Unit – Granulocyte, Erythrocyte, Macrophage, Megakaryocyte)<sup>158</sup>.

## **6.0     RESULTS AND DISCUSSION**

### **6.1     INFILTRATION PROCESSING**

As described in the first objective, a soluble Ca-rich phase should be introduced into HA ceramic. With this second phase, the HA degradation rate could be increased with higher concentration of  $\text{Ca}^{2+}$  released into the medium. Additionally, the soluble phase could be distributed in the HA ceramic so as to release  $\text{Ca}^{2+}$  over a 42 days period.

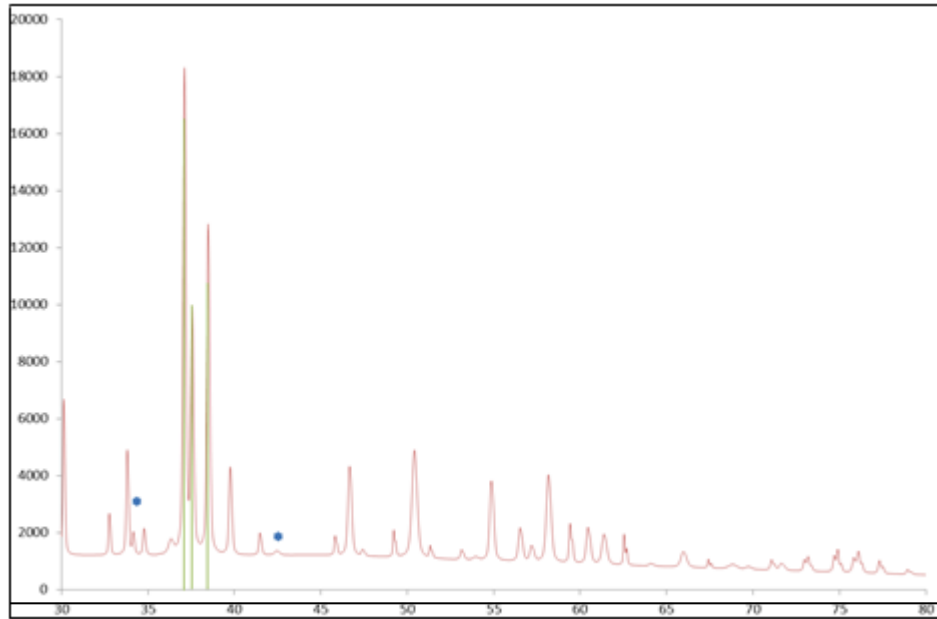
#### **6.1.1   Effect of the Infiltration on the Phase Distribution in Pellets**

Figure 6.1 shows the x-ray diffraction patterns for the infiltrated pellets. HA and  $\text{CaCO}_3$  were present in the infiltrated pellet surface. The  $\text{CaCO}_3$  standard peaks were labeled with stars in Figure 6.1. It is apparent that HA is the main phase found in the pellet surface. Fig 6.1 (a), shows the three main HA peaks were shown at  $37.07^\circ$ ,  $37.56^\circ$  and  $38.42^\circ$  as in the standard HA pattern. Also, Figure 6.1 also shows minor peaks at  $33.91^\circ$  and  $42.12^\circ$ , which belong to  $\text{CaCO}_3$ . The  $\text{CaCO}_3$  was formed after sintering by the reaction of the  $\text{CaO}$  second phase with moist air containing  $\text{CO}_2$  in ambient conditions.

With the x-ray diffraction result, the quantity of the  $\text{CaCO}_3$  was calculated using equation 6.1:

$$\frac{X\alpha}{X\beta} = \frac{I_{\alpha(hkl)} RIR_{\beta}}{I_{\beta(hkl)} RIR_{\alpha}} \frac{I_{\beta(hkl)}^{ref}}{I_{\alpha(hkl)}^{ref}} \quad \text{Eqn 6.1}$$

The quantity of the  $\text{CaCO}_3$  in the infiltrated foam was calculated to be approximately 3%, which is quite a small amount when compared with the HA phase.



**Figure 6.1** X-ray diffraction patterns of infiltrate HA pellet surface (\* stands for  $\text{CaCO}_3$  peak, green line stands for HA main peak)

Although the peak intensity of  $\text{CaCO}_3$  in the X-ray diffraction result was quite small, the existence of the peak proved that the infiltration process did introduce a Ca-rich phase into HA. Also, the new phase is  $\text{CaCO}_3$ , which has a much higher solubility than HA<sup>111</sup> and is therefore expected to release calcium into the media.

### **6.1.2 Microstructural Analysis of Polished Surfaces on Pellets**

Microstructural analysis of surfaces and the sections through the infiltrated HA pellets showed the second phase distribution derived from the infiltration process. As the Ca-rich phase is soluble with water, when polished with water, pits and defects appeared on the polished surface. In the Figure 6.2, polished surfaces of the infiltrated HA pellets shows pits on the surface while the pure HA pellets are still quite smooth and flat. Figure 6.2(A) is the HA pellet surface and there are no pits. Figure 6.2(B), (C), and (D), have defects which are created by dissolution of the  $\text{CaCO}_3$  during the polishing process. Also, the pellets infiltrated with higher calcium nitrate concentration did not show significant difference in the population of defects on the pellet surface.. In the infiltration process, the solution was introduced into the HA ceramic from the external surface and would be expected to create a gradient in the second phase which would diminish from the surface to the interior.

Even though the concentration of  $\text{Ca}^{2+}$  solution was increased, the external surfaces of the infiltrated HA pellets showed approximately the same amount of Ca-rich phase formation. This is probably due to concentration of the nitrate by precipitation on the surface during drying. This would lead to similar amounts of  $\text{CaCO}_3$  on the external surface since the nitrate would exceed its solubility limit at this location irrespective of the calcium nitrate concentration in the infiltrate.

The defects formed by dissolution of the  $\text{CaCO}_3$  are much larger than the second phase particles observed in SEM as shown in Figure 6.3(A) and (B., Therefore the dissolution of the  $\text{CaCO}_3$  must also be removing adjacent grains of hydroxyapatite. Also, the EDS result of Figure 6.3 (C) show that the Ca/P is 2.04, which is much larger than 1.67, the HA standard Ca/ P ratio.

This is thought to be due to the fact that most of the x-rays originate from the  $\text{CaCO}_3$  particle but some also originate from the surrounding HA grains.

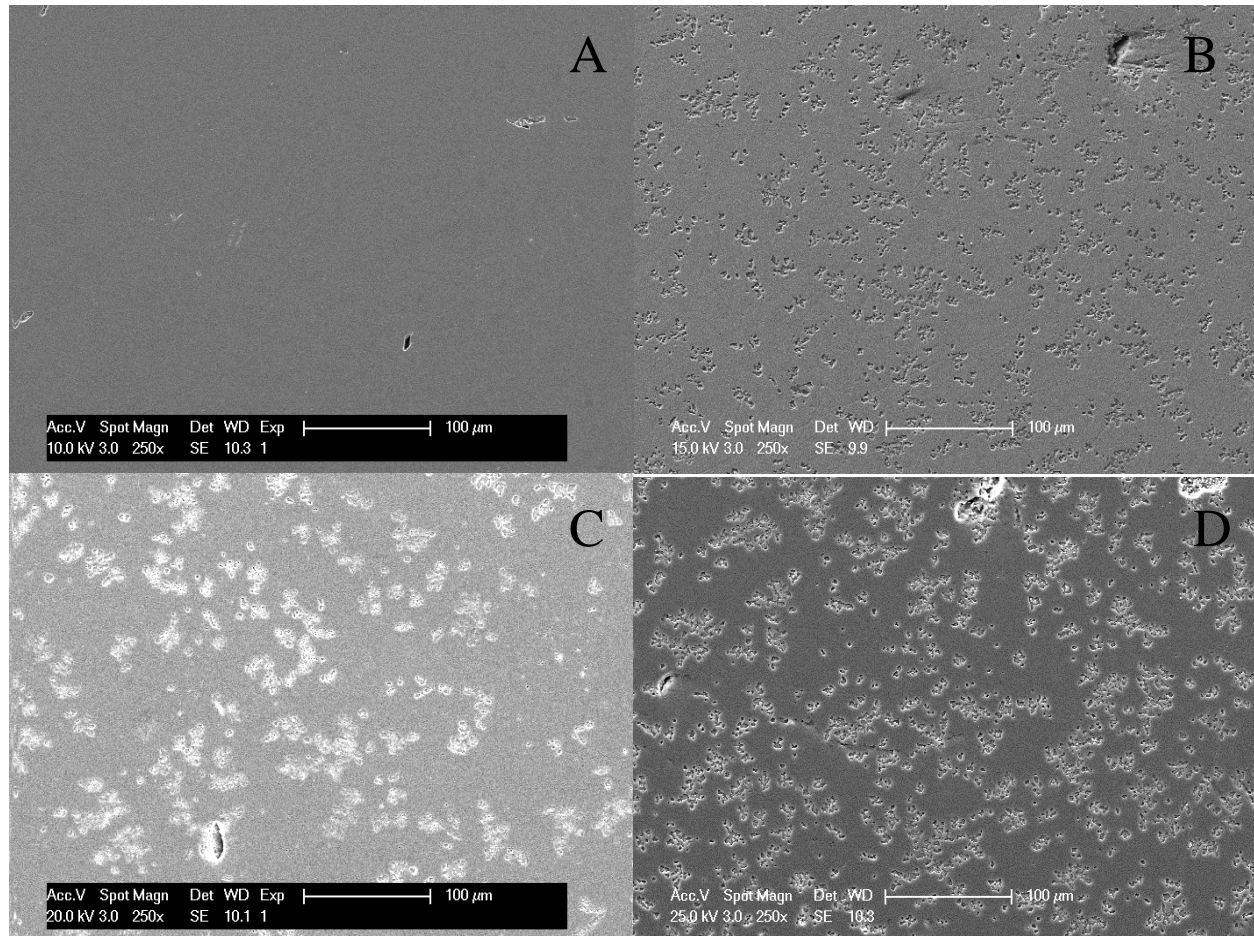


**Figure 6.2.** SEM for the surface of pellets. A) HA pellet surface; B) 0.5M calcium nitrate infiltrated HA pellet surface; C) 1M calcium nitrate infiltrated HA pellet surface; D) 2M calcium nitrate infiltrated HA pellet surface

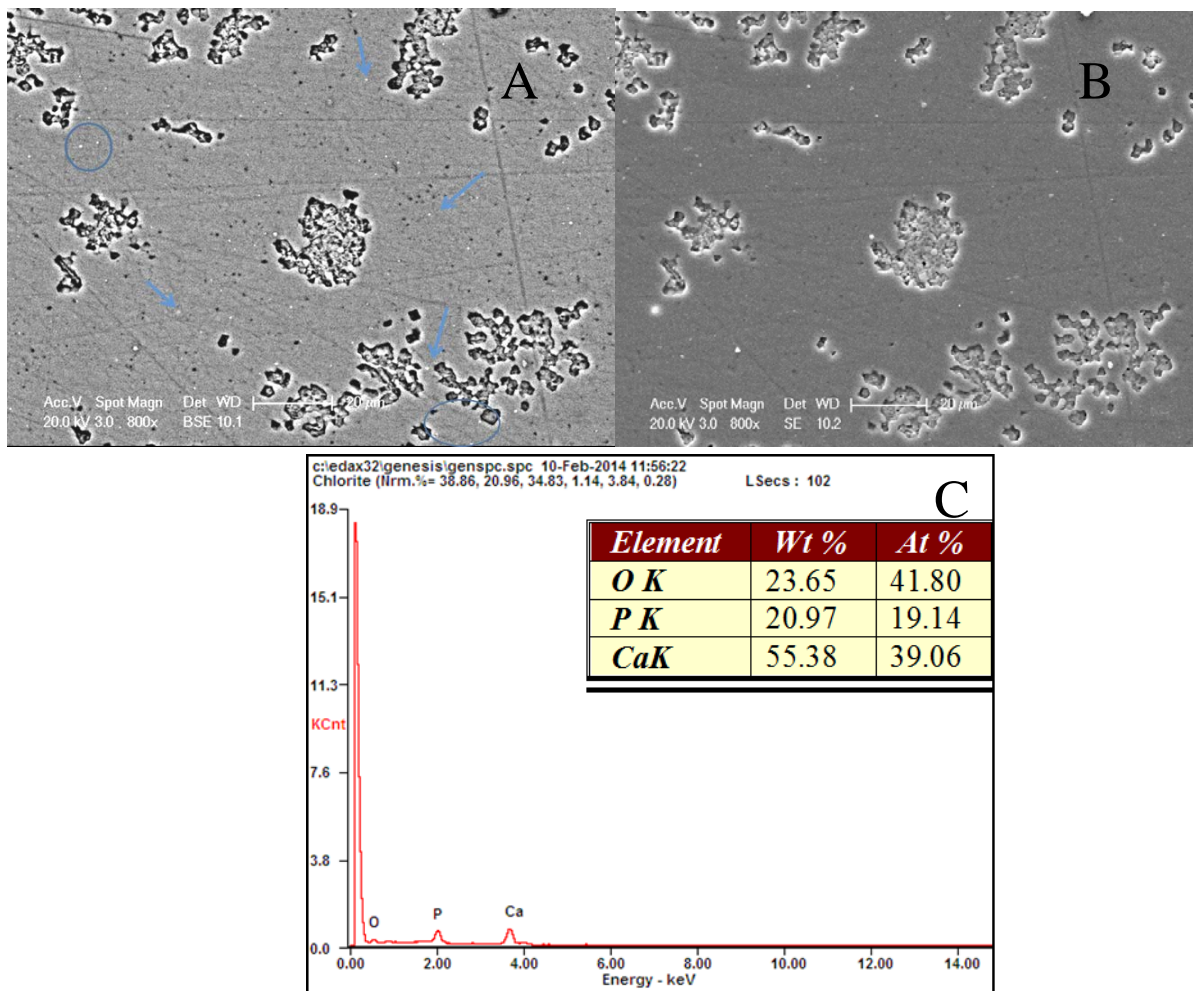


**Figure 6.3.** Polished surface of  $\text{Ca}^{2+}$  solution infiltrated HA pellet (A) BSE, (B) SEM, and (C) EDS

In Figure 6.4, shows the morphology at defects at higher magnification. The defects had faceted boundaries suggesting grains had been removed by the dissolution process, as Figure 6.4 (B), (C), and (D) demonstrates. Therefore the shape and size of the defects caused by dissolution result not only from the  $\text{CaCO}_3$  dissolution, but also from the removal of the HA grains that are coordinated to the  $\text{CaCO}_3$  particles. It is thought that,  $\text{CaCO}_3$  formation from  $\text{CaO}$  on exposure to water or moist air causes a volume change that cracks the surrounding material and allows coordinating HA grains to be removed.

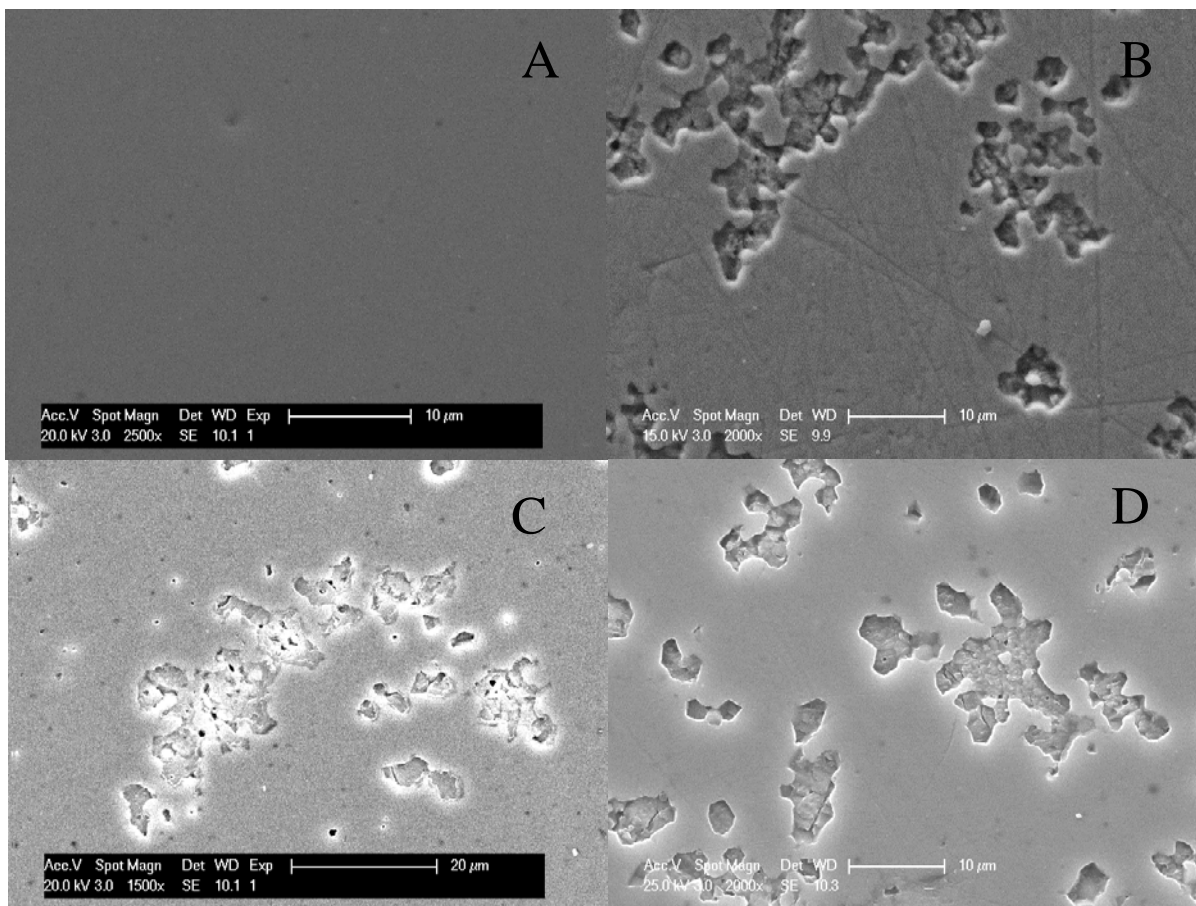


**Figure 6.4.** SEM on pellet surfaces: A) HA pellet surface; B) 0.5M calcium nitrate infiltrated HA pellet surface; C) 1M calcium nitrate infiltrated HA pellet surface; D) 2M calcium nitrate infiltrated HA pellet surface

Also, micrographs from the thermal-etched samples after polishing supported this conclusion. In Figure 6.5, the pellet was polished and then thermal-etched to show grain boundaries. According to this SEM picture, the defects are larger than a single HA grain and have a similar faceted shape as the grains. When back-scattered electron imaging was applied to more clearly observe the second phase, as in Figure 6.6, it is found that the size of the  $\text{CaCO}_3$  particles was much smaller than HA grains observed in Figure 6.5. In the Fig 6.6(A), the small white dots are calcium rich and thought to be  $\text{CaO}$  or  $\text{CaCO}_3$  phase,



**Figure 6.5.** Thermal-etched infiltrated HA pellet

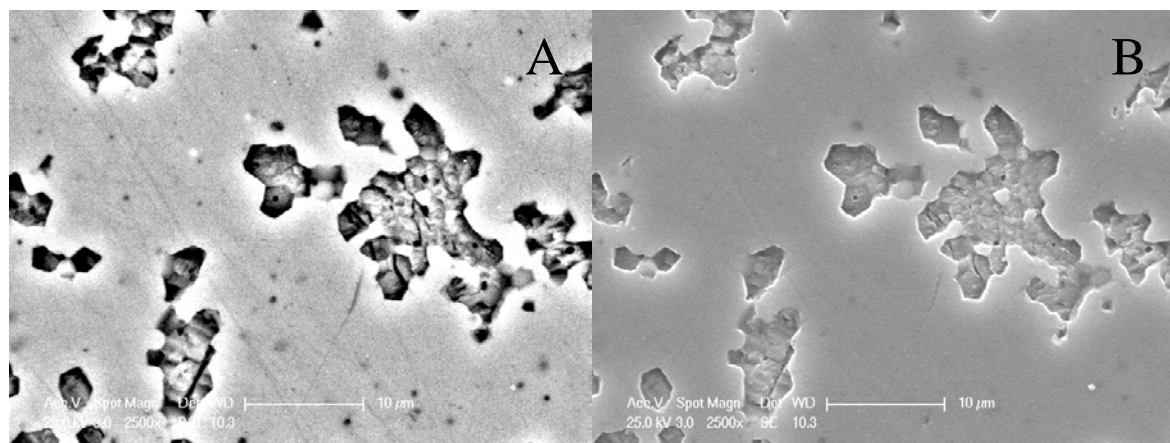


**Figure 6.6.** Polished surface of infiltrated HA pellet (a) BSE, (B) SEM

The  $\text{CaCO}_3$  was dispersed throughout the polished sample section but is concentrated towards the external surface. In other words, the  $\text{CaCO}_3$  distribution is heterogeneous but is present throughout the bulk of the ceramic.

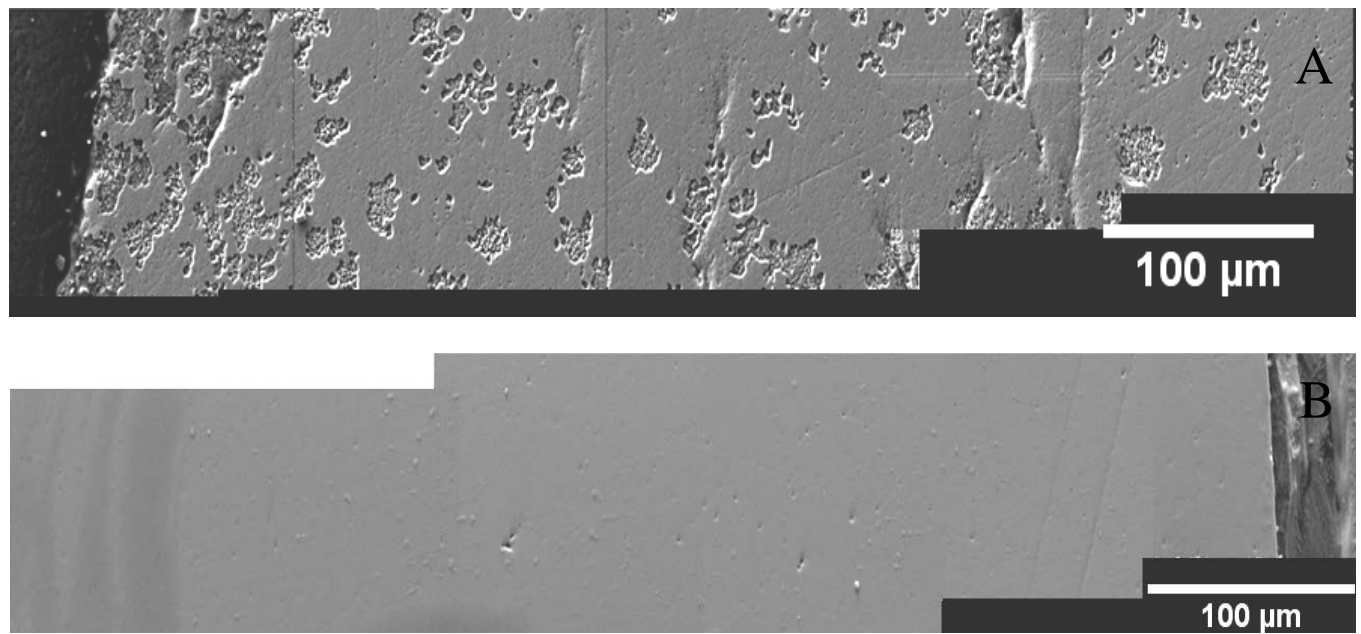


**Figure 6.7.** A) section of infiltrated HA pellets and B) section of HA pelltes

Figure 6.7, shows how the defects are dispersed throughout the section of the pellet when a cross-section is exposed to moisture during polishing, this suggests that the CaO second phase, is dispersed throughout the pellet. The results suggest that infiltration is a valid processing method for manufacture of these new biphasic ceramic containing a soluble second phases. However, there is a gradient in the CaO second phase fraction which decreases from the external surface towards the interior as previously observed by Lange et al in alumina infiltrated with zirconia ceramics<sup>164</sup>.

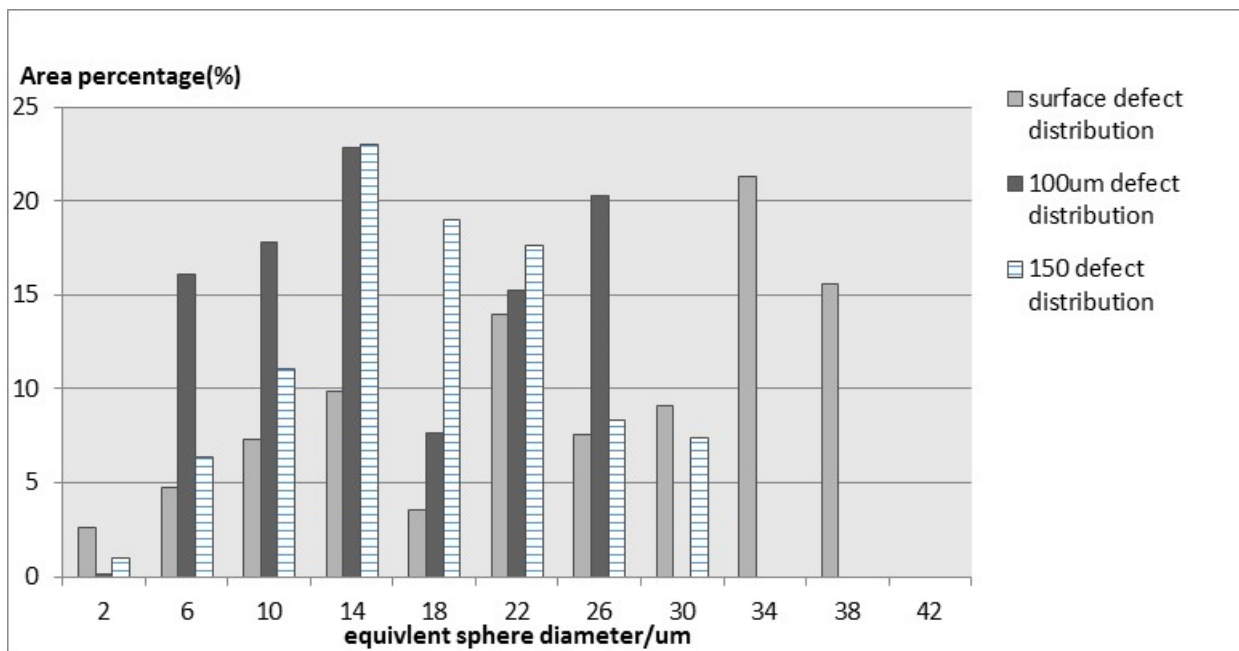


**Figure 6.8.** The defect size distribution on the section of infiltrated HA pellets in Figure 6.7

At the external surface, the defect area fraction was 29.6 ( $\pm 3$ ) %. After moving the fields of measurement into the interior, at the location of 100  $\mu\text{m}$ -away from external surface, the defect area fraction decreased to 20.3 ( $\pm 3$ ) %, and the measured pore size distribution shifted to smaller sizes. Figure 6.8 shows that adjacent to the pellet surface the pit size distribution was multi modal with modes at approximately 34  $\mu\text{m}$  (14 HA grain diameters) and 22  $\mu\text{m}$  (9 HA grain diameters). At the location 100  $\mu\text{m}$  from the surface the pore size distribution was still multimodal with the largest mode in pit size distribution ranging from 25.2-27.2  $\mu\text{m}$  (10.5-11.5 HA grain diameters) with a secondary mode between 13.2 and 15.2  $\mu\text{m}$  (5.5-6.5 HA grain diameters). Therefore the change in the defect area fraction reflects the expected decrease in the phase fraction of CaO with distance from the exterior surface of the sample in infiltrated samples but it is also interesting to observe the decrease in the size of the pits suggest that the spatial clusters of CaO that result in pits on transformation to  $\text{CaCO}_3$  are also smaller further into the interior of the samples. The decrease of the size corresponding to the defect modes continue on

moving 150 $\mu\text{m}$ -away from external surface, but the changes are small and not thought to be significant. The defect area fraction at a distance of 150  $\mu\text{m}$  was 19.2 (+/-3) %, and the first mode of the pit size distribution was, 12.8-14.8  $\mu\text{m}$  and the second mode of pit size distribution had decreased to 17.2-18.8  $\mu\text{m}$ . There appears to be no further change in pit fraction and pit size at larger distances from the external surface of the sample. Figure 6.9 (B), shows no faceted pitting defects on the section of the control HA sample.

Also, in order to confirm the defects are produced by water attacks, HA pellets and infiltrated pellets where sonicated with water and also with isopropanol.

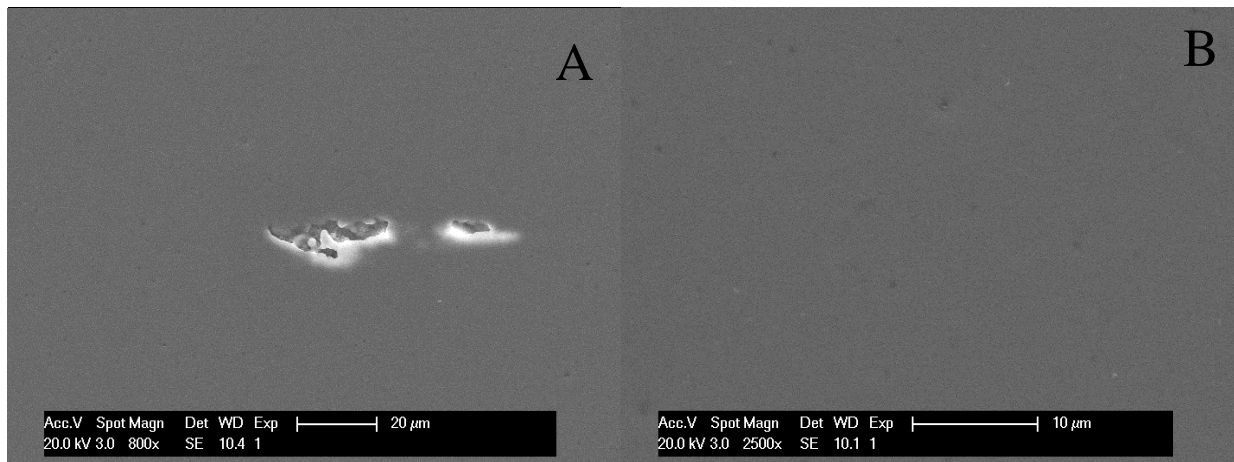


**Figure 6.9.** Polished HA pellet surface (A) with propanol, (B) with water

Figure 6.9, shows no significant difference between single-phase HA pellets that were ultra-sonicated with water or alcohol. Both of the pellets had smooth and flat surfaces without any defects, though some pores were present as shown in figure 6.9(A). However, Figure 6.10 shows that for the  $\text{Ca}^{2+}$  solution infiltrated pellets, ultra-sonicated with alcohol the defects were not present. When sonicated with water, the defects were throughout the sample as before.

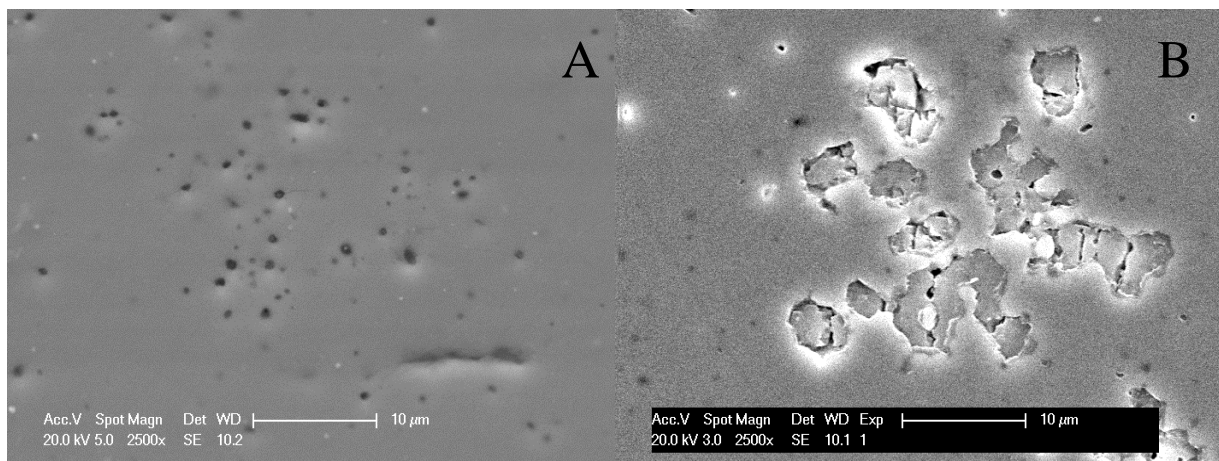


**Figure 6.10.** Polished surface of infiltrated HA pellet (A) with isopropanol, (B) with water

As the XRD results suggest that the  $\text{CaCO}_3$  is present in very small volume fractions (3 % to 5%). However, the defects produced on the surfaces of infiltrated pellets polished in water accounted for a much larger fraction of the surface. Again, this is consistent with HA grains being removed from the surface during transformation of  $\text{CaO}$  to  $\text{CaCO}_3$  and the dissolution of the  $\text{CaCO}_3$ . In summary, the  $\text{CaO}$  content in the ceramic body caused fragmentation of HA when the  $\text{CaCO}_3$  is formed and subsequently dissolved.

### 6.1.3 Effect of the $\text{CaCO}_3$ Phase on Dissolution and Damage Accumulation on Polished Surface of Pellets

As mentioned above, the infiltrated ceramic should be capable of releasing  $\text{Ca}^{2+}$  into the medium in the long term culture of HSCs. Also, in the HSCs culturing,  $\text{Ca}^{2+}$  should release at a steady rate through the culture period. Therefore the time dependent dissolution and damage accumulation of the biphasic CaP ceramic created using infiltration of HA must be studied. Two  $\text{CaCO}_3$  fractions were created as pellets by varying the concentration of the infiltrant solution (1 mol/L and 2 mol/L  $\text{Ca}(\text{NO}_3)_2 \cdot 6\text{H}_2\text{O}$  solution). As described previously, the pure HA pellet was a

negative control. The solubility of the pellets was tested in static condition, as described in the experimental procedures section.

The experiment shows significant differences in dissolution between the negative control and the infiltrated pellets. As shown in Figure 6.11, the infiltrated pellets released more  $\text{Ca}^{2+}$  ions in the saline than the HA pellets, especially for the 1 mol% samples at 28 days. Interestingly, the calcium released decreased more for 2 mol/L infiltrated HA pellets at 28 days, possibly due to precipitation of calcium phosphate. The range of the Ca probe in Cobas 211 is 0.04 to 40 mmol/L.

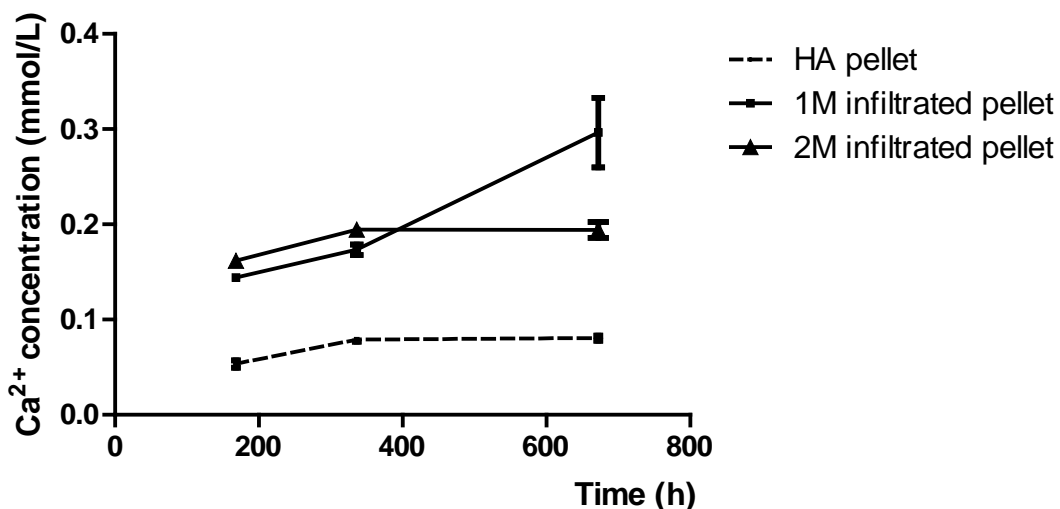


**Figure 6.11.**  $\text{Ca}^{2+}$  ion concentrations in the Tris-buffered saline were plotted as a function of time for static experiment on pellet samples.

The pellets used for the dissolution experiments were also observed in SEM on polished surfaces parallel to the sintered surface and as close to the sintered surface as possible. At the first two time points, 0.5 and 1 hour, there was no significant difference between the damage on the surface of the pellets at these two time points for the same condition. There were defects on

the surface of the infiltrated pellets, while there are no defects on the HA pellets at 0.5 and 1 hour samples.

However, the defects (Figure 6.12) in the 2M infiltrated pellets were deeper than the defects on 1M infiltrated pellets.

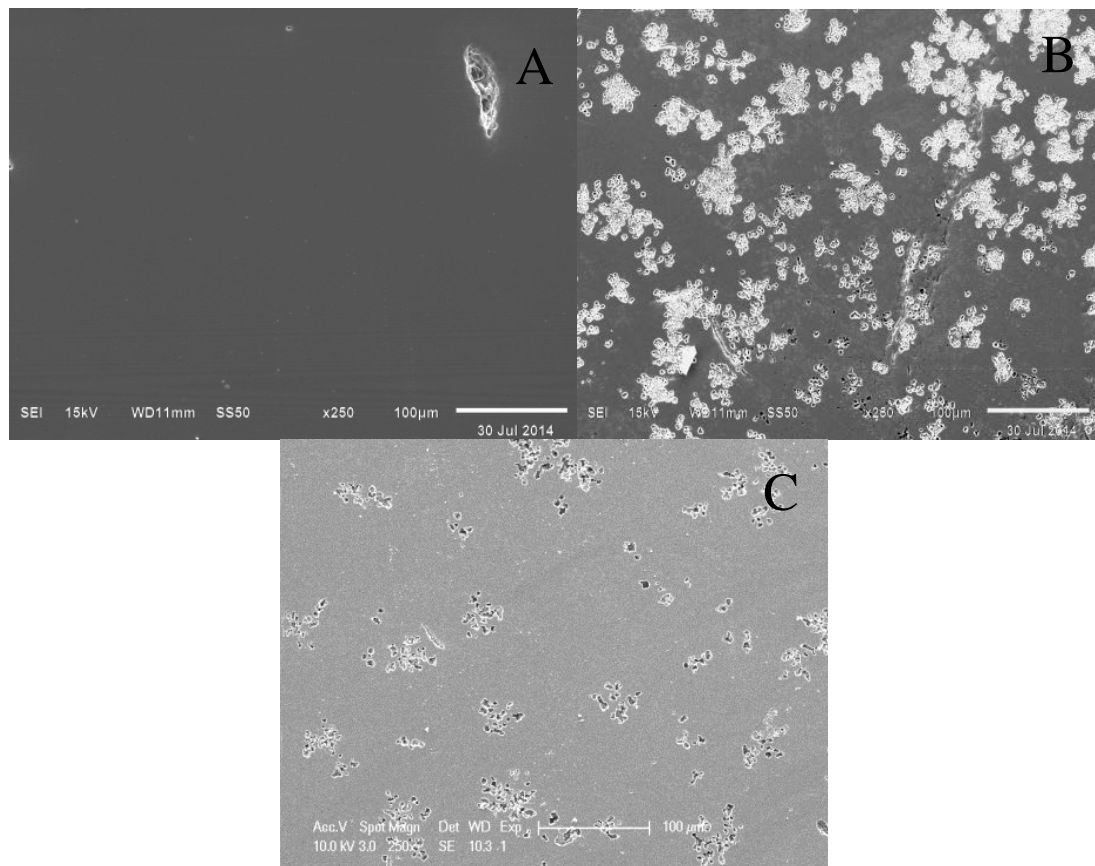


**Figure 6.12.** 0.5 hours microscopy for pellet surfaces (a) HA pellet, (b) 1M Ca<sup>2+</sup> solution infiltrated HA pellet, (c) 2M Ca<sup>2+</sup> solution infiltrated HA pellet

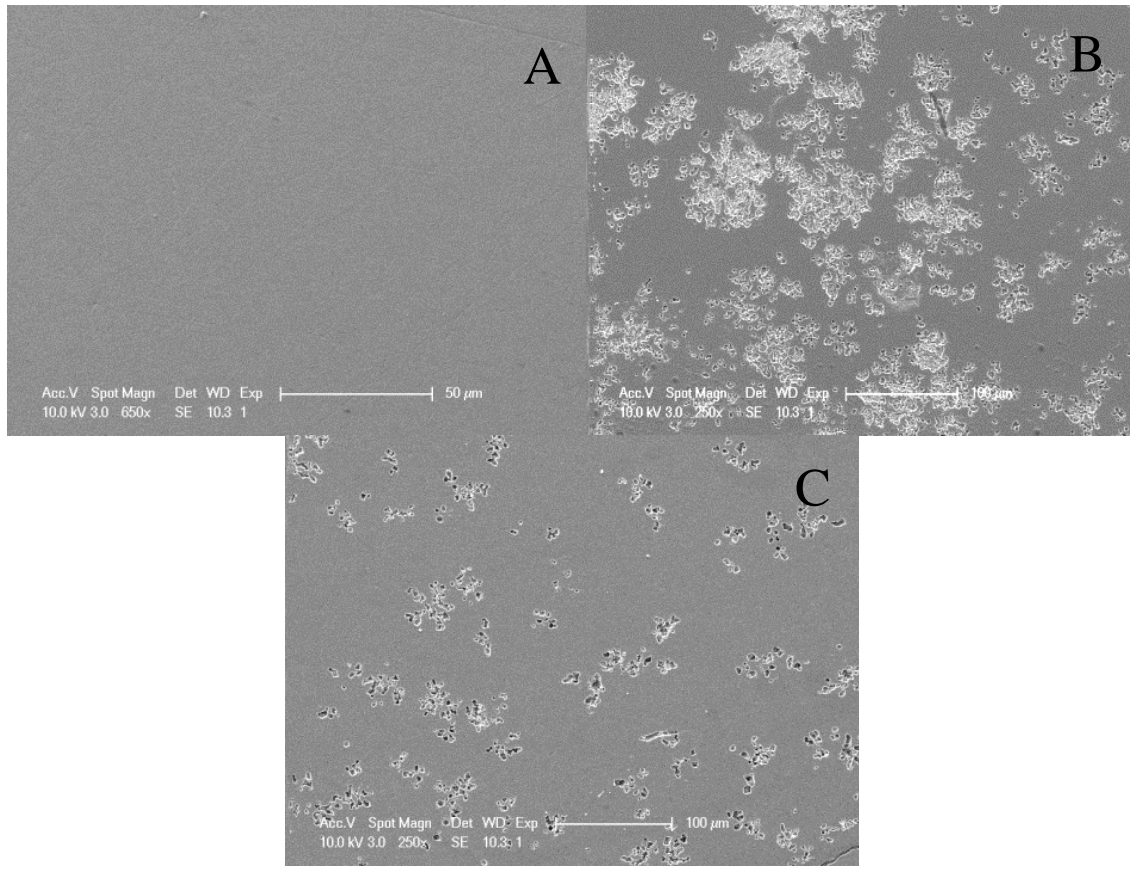


**Figure 6.13.** 1 hour microscopy for pellet surfaces (a) HA pellet, (B) 1M  $\text{Ca}^{2+}$  solution infiltrated HA pellet, (c) 2M  $\text{Ca}^{2+}$  solution infiltrated HA pellet

After 1 day, there were still no pits on the HA pellet surface. In the two infiltrated conditions, the defects grew deeper as time pass by and HA grains were removed layer by layer. This must involve a fragmentation process where exposure of  $\text{CaO}$  to moisture causes transformation to  $\text{CaCO}_3$  and the volume expansion cracks HA grain boundaries and allows the removal of adjacent HA grains. This exposes new  $\text{CaO}$  particles underneath and releases more  $\text{Ca}^{2+}$  ions into solution by dissolution of the  $\text{CaCO}_3$ . At Day 3, the defects began to appear on HA pellet surface but the resulting defects were much smaller than those on the -infiltrated pellets. The depth of the defects continued increasing for the -infiltrated pellets and some of the

defects began to connect with each other on the surface of 2M infiltrated pellet. The defects may have coalesced by removing the HA grains between them during fragmentation.

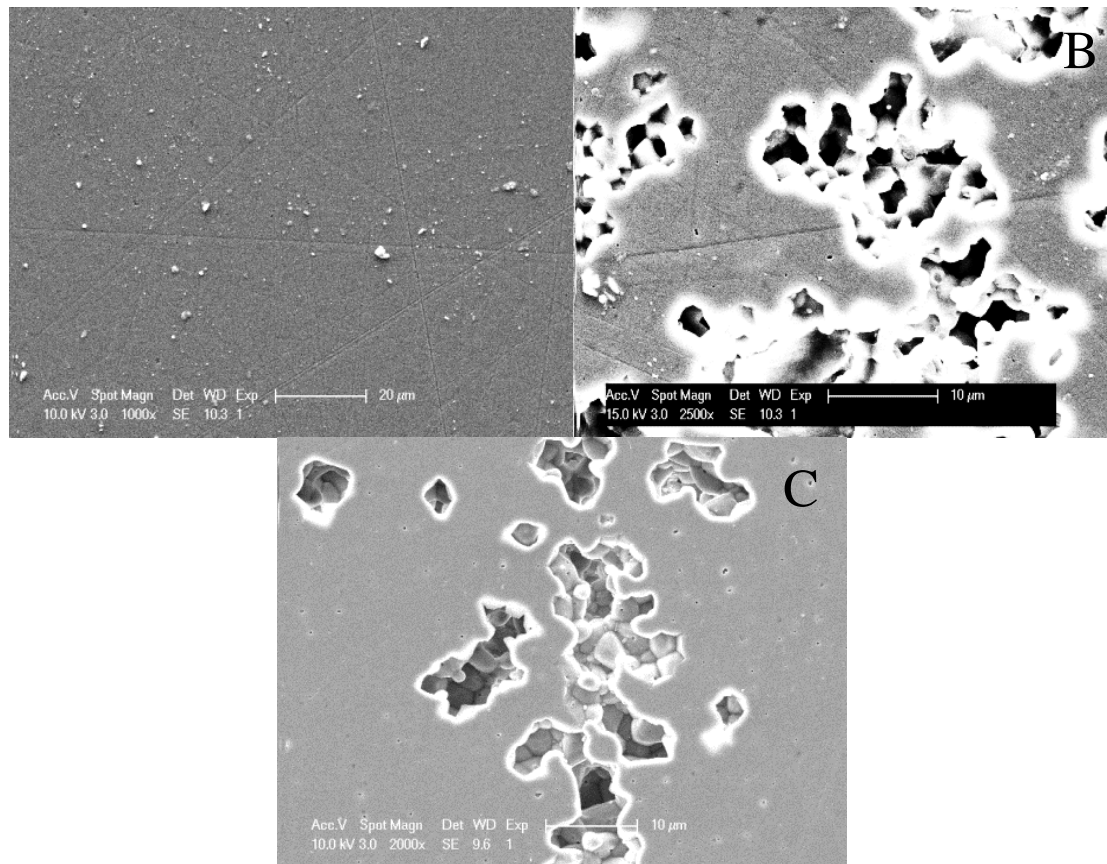


**Figure 6.14.** 1 day microscopy for pellet surfaces (a) HA pellet, (B) 1M  $\text{Ca}^{2+}$  solution infiltrated HA pellet, (c) 2M  $\text{Ca}^{2+}$  solution infiltrated HA pellet

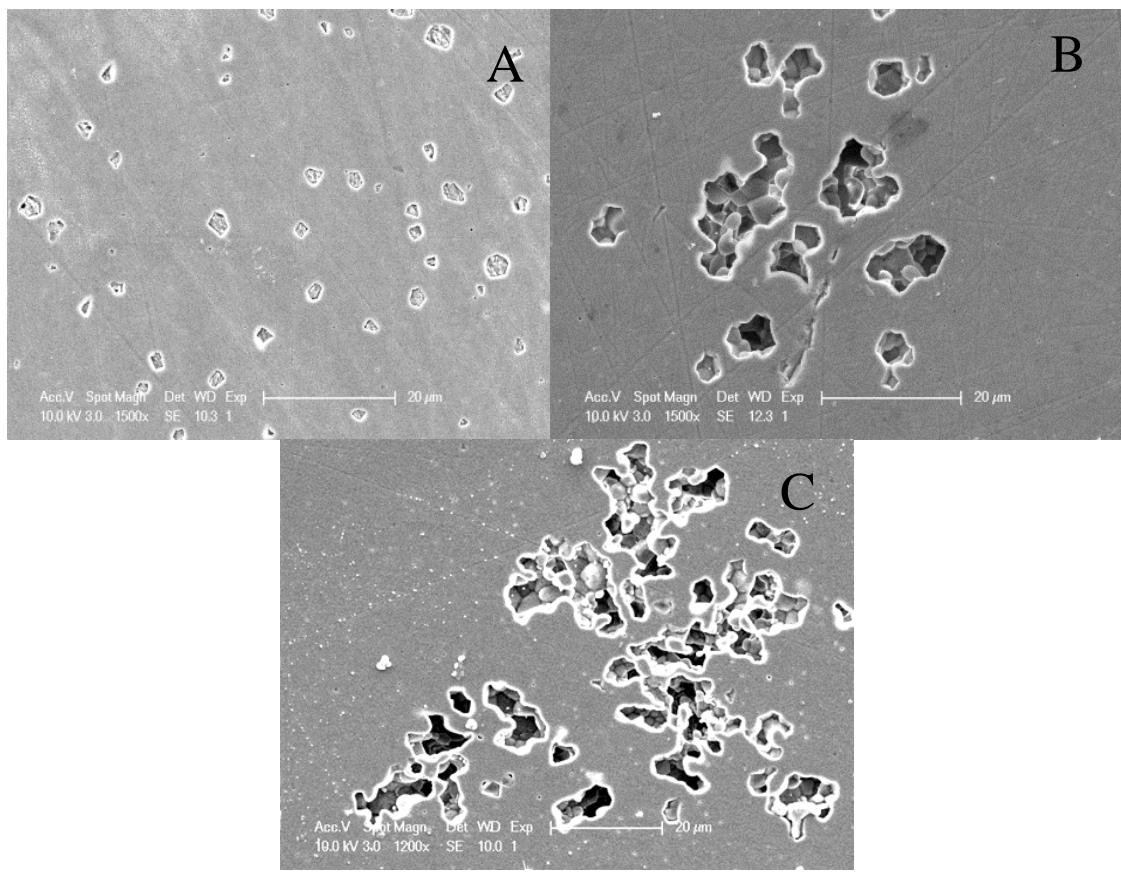


**Figure 6.15.** 3 day microscopy for pellet surfaces (a) HA pellet, (B) 1M  $\text{Ca}^{2+}$  solution infiltrated HA pellet, (c) 2M  $\text{Ca}^{2+}$  solution infiltrated HA pellet

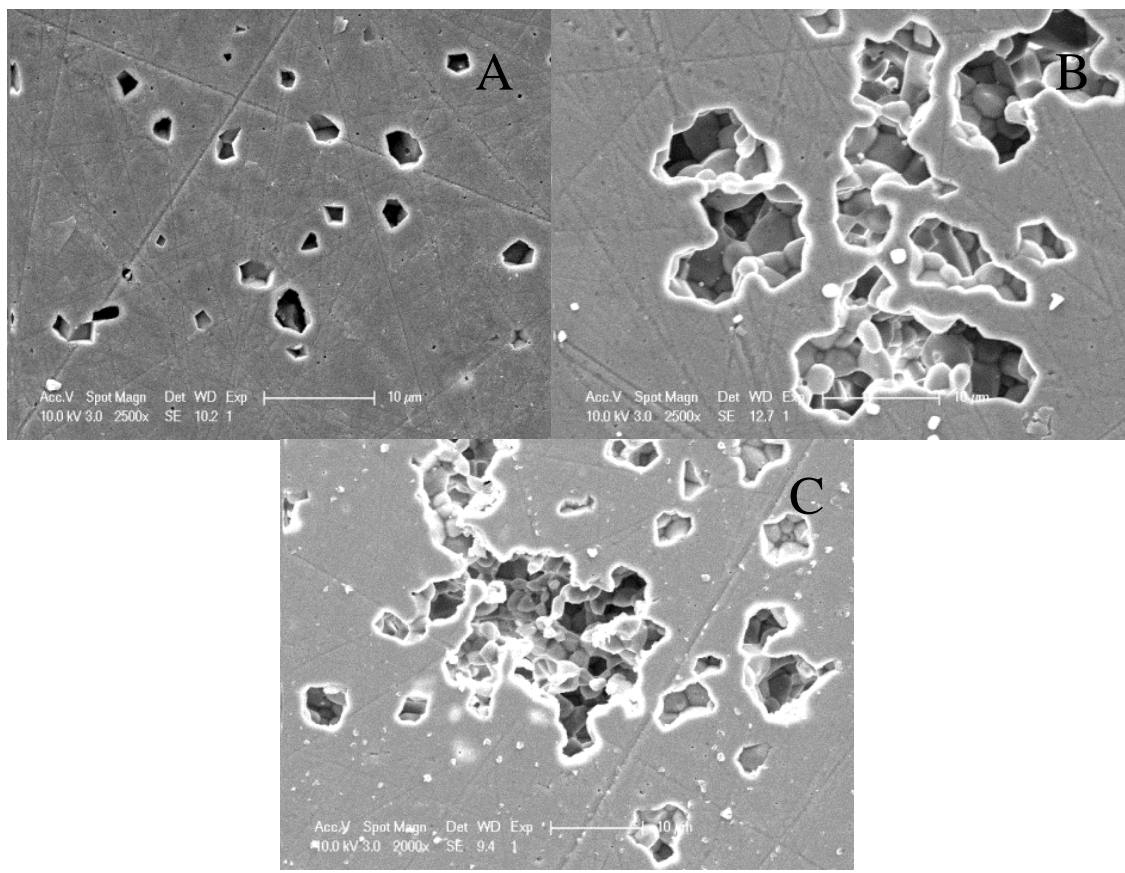


**Figure 6.16.** 7 day microscopy for pellet surfaces (a) HA pellet, (B) 1M  $\text{Ca}^{2+}$  solution infiltrated HA pellet, (c) 2M  $\text{Ca}^{2+}$  solution infiltrated HA pellet

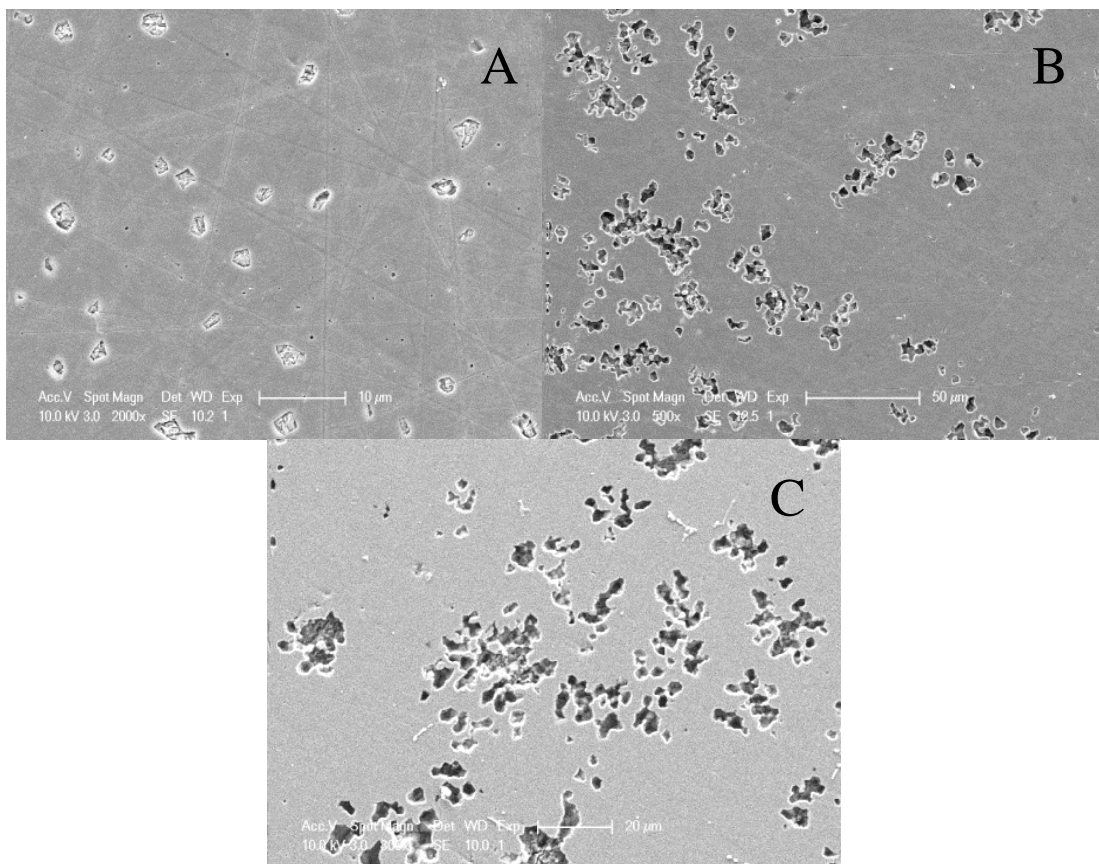


**Figure 6.17.** 14 day microscopy for pellet surfaces (a) HA pellet, (B) 1M Ca<sup>2+</sup> solution infiltrated HA pellet, (c) 2M Ca<sup>2+</sup> solution infiltrated HA pellet

The same trend in deepening of the defects appeared to continue at the next three time-points, Day 7, Day 14 and Day 28, as seen in Figure 6.16, 6.17 and 6.18. More and more HA grains were removed on the infiltrated pellets at the preexisting defect positions while defects continued to coalesce. Comparing the two Ca solution infiltrated pellet conditions, defects on 2M infiltrated pellets were more severe than the defects on 1M solution infiltrated pellets. The center of defects on the 1M solution infiltrated pellet was removed and created a quiet deep pit, as seen in the Figure 6.18(B). Figure 6.18, shows three large defects and the solid between them has been mostly removed. The three defects are connecting with each other, and the boundary between two of them had already been removed.

From the microscopy, it is found that the degradation of the ceramic is enhanced due to the presence of the second phase, which results not only in removal of a soluble phase but also in the fragmentation of adjacent HA.

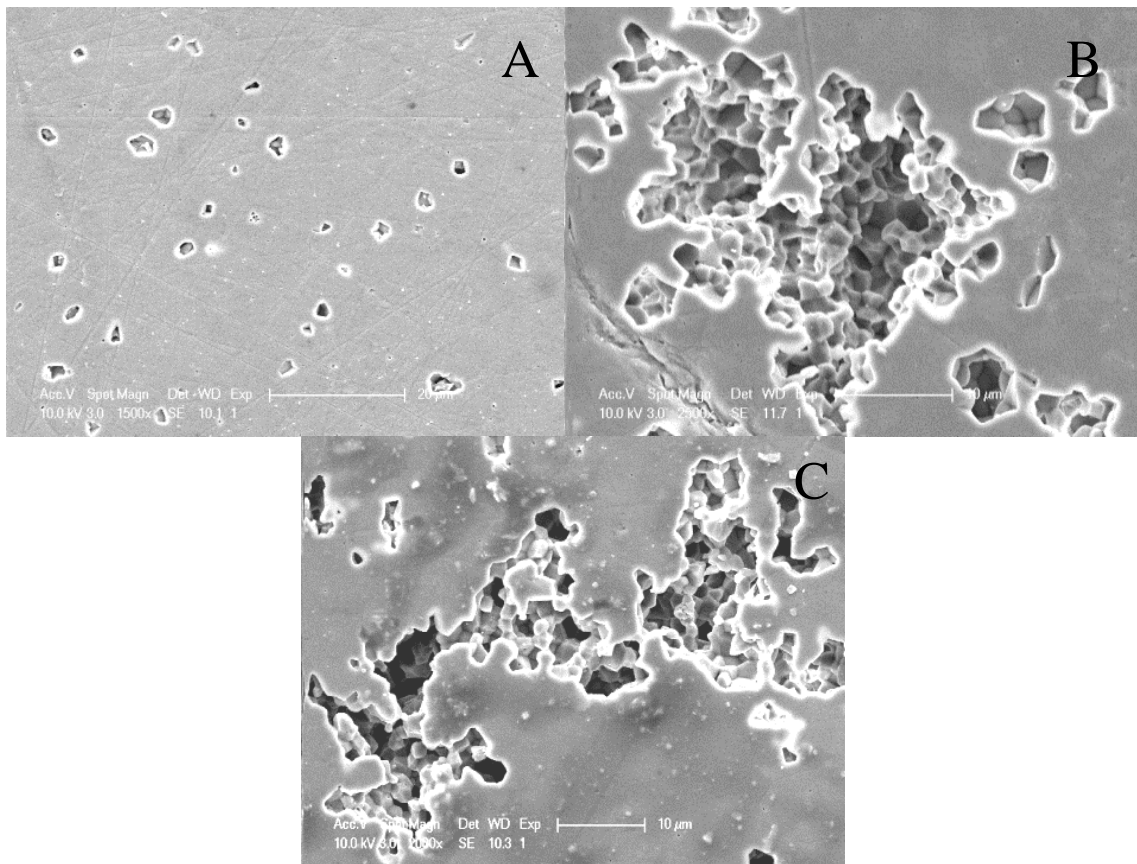


**Figure 6.18.** 28 day microscopy for pellet surfaces (a) HA pellet, (B) 1M  $\text{Ca}^{2+}$  solution infiltrated HA pellet, (c) 2M  $\text{Ca}^{2+}$  solution infiltrated HA pellet

Figure 6.18(A) shows that the pits in the HA were much smaller than those on the infiltrated samples. The size distribution of the pits was measured on the polished surfaces close to the sintered surface using image analysis. Significant differences were observed over the 4 weeks in saline. The size distribution of the defects on the pure HA pellets changed little by comparison with the distributions found on the infiltrated samples. For the HA control condition, the pits did not appear until the third day. Then, a size distribution with a single mode of

equivalent sphere size 1- 1.4  $\mu\text{m}$  was found .From Day 3 to Week 4 the pit area fraction on the HA samples only grew from 2.3 ( $+/-0.5\%$ ) to 2.4 ( $+/-0.5\%$ ). Figure 6.19 shows pit distribution on HA pellets for 4 different time points over a 4 week period. The size distribution is an order of magnitude smaller in size (0.8  $\mu\text{m}$  to 3.6  $\mu\text{m}$ ) and does not have the multimodal character of the pits on the surface of the infiltrated pellets. There is some evidence that the mode does increase slightly during 4 weeks of soaking. But they remain smaller than the HA grain size measured on the etched surface (Figure 6.19).

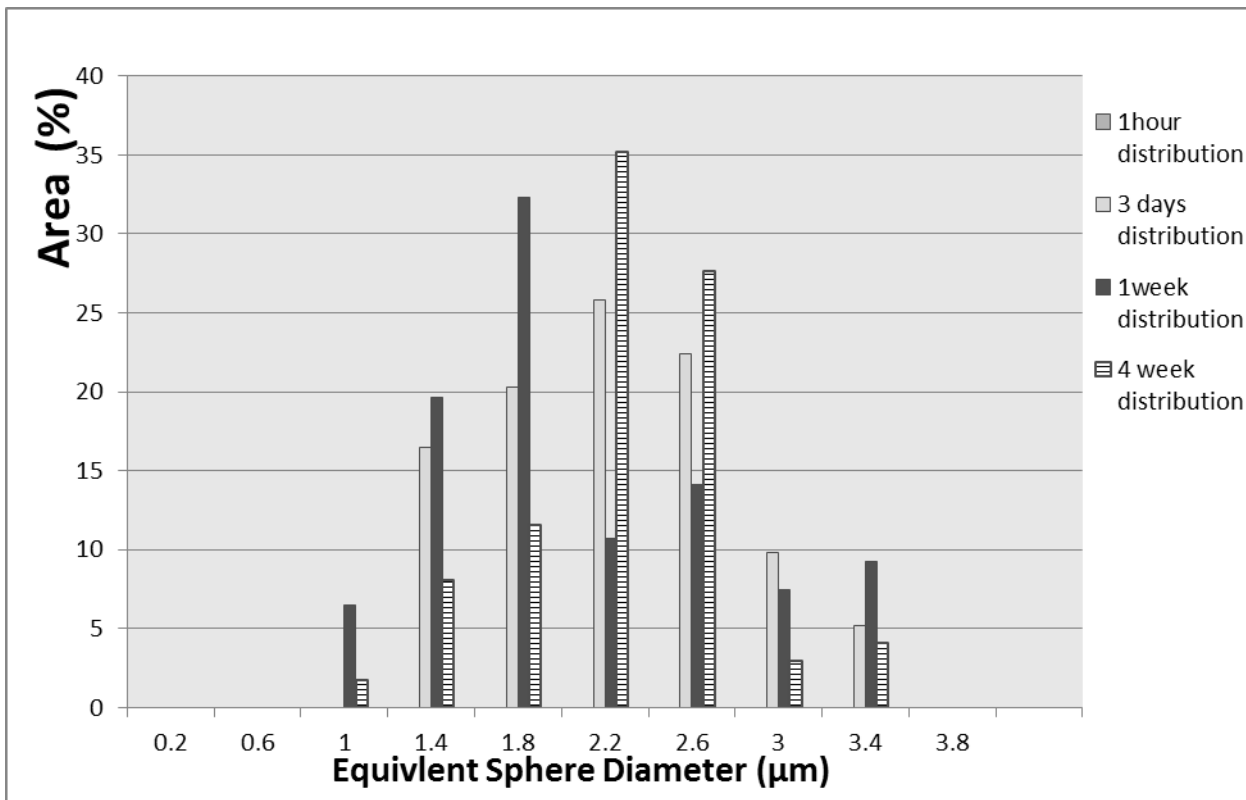


**Figure 6.19.** The defect distribution on HA pellet surface

For the 1M infiltrated pellets, the defect area fraction increased significantly from 22.6% after 1 hour and 23.1 % 3 hours, to 24.2% after 1 week and finally to 29.4% after 4 weeks. Figure 6.20 shows the distributions of pit size for the 1M infiltrated HA pellets. This figure

shows distributions for 4 time points from 1 hour to 4 weeks. Clearly, the distributions are multimodal and new modes appear at larger pore sizes at the longer soak times. The distinct multimodal distributions are thought to be due to the effect of the HA grain size on the pit coarsening mechanism.

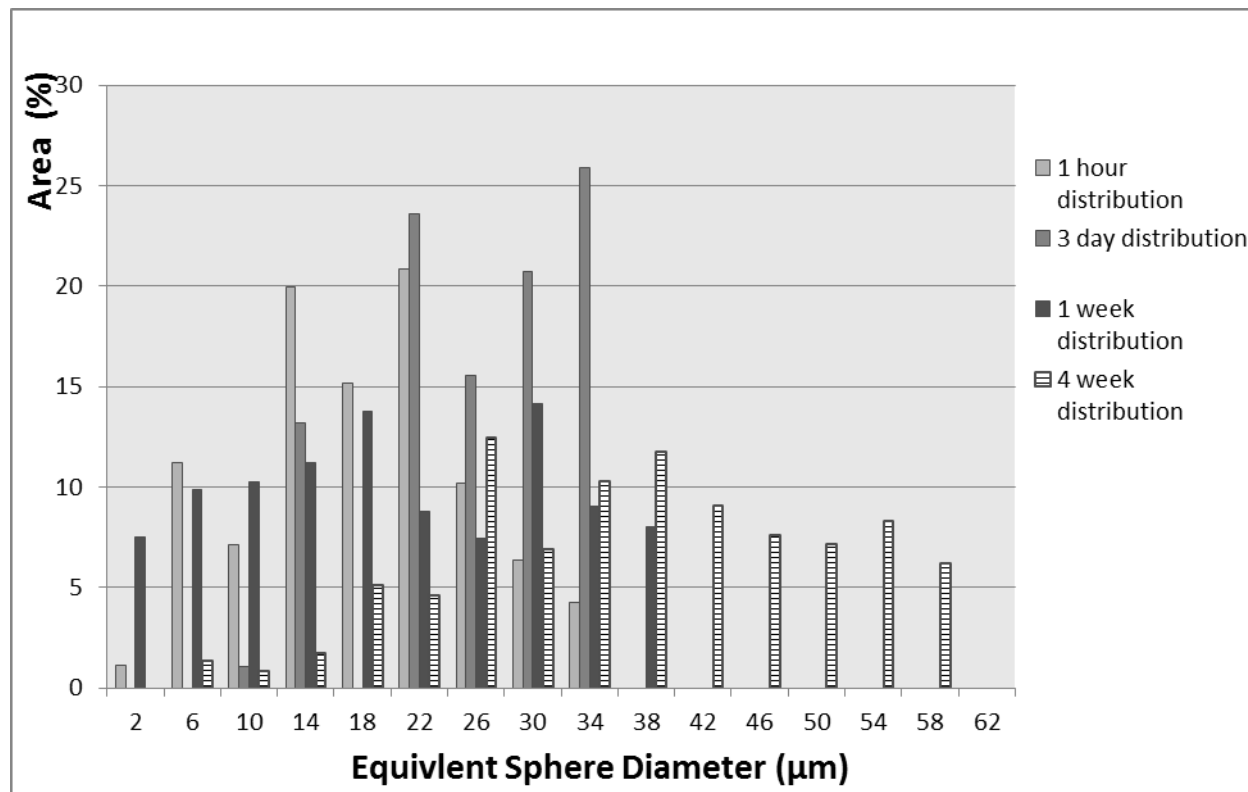


**Figure 6.20.** The defect distribution on 1M infiltrated HA pellets

Compared with 1M infiltrated pellets; the 2M infiltrated pellets showed the same trend in defect area fraction during the solubility experiment. The defect area fraction increased significantly from 18.8% after 1 hour and 20.1 % at 3 hours, to 24.2% after 1 week and finally to 30.1 % after 4 weeks. Figure 6.21 shows the distributions of defect size for the 2M infiltrated HA pellets. This figure shows distributions for 4 time points from 1 hour to 4 weeks. Comparing with 1M infiltrated HA pellets, the 2M infiltrated HA pellets had higher percentages of defects in

the size range from 6 to 18 $\mu\text{m}$  at short-term solubility test, 1hour and 3days. However, in the long term, 2M infiltrated pellets and 1M infiltrated pellets had similar multimodal distributions.

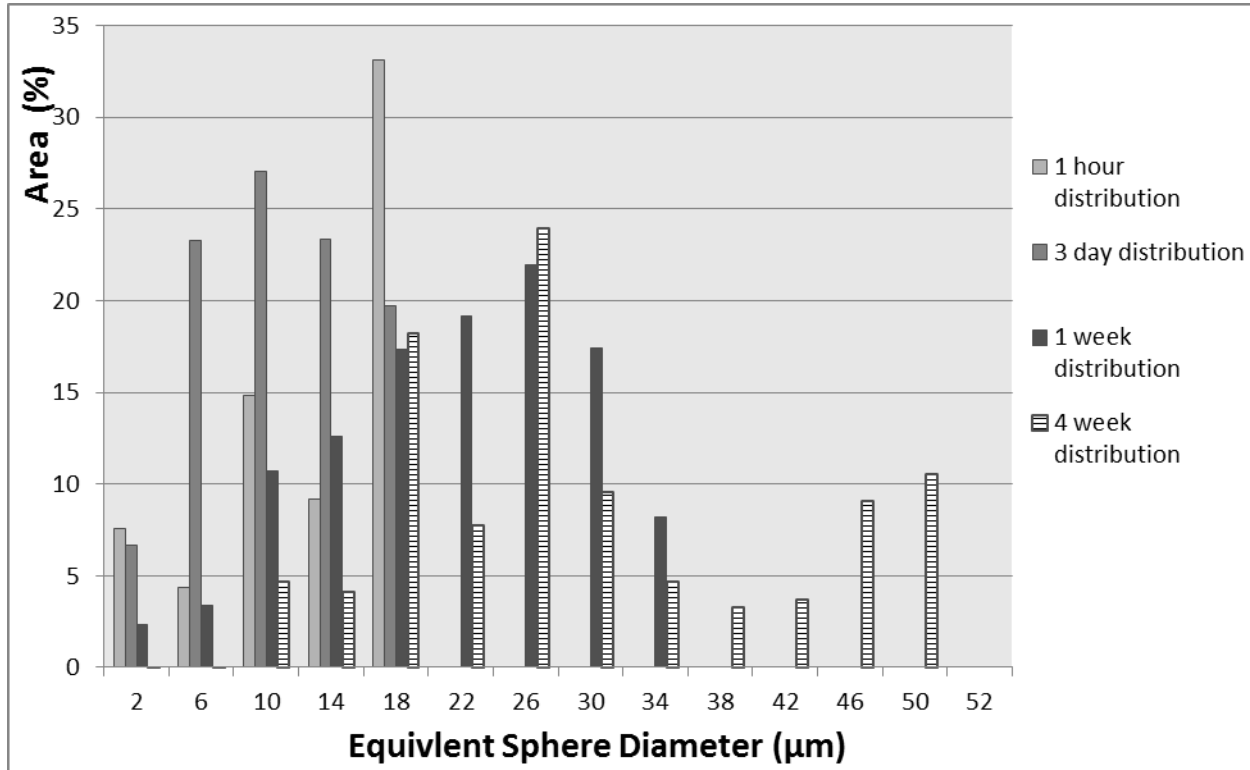


**Figure 6.21.** The defect distribution on 2M infiltrated HA pellets

As the soak time increased from 1 hour to 4 weeks the major mode in defect size grew from 14 (1M infiltrated HA) or 18(2M infiltrated HA)  $\mu\text{m}$  to 26  $\mu\text{m}$  and other modes appeared at larger equivalent sphere diameters after 4 weeks. This is thought to be a result of the degradation mechanism in which CaO grains in contact with saline on the surface transformed to  $\text{CaCO}_3$  and the resulting volume expansion caused cracking that removed adjacent HA grains and so the coarsening of the pits occurred in a discontinuous fashion by fragmentation events that removed whole HA grains or small groups of HA grains from preexisting defects and thereby exposed subsurface CaO grains to moisture which consequently transformed and led to other fragmentation events that deepened the defects and released more calcium ions..

The number of defects per unit area was also determined from the thresholded images. Figure 6.22 shows the plot of the number of defects/ unit area on the polished surface for the different degradation times. The numbers of pits per unit area on infiltrated HA pellets does not change significantly after 1 hour and for pure HA after 3 hours the number of pits per unit area is relatively constant. Hence, new pit formation does not seem to be significant after the very short soak times. The number of pits per unit area on the infiltrated samples is also higher than for the HA control samples.

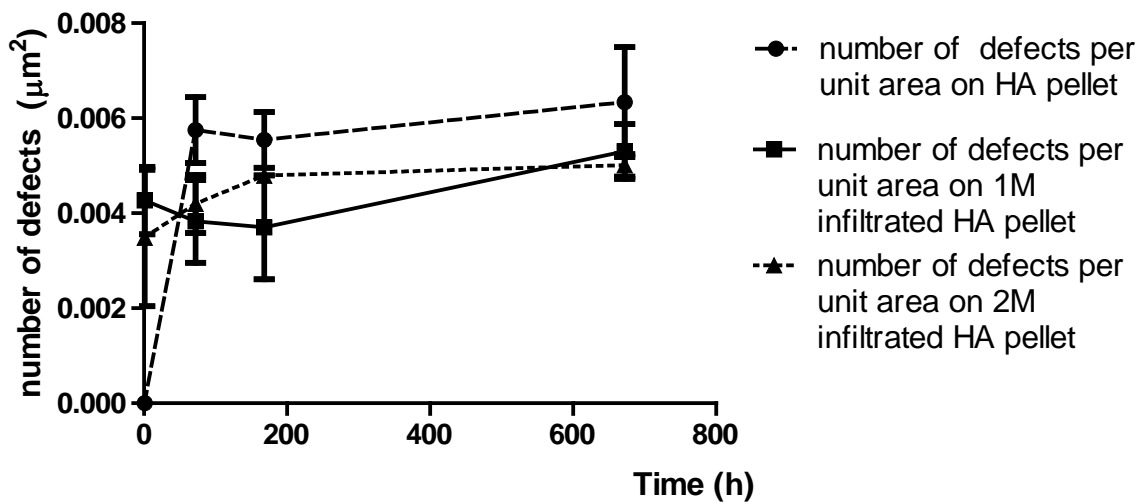


**Figure 6.22.** Number of defects/ unit area on the pellet surface

In summary, the area fraction of pits, the pit size and the depth of the pits increased on the surface of infiltrated pellets over 28 days due to the presence of CaO which not only dissolves rapidly but also transforms to  $\text{CaCO}_3$ . The volume increase on the transformation causes cracking of the HA grain boundaries and the enlargement of adjacent pits by the removal of HA grains by fragmentation. These grains are not thought to contribute much to the calcium content of the media but the exposure of new CaO grains by the fragmentation process leads to continued release of calcium into the media. This mechanism is reflected in the evolution of the

size distribution of the defects, particularly the appearance of new modes at larger defect sizes. Interestingly there is no further increase in the number of defects per unit area of the surface after the first hour and so the number of defects is mainly controlled by the initial transformation and dissolution of CaO grains on the surface. As the defects enlarge by fragmentation they must continue to produce new small satellite defect sections that intersect with the polished surface and then are merged with the adjacent larger pit at longer times. This would result in no significant change in the number of pits per unit area on the polished surfaces.

#### **6.1.4 Effect of the Infiltration on the Phase Distribution of Foams**

Figure 6.23 shows the x-ray diffraction patterns for the infiltrated foams. HA and CaCO<sub>3</sub> were present in the ground foam, which in the ground state represents the entire solid volume in the foam. The CaCO<sub>3</sub> standard peaks were labeled with stars in Figure 6.23 (B). It is apparent that HA is the main phase found in the ground powders. Fig 6.23 (A), shows the three main HA peaks were shown at 37.07°, 37.56° and 38.42° as in the standard HA pattern. Also, Figure 6.23 (B) also shows minor peaks at 33.91° and 42.12°, which belong to CaCO<sub>3</sub>. The CaCO<sub>3</sub> was formed after grinding by the reaction of the CaO second phase should with CO<sub>2</sub> in ambient conditions. The quantity of the CaCO<sub>3</sub> in the infiltrated foam was calculated to be approximately 3%, which like the pellets is quite a small amount when compared with the HA phase.

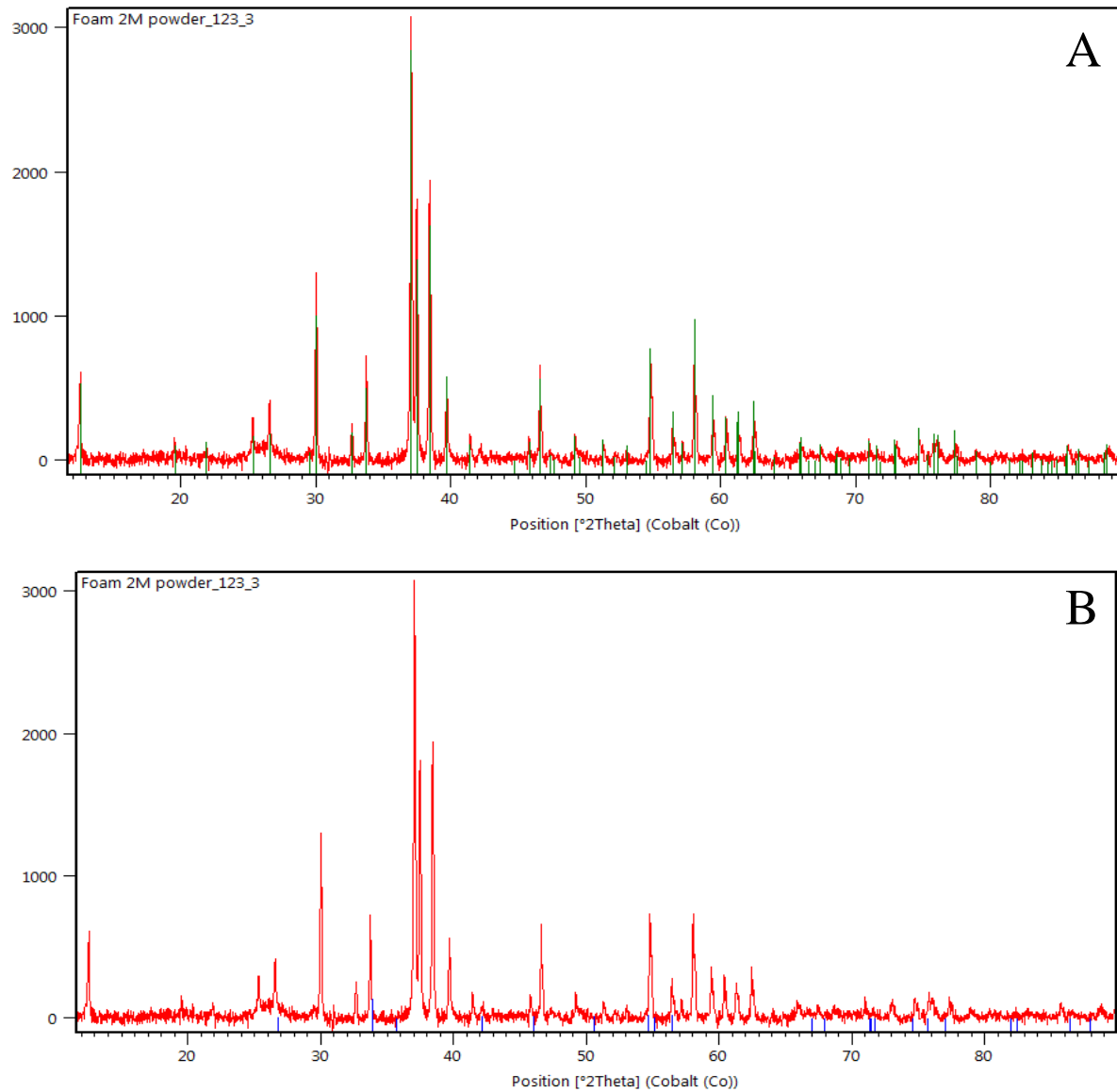


**Figure 6.23** X-ray diffraction patterns of (A) (B) ground foam

### 6.1.5 Infiltration of HA foams

In the pellet system, the CaO- HA biphasic system released  $\text{Ca}^{2+}$  into saline over 4 weeks and resulted in surface defects by dissolution and fragmentation. If these materials are to be used to culture HSC s in bioreactors, highly porous scaffolds are required. The dissolution behavior of the biphasic CaP ceramic should therefore be tested in this high porosity system, which has a

much higher surface area. As described previously, the pure HA scaffolds are used in the experiment as a negative control, with an infiltrated group made with 2mol/L  $\text{Ca}(\text{NO}_3)_2$  solution. By Micro-CT (Micro Photonics Inc., Allentown, PA), the open porosity of the scaffolds was measured at approximately 87% with total porosity 90% showing that the majority of the porosity is open. The solubility of the scaffolds was tested in static condition, as described in the experimental procedures section.

The experiment shows significant differences in dissolution between the negative control and the  $\text{Ca}^{2+}$  solution infiltrated scaffolds. Figure 6.24 shows, the  $\text{Ca}^{2+}$  solution infiltrated scaffolds released more  $\text{Ca}^{2+}$  ions in the saline than the HA scaffolds. At 0.5 hour, the Ca concentration in the 2M infiltrated HA scaffold condition is about 0.3mmol/L while in the HA scaffold condition it is smaller than 0.04 mmol/L. The Ca concentrations in the saline did not increase significantly until day 3. There is a peak in  $\text{Ca}^{2+}$  in the saline at 72 hours for the 2M infiltrated scaffolds with Ca concentration at approximate1.5 mmol/L. From 1 week to 4 weeks, the  $\text{Ca}^{2+}$  concentrations in the 2M infiltrated HA scaffold condition increased but not significantly. For the HA scaffold condition, the Ca concentration increased to 0.1 mmol/L s at 1 week. During the next two time points, the Ca concentration plateaued in the Figure 6.24.

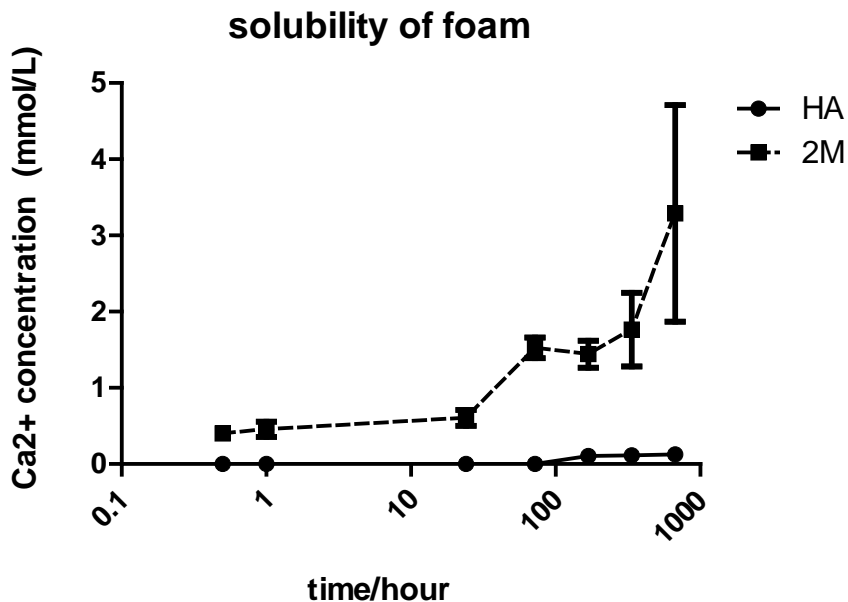


**Figure 6.24**  $\text{Ca}^{2+}$  ion concentration in the tris-buffered saline plotted as a function of time for static experiment.

In order to explain the trend in Ca release, the microstructure was observed by SEM. At the first two time points, 0.5 and 1 hour, There were defects on the surface of the infiltrated scaffold, while there is no defect observed on the HA scaffolds at these same time points. Interestingly, the defects (Figure 6.25) in the 2M infiltrated pellets were deeper than the defects on 2M Ca solution infiltrated pellets.

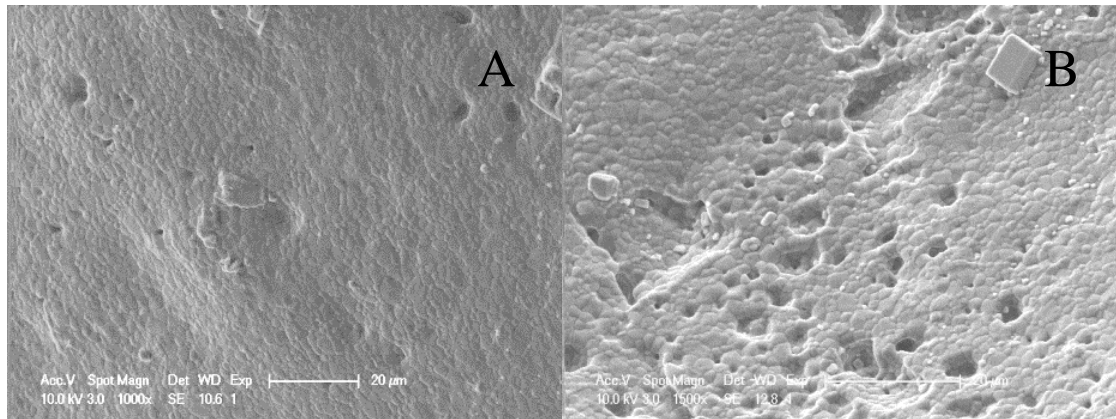


**Figure 6.25** 0.5 hour exposure for scaffold surfaces (A) HA, (B) 2M Ca<sup>2+</sup> solution infiltrated HA

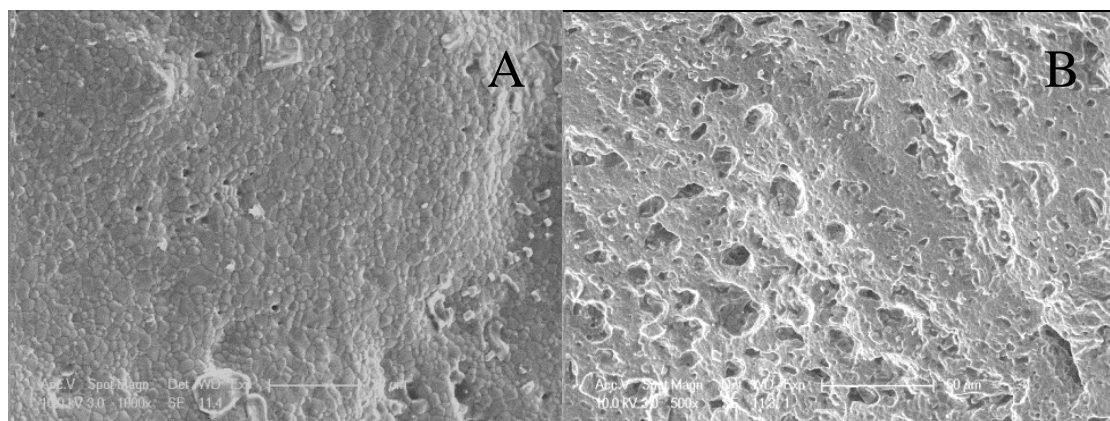


**Figure 6.26** 1 hour exposure for scaffold surfaces (A) HA, (B) 2M Ca<sup>2+</sup> solution infiltrated HA

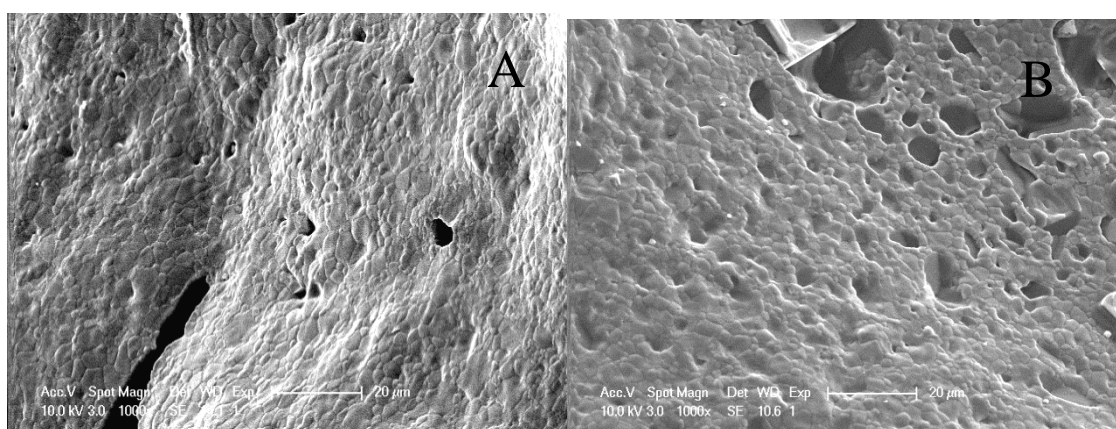


**Figure 6.27** 1 day exposure for scaffold surfaces (A) HA, (B) 2M Ca<sup>2+</sup> solution infiltrated HA

Figure 6.26 and Figure 6.27 shows there are no defects on the HA scaffolds surfaces, while the defects on the 2M infiltrated HA scaffolds surfaces became deeper and larger. From 1 day to 3 days, the defects began to connect with each other and more material has been removed. In consequence, the  $\text{Ca}^{2+}$  concentration in the saline increased significantly for the 2M n infiltrated HA in Figure 6.28.

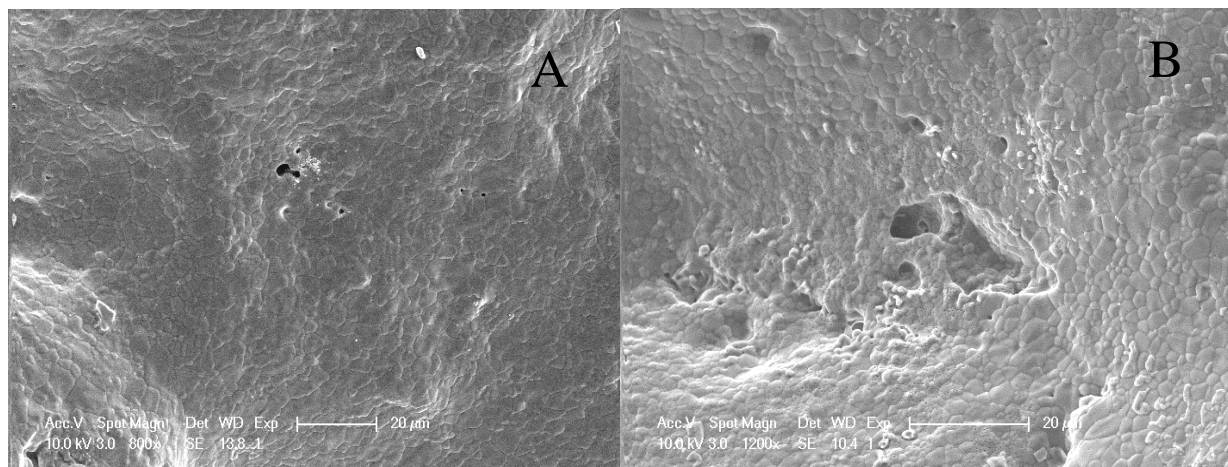


**Figure 6.28** 3 days exposure for scaffold surfaces (A) HA, (B) 2M  $\text{Ca}^{2+}$  solution infiltrated HA

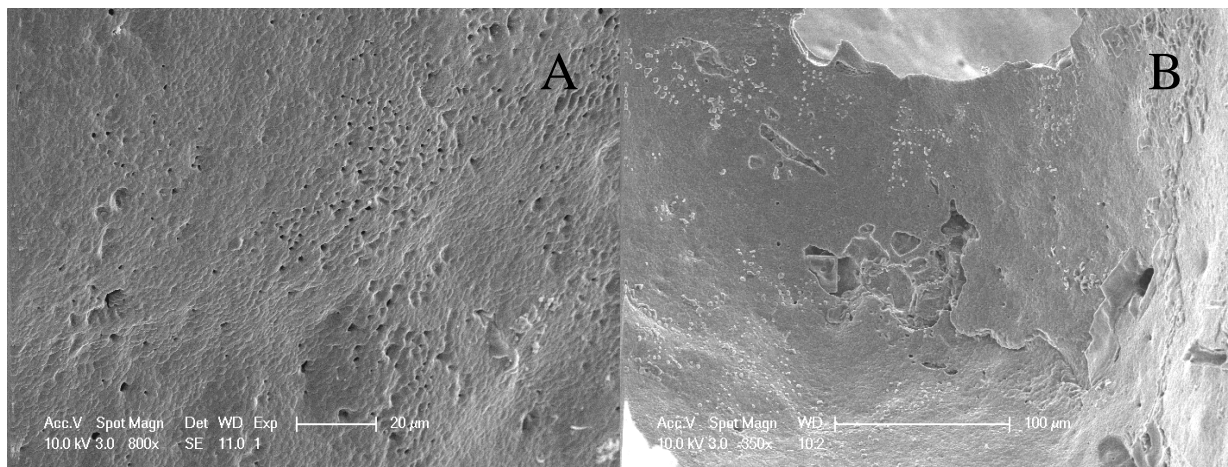


**Figure 6.29** 7 days exposure for scaffold surfaces (A) HA, (B) 2M  $\text{Ca}^{2+}$  solution infiltrated HA

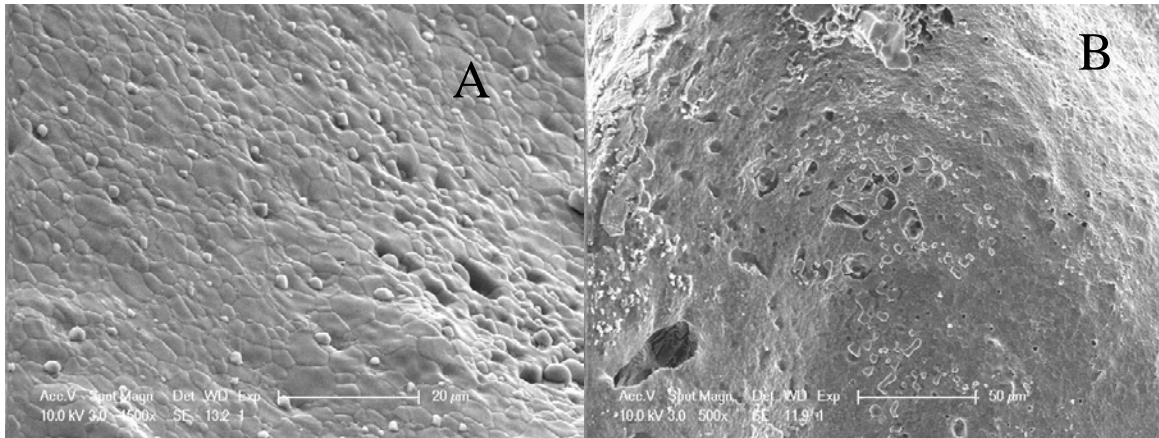


**Figure 6.30** 14 days exposure for scaffold surfaces (A) HA, (B) 2M  $\text{Ca}^{2+}$  solution infiltrated HA

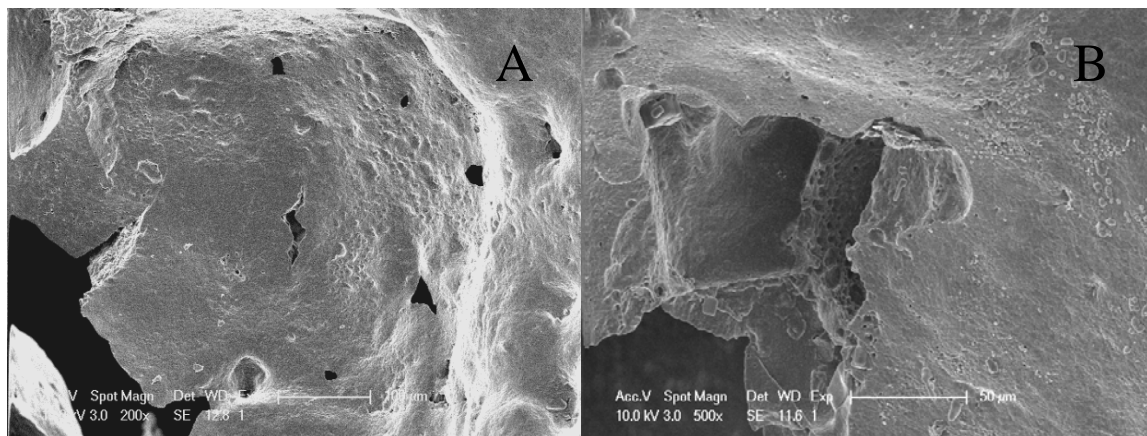


**Figure 6.31** 28 days exposure for scaffold surfaces (A) HA, (B) 2M  $\text{Ca}^{2+}$  solution infiltrated HA

From 7 days to 28 days, some defects were observed on the surfaces of the infiltrated HA scaffolds and became more numerous with increased soaking time. On the 2M infiltrated HA scaffolds, the defects became larger and made the scaffolds more fragile. Compared with the defects on HA scaffolds, the defects on the 2M infiltrated HA scaffolds showed many more defects (Figure 6.28(B)). In the Figure 6.31 (B), a piece of the scaffold was removed by the fragmentation. The increase in structural damage correlated with the enhanced  $\text{Ca}^{2+}$  concentration in the saline after 28 days for the 2M infiltrated HA scaffold.

In summary, the Ca-rich phase enhanced the  $\text{Ca}^{2+}$  ion concentration in the saline to much higher levels compared with the pellets and also resulted in defects that could be clearly observed on the scaffold surface.

## **6.2 HUMAN UMBILICAL VEIN ENDOTHELIAL CELLS CULTURING**

The first intended cell source for this study was a human umbilical vein endothelial cell line (HUVEC) which is commonly used as cell type that contains a large fraction of endothelial progenitors but no HSCs. Three biological repeats were applied to test the biocompatibility of the biphasic materials produced in this study. The endothelial cells are the cells that form the vessels in the human body and will be extremely important to the process of vascularization during tissue formation in vitro cell culture.

### **6.2.1 Genomic DNA data and Medium Analysis during Culture**

Three parallel repeats were studied for the HUVECs proliferation. In order to study the cell proliferation, genomic DNA was taken from harvested cells at each culture time point in all three repeats. The three different conditions used were: (A) the HUVECs cultured without any scaffold as a negative control, (B) the HUVECs cultured with HA scaffold, and (C) the HUVECs cultured with 2M Ca solution infiltrated HA scaffold. This will allow for the study of the effect of the scaffold and the effect of calcium concentration on the fate of the HUVEC cells. The cell number was calculated by measuring the total amount of DNA in each sample and comparing this number to the DNA from a known amount of cells.

As it is shown in the Figure 6.32, in the first 15 days, the cell numbers increased in all three conditions from 1E4 cells/well initially. From day 5 to day 15, there were changes in the cell numbers for three conditions. The increase for the no-scaffold condition was significant as well as for the infiltrated scaffold over the first 15 days in these samples in comparison there was a decrease in total cell number for the HA scaffold between day 5 and day 15. This general proliferation might be due to the cells becoming attached to the surface of culture wells or the scaffold and starting to proliferate. However, after 42 days, the number of cells significantly decreased in all conditions, which is not surprising for static culture where the cells do not proliferate after this length of time without passaging due to confluence and consequent cell depth. At all three time-points the results showed that the no-scaffold condition had the largest cell number. This might be because of the surface morphology difference between the material of the culture well and the scaffold. HUVECs are more likely to attach to the polystyrene surface of culture wells than to the ceramic surface of the HA scaffold. As mentioned previously, the decrease in the number of cells between day 15 and day 42 samples is expected if the cells are not proliferating. The life expectancy for HUVECs as 50 to 60 population doublings (population doublings refers to the times one cell is able to divide into two, and has nothing to do with the number of passages)<sup>159</sup>. With a certain life-time period, a cell cycle time of 19.9+-2.73 h for early passage HUVECs compared with 23.3+-1.32 h for late passage cells, the total life-time of most HUVECs is 30 to 38 days. The time period is shorter compared to our culture time, so the amount of cells would be expected to decrease drastically by 42 days, if there was no cell expansion or proliferation.

In order to prove this point, the glucose and lactate secretion was measured over the 42 days period and is shown in Figure 6.33(A) and (B). The glucose is a protein that cells would

consume for activity while the lactate would be secreted. If the cells are active, the glucose consumption rate and lactate secretion rate increase. On the other hand, the rate of glucose and lactate increase would be lower if the cells are in-active. For the glucose and lactate comparison, the two metabolic parameters are presented in terms of accumulation with linear regression linear applied. The regression lines were analyzed by one-way ANOVA test for statistical significance. In the comparison of accumulated glucose, the no-scaffold condition indicates that more glucose was consumed and more lactate secreted in the culturing than was consumed in the cultures containing HA and Infiltrated HA. In addition the glucose consumption and lactate secretion for the scaffold conditions appears to plateau between 20 and 30 days but not for the no-scaffold condition. But the difference between the rates of accumulation between the three conditions was not significant based on the ANOVA test. Also, it is obvious that the glucose consumptions of the HA and infiltrated HA conditions are similar while the amount of DNA in HA condition is smaller than the amount in infiltrated HA condition. The difference between the two results suggested that the cells in infiltrated HA were less active than HA condition but infiltrated HA scaffold could still maintain more HUVECs.

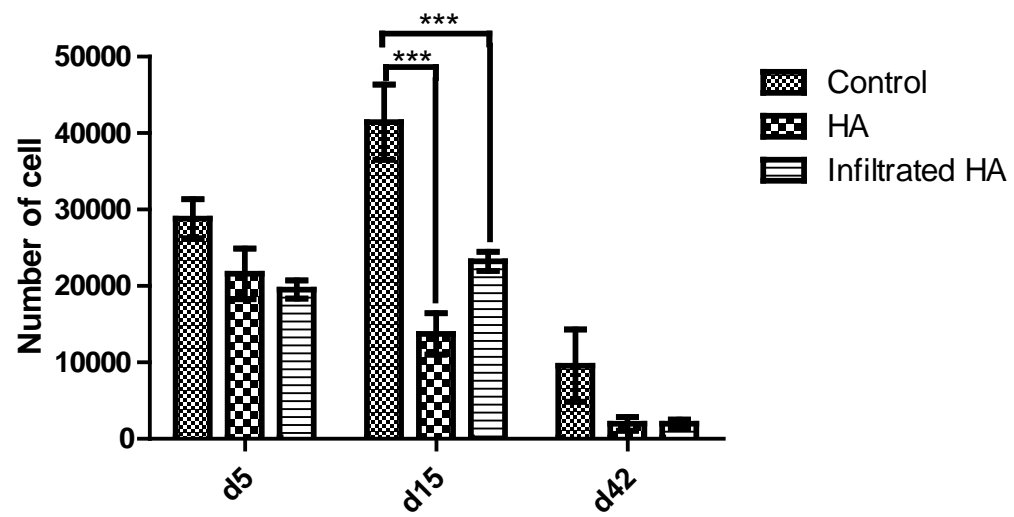


**Figure 6.32** DNA amounts of samples in 42 days

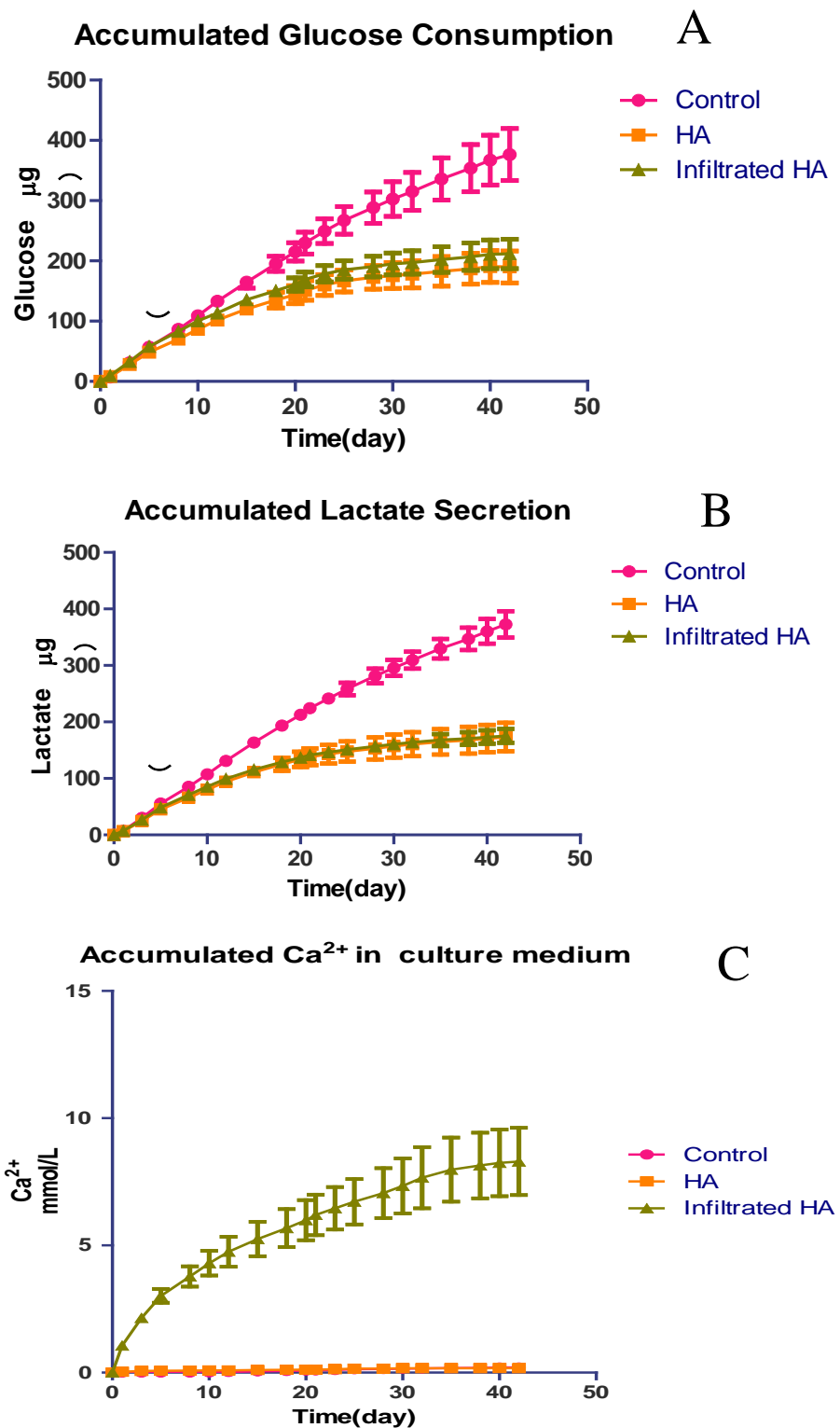


**Figure 6.33** Cumulated secretions and  $\text{Ca}^{2+}$  concentration in culture medium (A) accumulated glucose consumption (B) accumulated lactate consumption (C) accumulated  $\text{Ca}^{2+}$  concentration

Figure 6.33(C) shows that there was little difference between the calcium content of the culture over 42 days for the no scaffold condition and the condition with the HA scaffold. However, the calcium release from the 2M infiltrated sample increased continuously over the 42 days. This latter scaffold condition released more calcium than the pellets studied earlier because of the higher surface area. The Ca release occurred over a long period of time because of the fragmentation mechanism that continuously exposes new CaO, leading to the conversion to CaCO<sub>3</sub> and more release of Ca into solution and deepens the already existing defects. The gradient of decreasing CaO into the interior of the infiltrated samples would result in the observed decrease in Ca releasing rate at longer times due to fewer fragmentation events. Note that at all time points the calcium concentration in the media was below levels considered toxic to cells. The calcium concentration limit is 3mM for general extracellular concentration<sup>160</sup> while it could up to 40mmol/L in bone marrow<sup>18</sup>.

### **6.2.2 Real Time Polymerase Chain Reaction (RT-PCR)**

In order to exam the gene expression and give insight into the cell development in the culture, real-time PCR was applied to the samples. The statistics from the estimates of gene expression are divided by the number of cells and are normalized to the gene level of each marker in day 0. In this experiment, six genes were examined: vWF, CD144, CD31, CD34, KI-67 and Ang-1. Among those, vWF, CD144, CD31, CD34 represent different stages in the lineage of endothelial cells derived from HUVECs. The KI-67 is the marker for any cells in a proliferative stage, and Ang-1 is the marker for cell-matrix attachment protein expression, which will activate Tie-2 receptor on the HSCs and promote tight adhesion of HSCs to their niches if HSCs can develop from the HUVECs since both show hemangioblast character suggesting they are both related by

an early progenitor. As the PCR result is an average level of the gene marker expression inside the cells, the same level of a gene marker expression might indicates a gene was expressing inside a large amount of cells at a lower level or by a small number of cells at a higher level. So while PCR can be used to examine the development of HUVEC into other types of cells during culture it cannot be directly related to cell number. The results are shown in Figure 6.34.

For CD 144 and CD 31, the two immature endothelial cell markers, the gene expression increased between day 0 and day 5. , the no-scaffold condition expressed the highest levels of both gene markers at day 5. But these differences were not significant. There is also no significant difference between the HA foam condition and the Infiltrated HA foam condition for these two gene markers. Also, the expression levels of the two gene markers are almost the same for the Day5 and Day 42 samples.

For CD34, a marker shared by immature endothelial cells and HSCs, the level of expression increased a great deal between day 5 and day 42. For the Day 5 samples, the no scaffold condition expressed more than infiltrated HA foam condition while the infiltrated HA foam culture expressed higher amounts of CD34 than the HA foam condition. Between the groups, the differences were significant. After 42 days, the no-scaffold condition still expressed the most but the HA foam condition now expressed higher amounts than infiltrated HA foam condition. Again the differences between the groups were significant.

vWF is a gene marker for mature endothelial cells. Expression of vWF increased over the 42 days of culturing. At Day 5, the no-scaffold condition expressed significantly more vWF marker than HA foam condition and infiltrated HA foam condition). After 42 days, HUVECs cultured with the scaffolds expressed more vWF than the no scaffold condition. The expression of vWF was 2-3 times more than at the day 5 time points. This shows that the surface of the HA scaffold is the best condition examined to expand HUVECS into mature endothelial cells and serves

as an incentive to study the use of HA scaffolds to promote the formation of vascular-like channels using HUVECs. As discussed in section 2.3.5, Ca ion channels play an important role in endothelial cell growth and subsequent vascularization<sup>161</sup>. The resorption/dissolution and the release of Ca ions from the scaffold material might create a microenvironment near the surface of the HA that is rich in these ions. Such calcium ions might contribute to the maintenance of endothelial cells and also the formation of vascular tissue by passing through channels on the surface of these cells to trigger these events.

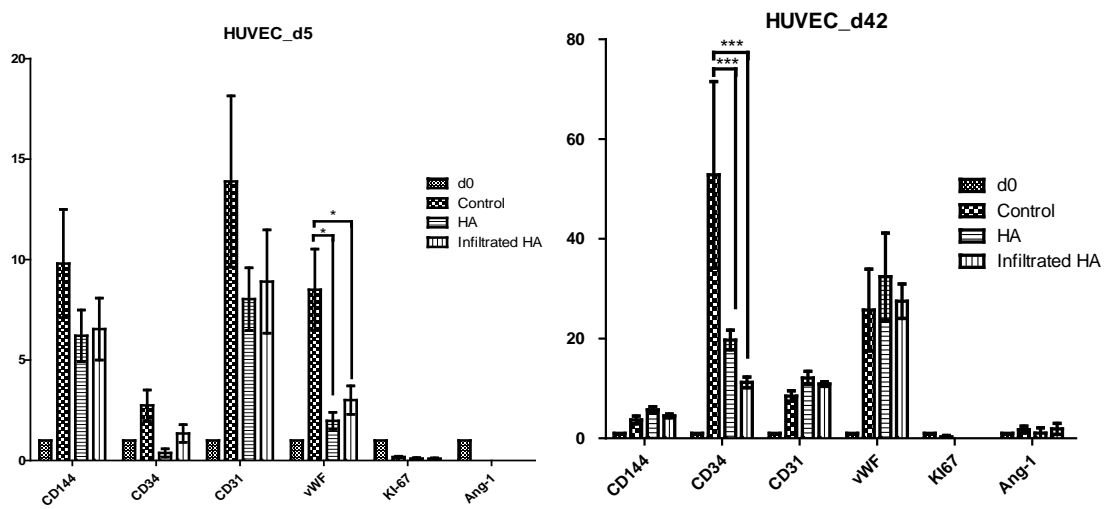


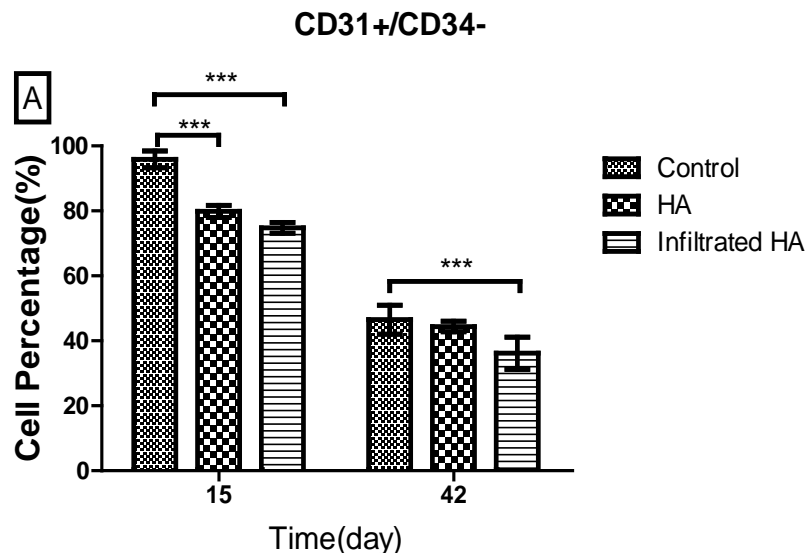
**Figure 6.34** Gene expression data for HUVECs normalized to day 0 cells (\*\*\*(p<0.001, \*\*p < 0.01, \*p < 0.05)

According to the RT-PCR results, there is no significant difference between the three conditions for KI-67 and Ang-1 marker. Also, the KI-67 and Ang-1 marker expression levels are quite low, which indicates that angiogenesis was not active in the HUVEC culture.

### 6.2.3 Fluorescence Activated Cell Sorting (FACs)

In order to isolate the fraction of the cell population that had certain cell character during culture, Fluorescence Activated Cell sorting (FACs) was used. Since PCR showed an increase in CD34 expression and the fact that this marker is expressed by endothelial progenitors and HSCs, it was decided to use cell marker CD45, which is used to detect mature hematopoietic cells to see if the culture could guide HUVECs to differentiate down the hematopoietic cell line. In FACs, the percentages of HUVECs were analyzed at 2 time points, Day 15 and Day 42. The markers used in FACs included: CD 235a+ for erythrocytes, CD45<sup>+</sup> for mature hematopoietic cells, Lin+ for mature hematopoietic lineage cells, including lymphocytes, T-cells, B-cells, granulocytes, and macrophages; CD34<sup>-</sup>/CD31<sup>+</sup> for endothelial progenitors, and Lin<sup>-</sup>, CD34<sup>+</sup>, CD38<sup>+</sup> for hematopoietic stem cells.

The CD34 and CD31 makers' combination could present several type of cell, including CD31<sup>-</sup>CD34<sup>+</sup> for hematopoietic progenitor cells, CD31<sup>+</sup> CD34<sup>+</sup> for endothelial progenitor cells, and CD31<sup>+</sup>CD34<sup>-</sup> for more mature endothelial cells.



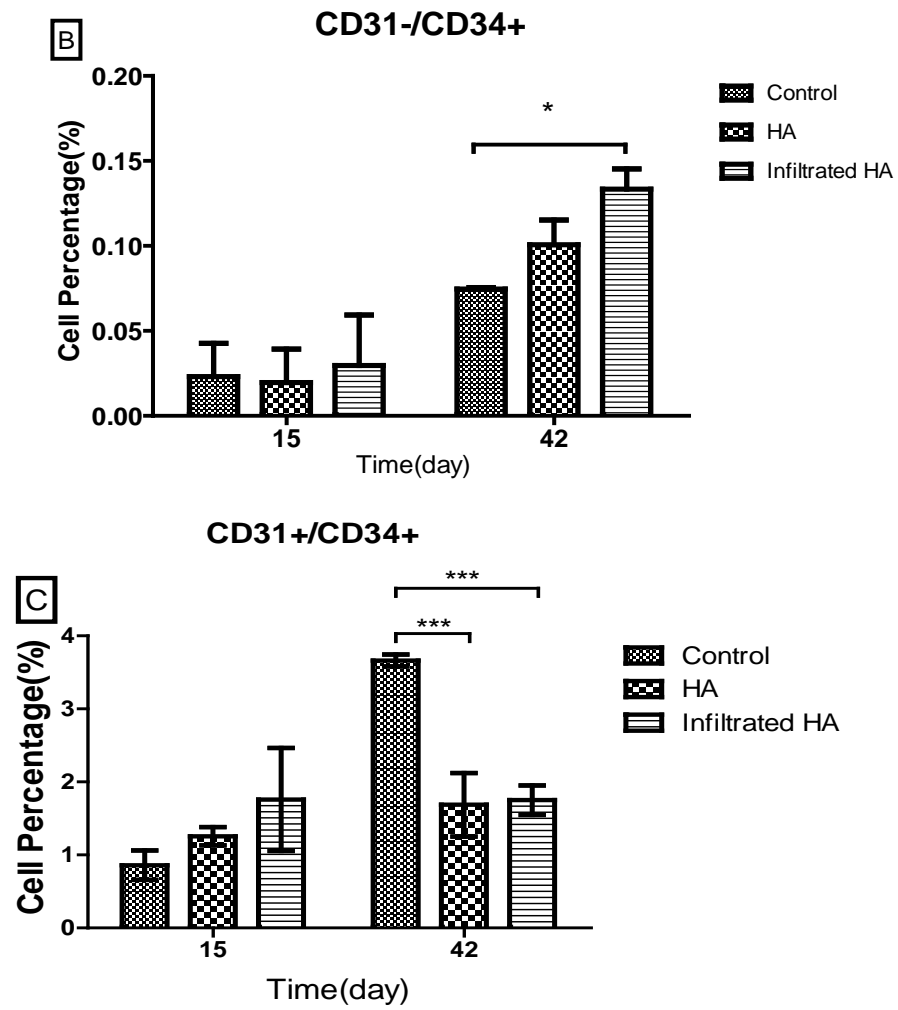


**Figure 6.35** (A) more mature endothelial cell percentages, (B) hematopoietic progenitor cell percentages, and (C) endothelial progenitor cell percentages for three conditions at Day 15 and Day 42 (\*\*p<0.001, \*\*p < 0.01, \*p < 0.05)

For the more mature endothelial cells in the HUVEC population, figure 6.35(A) shows that at day 15 most of the HUVC cells are indeed more mature endothelial cells and there are significant differences between the conditions at Day 15 and Day42. At day 15, the fraction of CD31<sup>+</sup>CD34<sup>-</sup> cells for the no-scaffold condition is significantly higher than for the infiltrated HA condition and the HA condition. For the long-term culture, day 42 shows that the fraction of CD31<sup>+</sup>CD34<sup>-</sup> cells decrease between day 5 and day 42 for all scaffold conditions and they are

now less than 50% of the cells present. The fraction in the no-scaffold condition was still significantly higher than the fraction of CD31<sup>+</sup>CD34<sup>-</sup> cells in the infiltrated HA condition. Figure 6.35 (B) shows the very small fractions of hematopoietic progenitors (CD31<sup>-</sup>CD34<sup>+</sup>) in the samples, these fractions increased for all the scaffold conditions from day 15 to day 42 and the infiltrated HA condition gained a significant higher fraction of these cells than the no-scaffold condition at day 42 while no significance appeared at day 15. From Figure 6.35 (C) endothelial cell progenitor (CD31<sup>+</sup> CD34<sup>+</sup>) percentages were also quite small but not as small as for the (CD31<sup>-</sup>CD34<sup>+</sup>) cells. Again the fraction of these cells increased between 15 days and 42 days. The no-scaffold condition is significantly higher than the HA condition and the infiltrated HA condition after 42 days culture. In Figure 6.35 (B) and (C), significant differences are obtained at day 42, while there are significances for mature endothelial cells at both time points.

Figure 6.36 (A) shows that the percentages of HSCs (Lin<sup>-</sup>CD34<sup>+</sup>CD38<sup>-</sup>) cells were between 0.5% and 2% after 15 days but increased to between 2% to 5% after 42 days suggesting that the fraction of HSCs derived from HUVEC cells were increasing in long term culture. The scaffold conditions gave higher percentages than the no-scaffold condition after 15 days and the percentage for the infiltrated HA is significantly higher than the no-scaffold condition at this time point. After 42 days (Figure 6.36B) the fraction of Lin<sup>-</sup>CD34<sup>+</sup>CD38<sup>-</sup> increased in all three conditions although the trends seen at 15 days were now reversed with the no-scaffold condition showing the highest fraction.

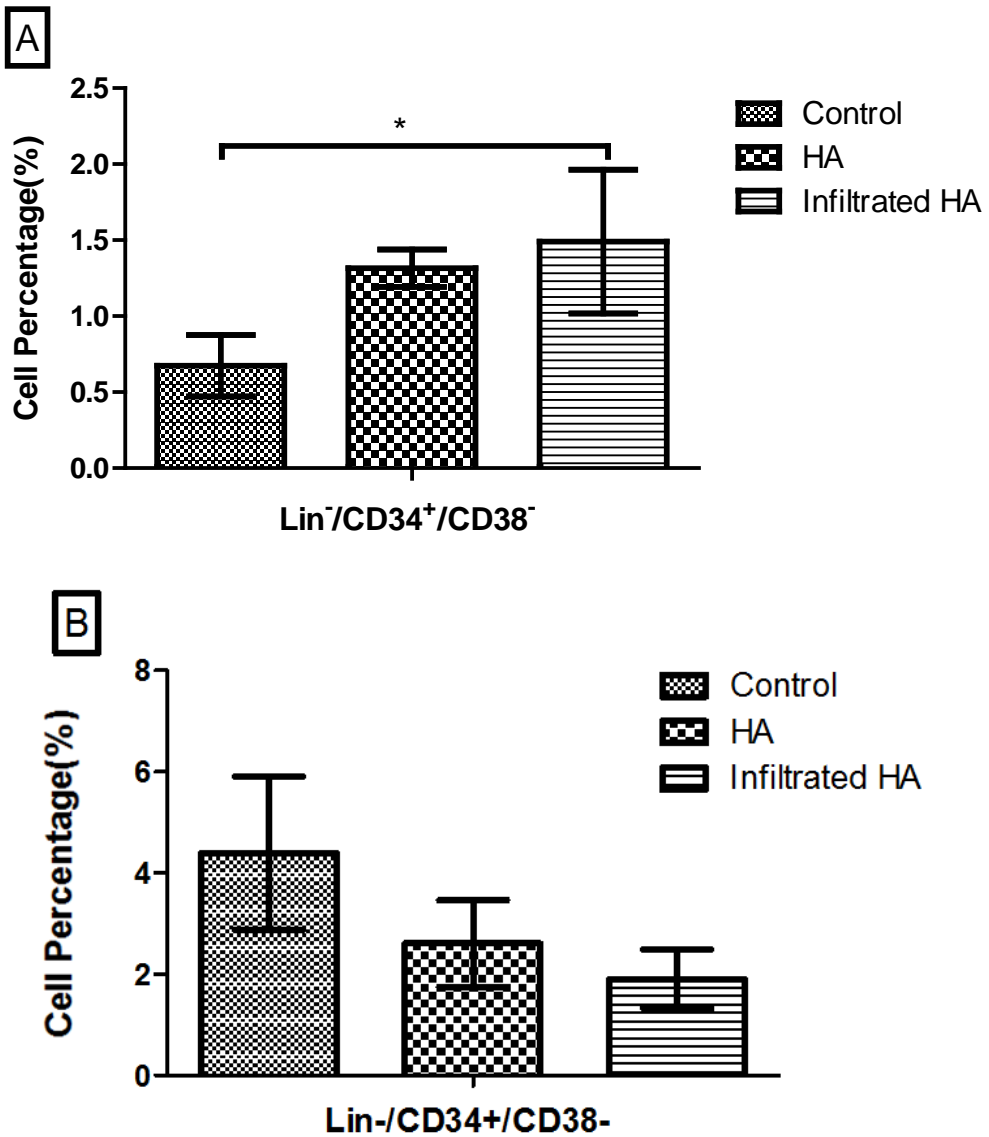


**Figure 6.36** Hematopoietic stem cell percentages for three conditions at (A) Day 15, and (B) Day 42

Significant differences were showed (\* $p < 0.05$ )

For the hematopoietic cell markers, Figure 6.37 (A) showed that the cell percentages expressing CD235a and Lin tended to increase from the no-scaffold to the HA scaffold condition and were the highest for the infiltrated scaffold condition after 15 days. Also the fraction of  $\text{CD235}^+$  cells increased noticeably for all scaffold conditions between day 15 and day 42. There was significantly more  $\text{Lin}^+$  for the infiltrated HA scaffold compared to the control condition at

day 15. These trends continued to develop and by 42 days and the expression for the infiltrated HA scaffold condition was significantly higher than the no-scaffold condition for all hematopoietic markers including: Lin<sup>+</sup>, CD45<sup>+</sup> and CD235a<sup>+</sup> (Figure 6.37B). Also, at Day 42, the expression for the infiltrated HA scaffold condition was significantly higher than the HA scaffold condition for the CD45<sup>+</sup>, the mature hematopoietic cell marker.

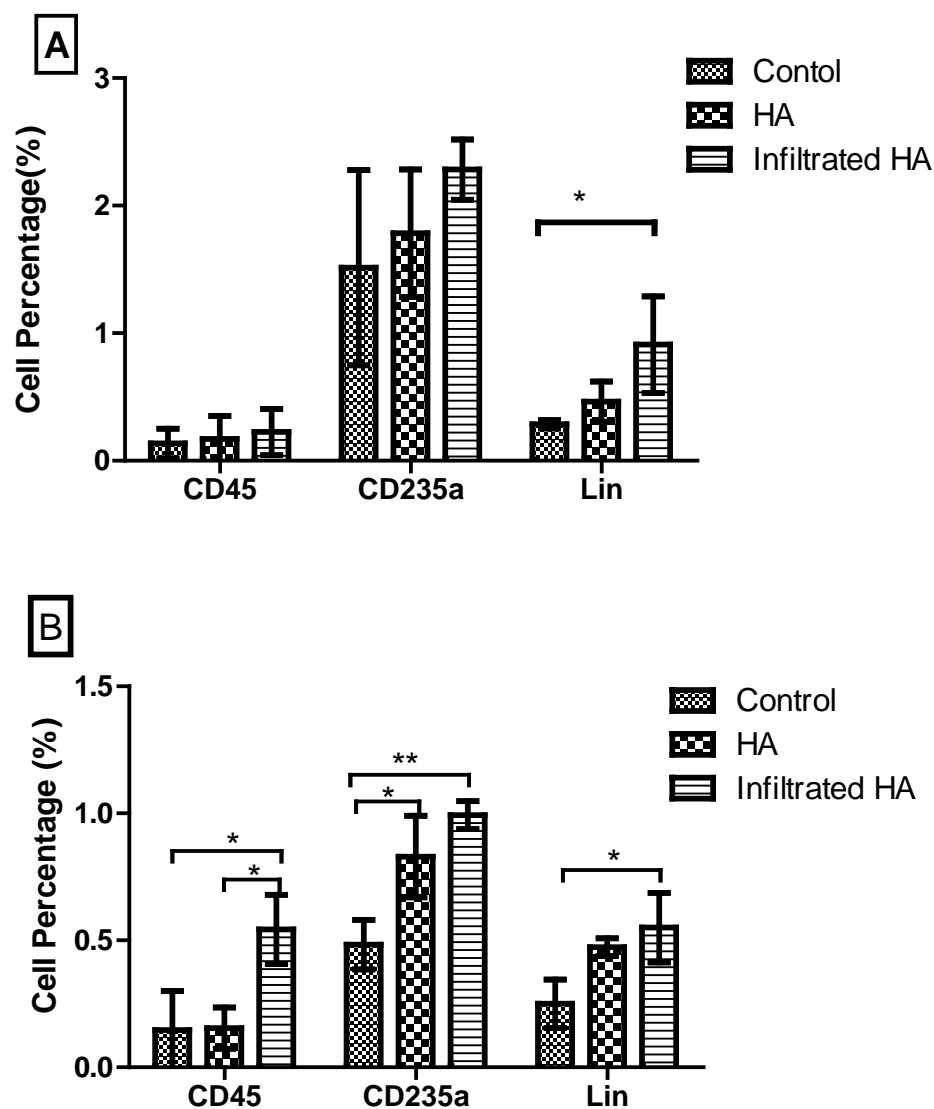


**Figure 6.37.** CD45, CD235a and Lin positive cell percentages for three conditions at (A) Day 15 and (B) Day 42. Significant differences were showed (\*\*p < 0.01, \*p < 0.05)

In this research, HUVECs, which are commonly used as an endothelial cell lineage model, seem to regain HSC functionality during long term culture, particularly in the presence of the scaffolds. The presence of mature hematopoietic cells, such as CD235a<sup>+</sup> (erythrocytes) and CD 45<sup>+</sup> (lymphocytes), confirms that endothelial cells can be stimulated into the hematopoietic lineage. The infiltrated HA scaffold which released more calcium into the culture, induced more of the HUVECs to differentiate into lymphocyte lineage At Day 15, the CD45 fraction for the infiltrated HA scaffold condition is significantly higher than that of the HA scaffold condition. After 42 days, the CD 45 fraction for the infiltrated HA scaffold condition is significantly higher than for the control and the HA scaffold condition. Therefore, Ca<sup>2+</sup> ion concentration may play an important role in the differentiation of cells with hemangioblast character (HSCs and HUVECS) down the hematopoietic lineage and more study is needed here.

#### **6.2.4 Colony Unit Forming Assay**

In order to investigate the efficacy of hematopoietic progenitors to differentiate down the hematopoietic cell line, the Colony Forming Unit Assay was performed. The HUVECs without culturing were assayed as Day 0 as a negative control. Then the HUVECs cultured for 15 or 42 days under the three scaffold conditions were subject to the CFU assay and the results and compare to the Day 0 result (as Table 7). Statistical analysis showed no significant between all conditions at Day 15 and Day 42. However, the presence of CFU-E and CFU-GM in the assay proved the existence of functional hematopoietic progenitors in the HA and Infiltrated HA scaffold conditions after 15 days and 42 days of culture. In both Day 15 and Day 42, there was no colony formed in the control conditions, which indicates that the cells cultured in the control condition are not able to differentiate down the hematopoietic cell lineage.

**Table 7** CFU accounting for HUVECs

Sample	CFU-E	BFU-E	CFU-GM	CFU-GEMM
Day0	0	0	0	0
Day 15 Control	0	0	0	0
Day 15 HA	0.67±0.67	0	0.67±0.67	0
Day 15 Infiltrated HA	0.67±0.67	0	0.67±0.67	0
Day 42 Control	0	0	0	0
Day 42 HA	0.67±0.67	0	1±1	0
Day 42 Infiltrated HA	0.67±0.67	0	0.33±0.33	0

With the CFU testing, the results showed that the HSCs derived from the HUVEC population were able to differentiate into erythrocytes and form macrophages. in the presence of the scaffolds but not in the control condition in which they appear to retain their stem cell character. The ability of HUVEC to acquire HSC lineage is perhaps not surprising given their shared hemangioblast character. Importantly, the CFU results indicates that HUVECs will not differentiate into hematopoietic lineages spontaneously in the negative control, but have the capacity to differentiate into hematopoietic progenitors and hematopoietic lineage cells in the presence of the scaffolds. With HA scaffolds and infiltrated HA scaffolds, the HUVECs appear to have attached, proliferated and differentiated, with higher percentages of hematopoietic lineages cells produced, such as erythrocytes, lymphocytes, macrophages.

### **6.3 HEMATOPOIETIC STEM CELLS AND OSTEOBLASTS CO-CULTURING**

The second cell model for this study was the hematopoietic stem cells (HSCs) / osteoblasts co-culture system. The osteoblasts are from the Saos-2 cell line and the HSCs are primary human bone-marrow derived stem cells. Three biological repeats, each having HSCs from a different donor, were applied to test the biocompatibility of the biphasic material developed in this study.. As the cell sources for HSCTs, HSCs are used widely and are difficult to maintain and proliferate during long term in-vitro culture<sup>162</sup>. There are two types of in-vitro culture model for bone marrow derived HSCs, each based on a microenvironment (niche) in which the HSCs are found in bone marrow., The first is the endosteal niche, close to the bone surface, and the second is the vascular niche close to blood vessels. In the endosteal niche, in which HSCs can self-renew and differentiate into mature hematopoietic cells, the HSCs are immobilized in association with osteoblasts that are attached to the bone surface. Hence, the osteoblast and HSCs co-culture cell model is widely accepted for the HSCs maintenance in this microenvironment, which is most pertinent to this study. According to Calvi et al<sup>163</sup> there is a parallel relation between the osteoblast population increase and the HSCs cell number increase. Therefore it is expected that this co-culture would be most appropriate for expanding the HSC population and controlling their fate in in-vitro culture.

#### **6.3.1 Cell Population and Culturing Observations**

In the three biological repeats of this study, the HSC/Saos-2 co-culture, the total cell number for each scaffold condition was counted by microscopy at each harvest time point. Four different conditions were used in this experiment, including: (i) the HSCs/Saos-2 cultured without any

scaffold as a positive control, (ii) the HSCs/Saos-2 cultured with an HA scaffold, (iii) the HSCs/Saos-2 cultured with a 1M Ca<sup>2+</sup> solution infiltrated HA scaffold, and (iv) the HSCs/Saos-2 cultured with a 2M Ca<sup>2+</sup> solution infiltrated HA scaffold.

As it is shown in the Figure 6.38, the total cell number increased with time for all scaffold conditions. Unfortunately there is no significant difference between the time points for any of the scaffold conditions because of the variability between the behaviors of the HSCs from the donors. Such variability is not unusual for primary human HSCs but it does effect the interpretation of significance in this case, especially at day 28 and day 42. The large error bars on the cell number are due to the donor individual variation.

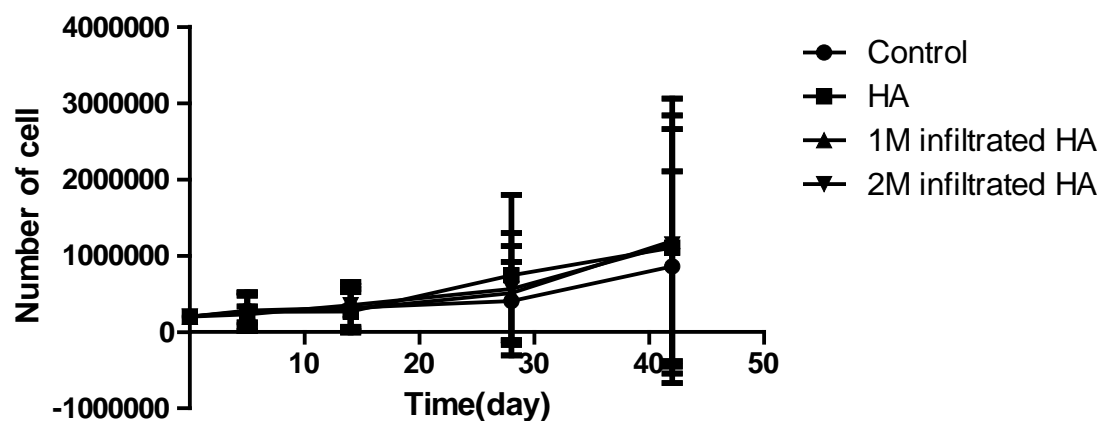


**Figure 6.38** Total cell number in the samples over a 42 day period samples in 42 days

In order to further examine the differences for the total cell population between the scaffold conditions, the glucose and lactate secretion was measured in media samples extracted from the culture every three days over the 42 days period and is shown in Figure 6.36. As described above in the HUVECs culture experiments, the glucose consumption and the lactate secretion could reflect the cell activity level.

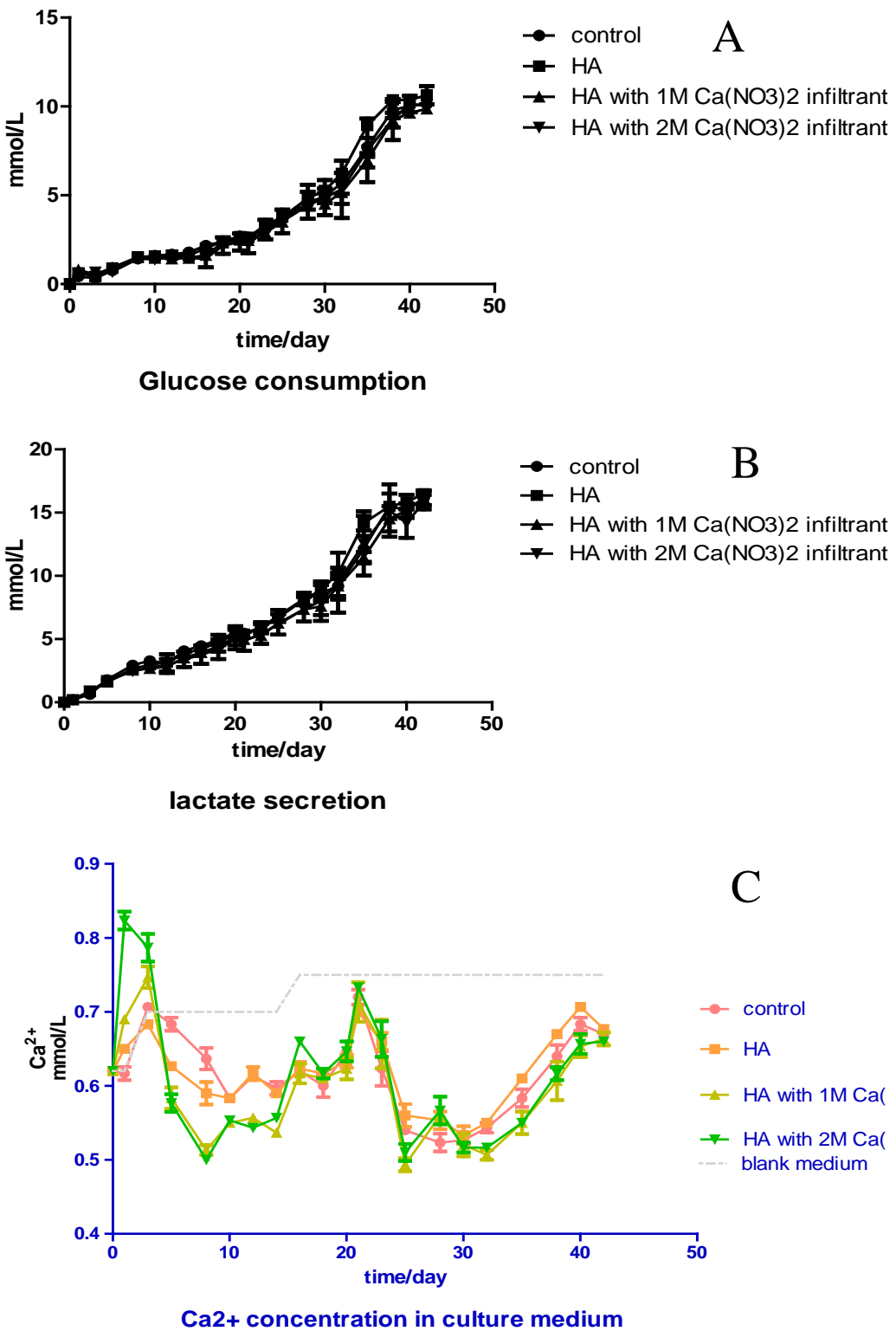


**Figure 6.39** (A) accumulated glucose consumption (B) accumulated lactate secretion, and (C) Ca<sup>2+</sup> concentration over a 42 day period

In the comparison of glucose and lactate, there is no significant difference between the scaffold conditions at any particular time point. The consumption of glucose and the secretion of lactate increased with time in much the same way for all the co-culture wells during 42 days. Thus, the four scaffold conditions appear to have similar effects on biocompatibility for the HSCs/ Saos-2 co-culture.

Between the infiltrated scaffolds and pure HS scaffolds, there is a significant difference in the  $\text{Ca}^{2+}$  concentration measured in samples of the medium extracted every three days over the 42 day period. With the Ca-rich phase, the infiltrated scaffolds provided a higher Ca concentration over the first 3 days as shown in Figure 6.39 (C). This enrichment was greater for the scaffold infiltrated with the higher calcium nitrate concentration. Since this should result in more soluble second phase it is not surprising that the calcium concentration in the media should be higher. In the HA scaffolds condition, the Ca concentration is significantly lower than the infiltrated scaffolds but significantly higher than the medium of the no-scaffold control condition at 1 day. Again, this is consistent with the fact that the HA scaffold does not contain the soluble second phase but does degrade a little in the culture medium. From day 5 to day 14, the  $\text{Ca}^{2+}$  concentration of the extracted media samples for the infiltrated scaffolds decreased sharply and had a significantly lower  $\text{Ca}^{2+}$  concentration than the HA condition and the no-scaffold control condition. This was indeed surprising but this could be an active cell differentiation period (osteoblast or erythrocytes), for the infiltrated scaffolds conditions and the new cells thus produced could then consume the calcium in the media<sup>164</sup>. This will be examined later in the presentation of the FACS results, such as ALP and CD235a markers.

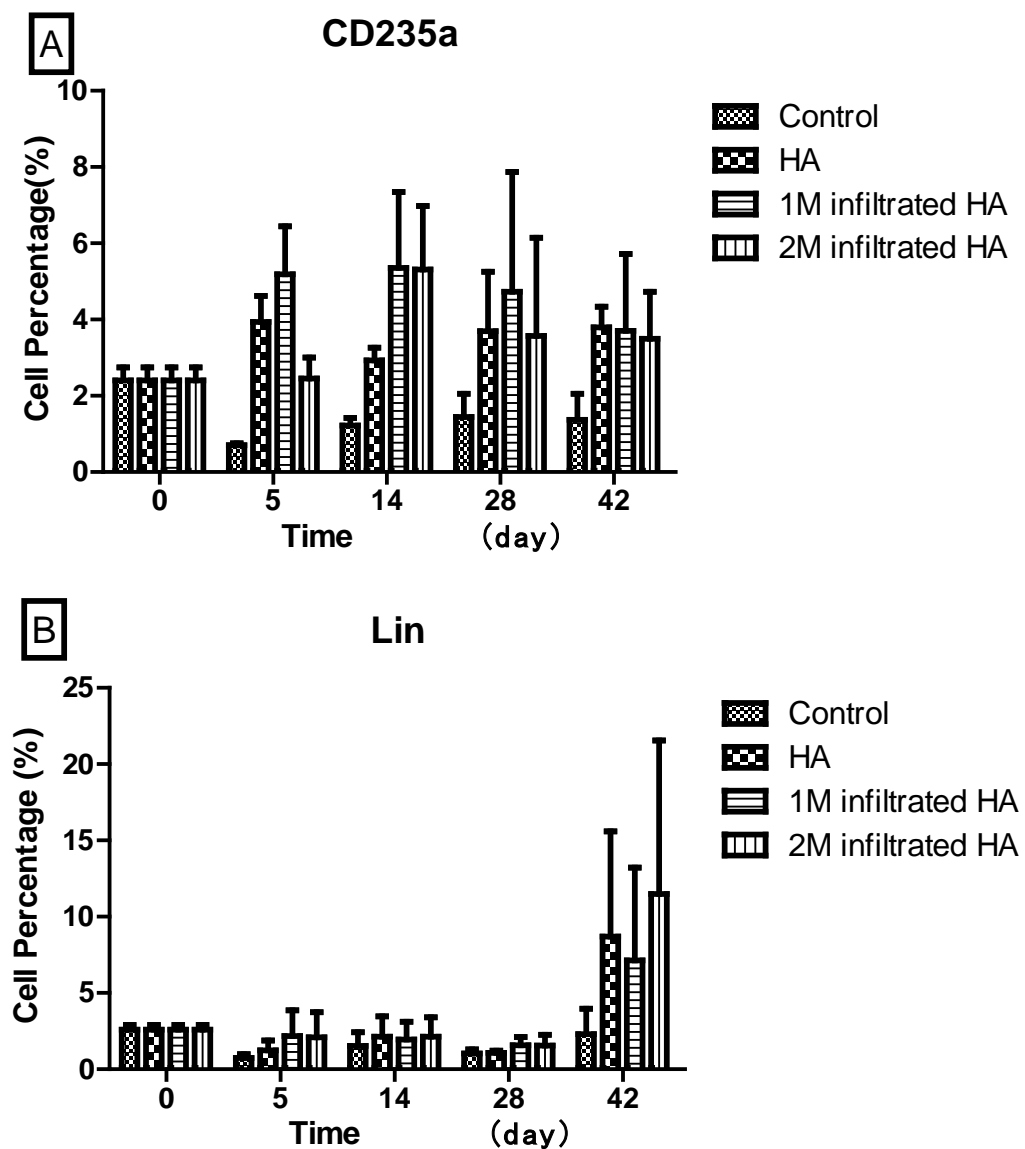
From day 16 to the day 42, the  $\text{Ca}^{2+}$  concentrations in the four conditions became similar, with no significant differences between each other. Interestingly the Ca concentration peaked

once again for all the scaffold conditions at around 20 days and then decreased to a minimum between 25 and 30 days and then finally rose once more to a peak at 40 days. There is clear cyclic behavior in the  $\text{Ca}^{2+}$  concentration of the media for all the scaffold conditions which could be associated with the cell activity. Note that the  $\text{Ca}^{2+}$  concentration from the medium of the osteoblast/HSC co-culture has a quite different trend with time when compared with the HUVEC culture. We hypothesized that difference between the two experiments is caused by the activity of the different cell types. According to the researches who have previously studied osteoblasts<sup>165</sup>, these cells prefer higher  $\text{Ca}^{2+}$  concentration and consume  $\text{Ca}^{2+}$  ions medium during culture. In addition, the  $\text{Ca}^{2+}$  dependence of  $\text{Ca}^{2+}$ -ATPase in erythrocyte membranes polyphosphoinositide metabolism has been reported by Buckley<sup>166</sup>, suggesting that erythrocytes will also consume calcium. The general osteoblast culture medium, McCoy's 5A medium, has a 0.9mM calcium concentration while HSC culture medium has a calcium concentration of only 0.7mM. Therefore high  $\text{Ca}^{2+}$  concentration in the scaffold condition is expected to correlate most with higher osteoblasts and erythrocytes activity in culture.

### **6.3.2 Fluorescence Activated Cell Sorting**

In order to tracking the cell fate and the differentiation of the cells in the co-culture, fluorescence activated cell sorting (FACs) was applied to the three repeats for each scaffold condition for the day 5, day 14, day 28 and day 42 time points. In the FACs examination, six antibodies were applied, including FITC-Linage cocktail (Lin), PerCP Cy-CD34, BV421-CD31, PE-CD38, AF647-ALP, and AF700-CD235a. Linage cocktail (Lin) represents for a collection of lymphocytes, such as T-cells, B-cells, and macrophages. As a progenitor marker, CD34 was used in combination with CD38 to evaluate  $\text{CD34}^+$ / $\text{CD38}^-$  for HSC stem cells.. CD235a is the marker

for erythrocytes, and ALP is used to detect osteoblasts. The CD31 is a marker used for endothelial progenitor cells.



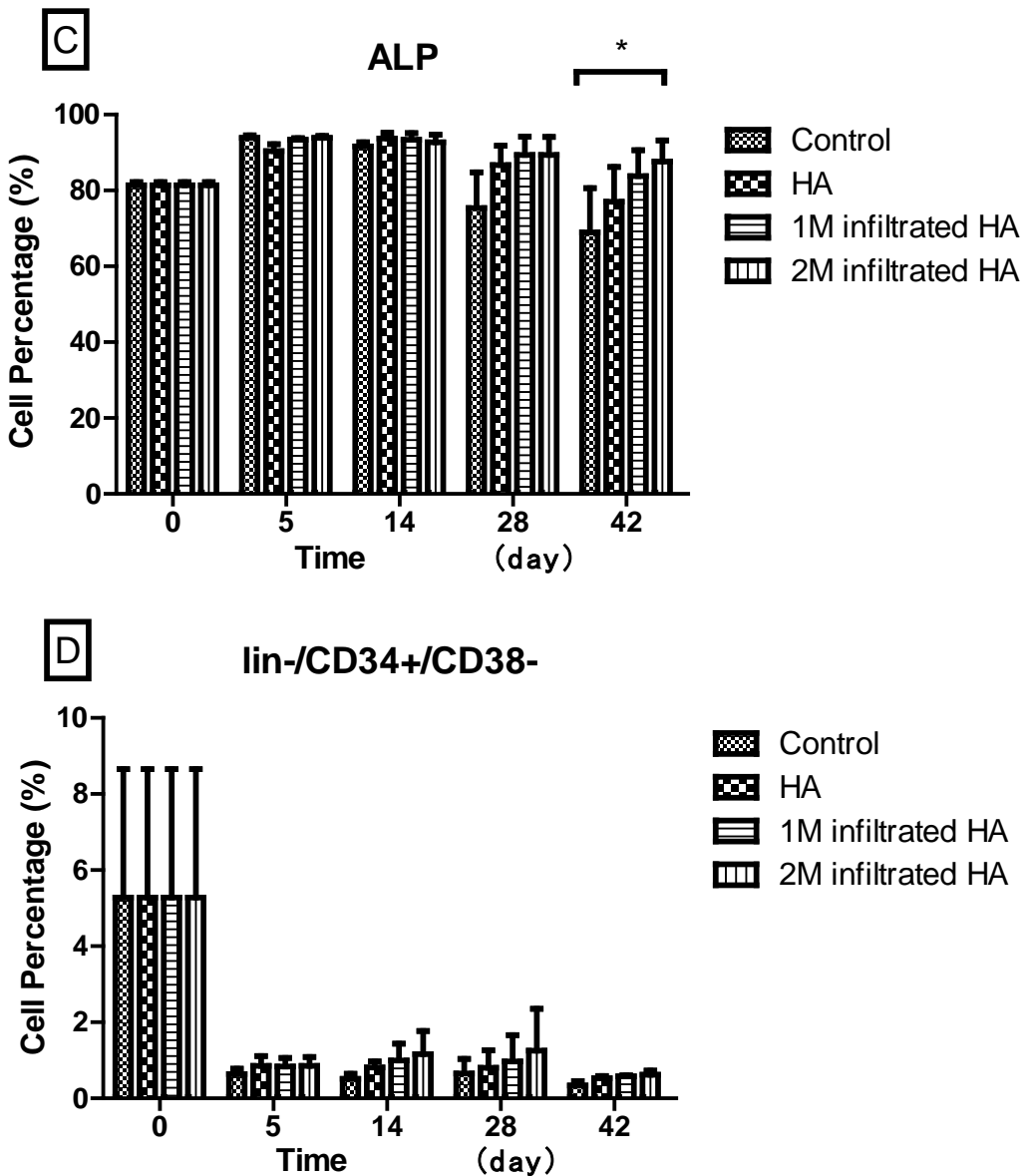


**Figure 6.40** FACs results for HSC/Saos-2 for (A) CD235a, (B) Linage, (C) ALP, and (D) HSCs cell for all the conditions during 42 days of culture

In Figure 6.40 (A), comparing with day 0 fresh cells, the erythrocytes percentages decreased in the control no-scaffold condition by 5 days and although the percentage of these cells in the control increased at longer times it never regained the percentage in day 0. However, for the other three scaffold conditions, the erythrocytes percentages increased. Erythrocytes can

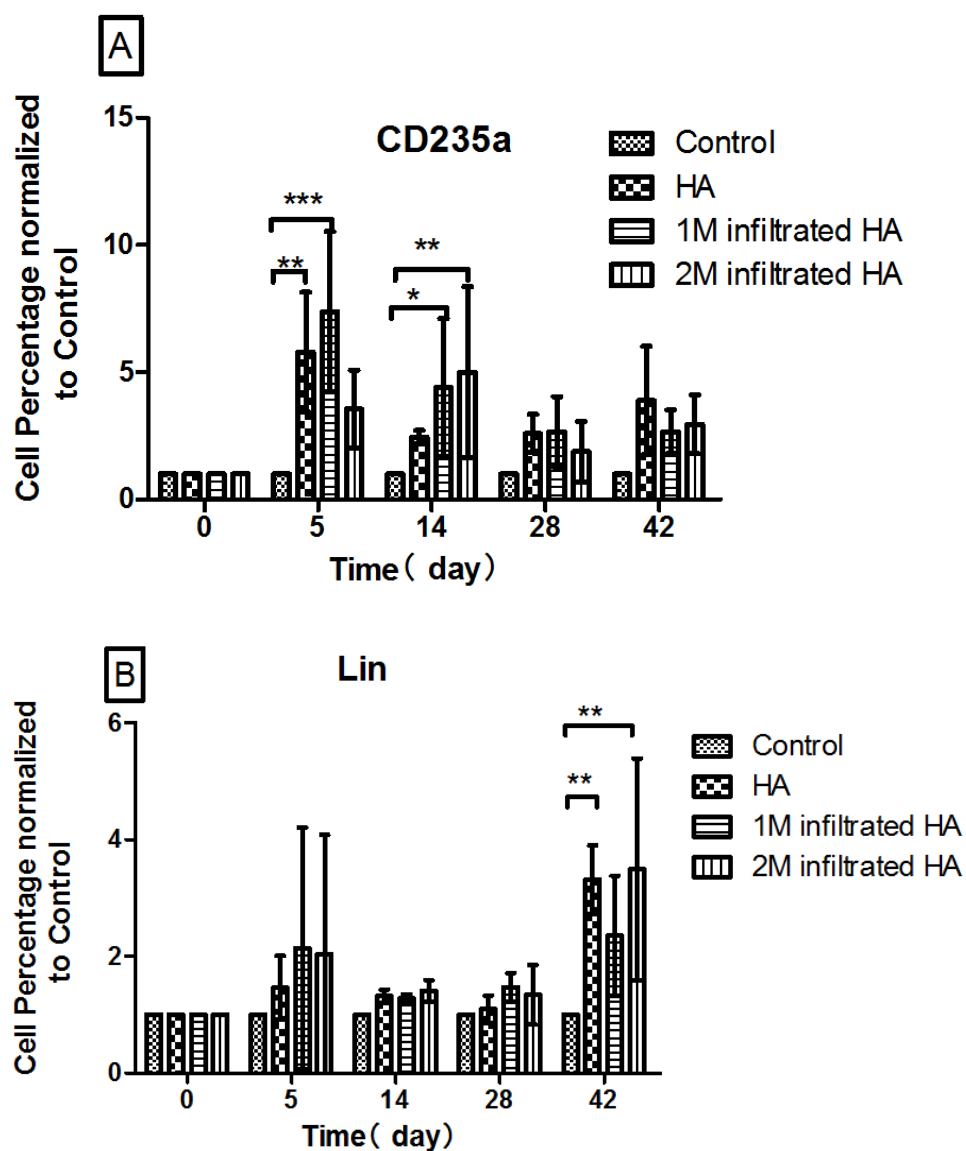
live for a maximum of 2 weeks and usually die well before that. In addition they are not capable of differentiation themselves and must be derived from HSCs present in this culture. The results indicated that erythrocytes are present throughout long term culture and the fraction increases for the scaffold conditions. This suggests that HSCs are differentiating into erythrocytes throughout the culture period and that the scaffolds seem to promote this.

There is a different trend for the Lin positive cells, which are lymphocytes derived for HSCs. There is no significantly change in the cell percentage until 42 days. At 42days Figure 6.40 (B), shows the cell percentage expression Lin was sharply higher for the scaffold conditions. The control condition with no scaffold still had a low and stable percentage of Lin positive cell percentage. The large variability between the biological repeats with different donors contributed to the large error bars and no significant differences.

Since the medium was chosen for HSC culturing rather than the culturing of osteoblasts, it is no surprise that the cell percentage for ALP (Figure 6.40(C)), osteoblast cell marker, decreased in the control condition as the culture time increased. At day 42, there is a significant difference between the percentages of cells expressing ALP in the control condition and the 2M  $\text{Ca}^{2+}$  solution infiltrated HA scaffolds condition. In the scaffolds conditions, the ALP marker percentages increased with culture time for the HA scaffold condition, 1M  $\text{Ca}^{2+}$  infiltrated HA condition and the 2M  $\text{Ca}^{2+}$  infiltrated condition.

Figure6.40 (D) shows there is large decrease in the fraction of HSCs within the first 5 days and then there is no significant difference between the scaffold conditions at each time point. However, the results at day 42 for all the scaffold conditions indicated that the HSCs were then maintained in long term culture over 42 days.

In the FACS results, the large error bars appeared due to the biological variation between different HSC donors. In order to reduce the individual difference, the normalization is applied to the FACS result. At each time point, the FACS results for the four scaffold conditions were normalized to the control in each repeat. The normalized FACS results are shown in Figure 6.41 (A) to (D).



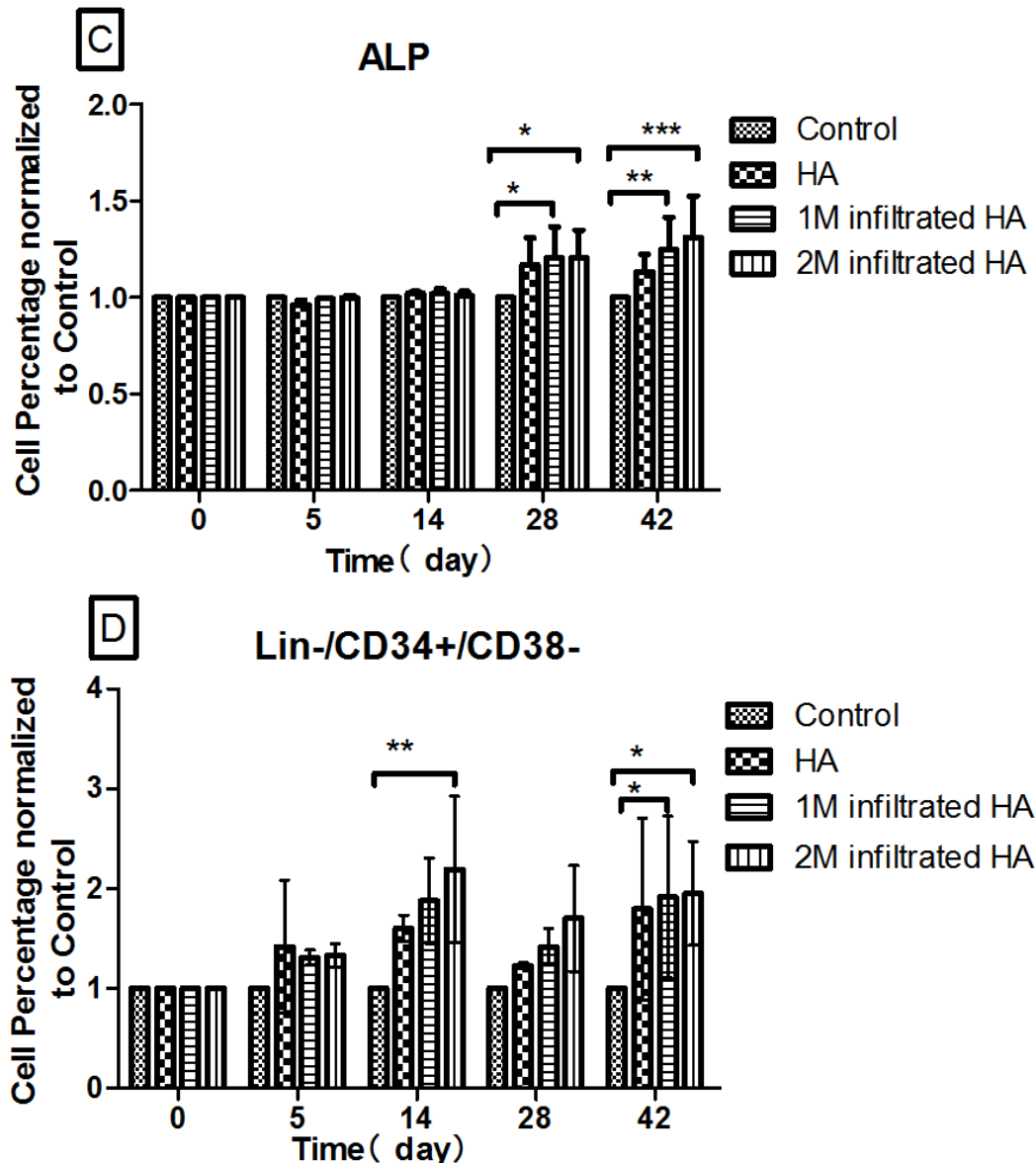


**Figure 6.41** Normalized FACs results for HSC/Saos-2 for (A) CD235a, (B) Linage, (C) ALP, and (D) HSCs cell for all the conditions during culture

After normalizing, the variation between the donors is reduced and there are significant differences between the scaffold conditions. For the CD235a erythrocyte marker, the cell percentages for the HA scaffold condition and the 1M infiltrated HA scaffold condition are significantly higher than the no-scaffold control on day 5. 2M infiltrated HA scaffold condition and 1M HA scaffold infiltrated condition are also significantly higher than the control condition

on Day14. The erythrocytes expression enhancement on the scaffolds conditions maintained at the longer time points but is no longer significant. These results suggest that HSCs are more likely to differentiate into erythrocytes on the scaffolds, perhaps due to the release of calcium.

The normalization reveals differences between the scaffold conditions for the Lin marker at the longer time points. Both of the HA condition and the 2M infiltrated HA condition expressed for significantly higher cell percentages of Lin marker than the control at day 42. The significances between the control and the scaffolds conditions demonstrated once again that the scaffolds introduced into the HSC/Saos-2 co-cultures could facilitate HSC differentiation.

For ALP, the osteoblast cell type marker, there are greater significance to the enhancement at longer sintering times compared to the control. Significantly more osteoblasts were maintained in the two infiltrated scaffolds conditions compared to the control condition ( $p<0.05$ ) at day 28. After another 2 weeks, the differences became more significant with  $p<0.001$ . Meanwhile, there is no significant difference at each time point between the HA condition and the other scaffold conditions, as well as between the 1M infiltrated HA scaffolds condition and the 2M infiltrated HA condition during 42 days. It is clear that the scaffolds allow the osteoblast population to be maintained and even increase whereas the control results in a decrease in osteoblasts through the culture period. This could be due to osteoblast attachment to the scaffolds and the calcium content of the media.

Figure 6.41 (D) shows the HSC cell percentages are defined by the marker combination of Lin negative, CD34 positive and CD38 negative. This removed more mature hematopoietic progenitors and also endothelial progenitors that may express CD34. The infiltrated HA scaffolds conditions had significantly higher HSC cell percentages than the control condition at

day 42 with  $p < 0.05$ . Also, in the culture of the 2M infiltrated HA condition, HSC percentages are significantly larger than that in the control condition at day 14.

In summary, the FACs results show that there are significant increments in cell percentages for the infiltrated HA conditions over the control condition for erythrocytes, osteoblasts, and HSCs. For the hematopoietic lineage cell percentages, there is a significant difference between the HA condition and the control condition at long time points.

### **6.3.3 Colony Forming Unit Assay**

In HSCs in-vitro culture experiments, Colony Forming Unit Assay (CFU) is an important and necessary method to investigate the ability of hematopoietic progenitor cells and HSCs to differentiate after being cultured. In the CFU testing, 5000 cells were extracted for cultures of each scaffold condition at each harvest time point, mixed with CFU assay, and cultured for another 15 days. After 15 days, the wells were observed under a microscope to identify the types of colonies formed by differentiation of HSCs and count the colony numbers. Four different types of colonies were identified in this study and their frequencies compared to expected numbers as given by the manufacturer: These included: CFU-E (Colony Forming Unit – Erythrocyte), BFU-E (Burst Forming Unit – Erythrocyte), CFU-GM (Colony Forming Unit – Granulocytes, Macrophage) and CFU-GEMM (Colony Forming Unit – Granulocyte, Erythrocyte, Macrophage, and Megakaryocyte)<sup>158</sup>. The results are shown in Figure 6.42.

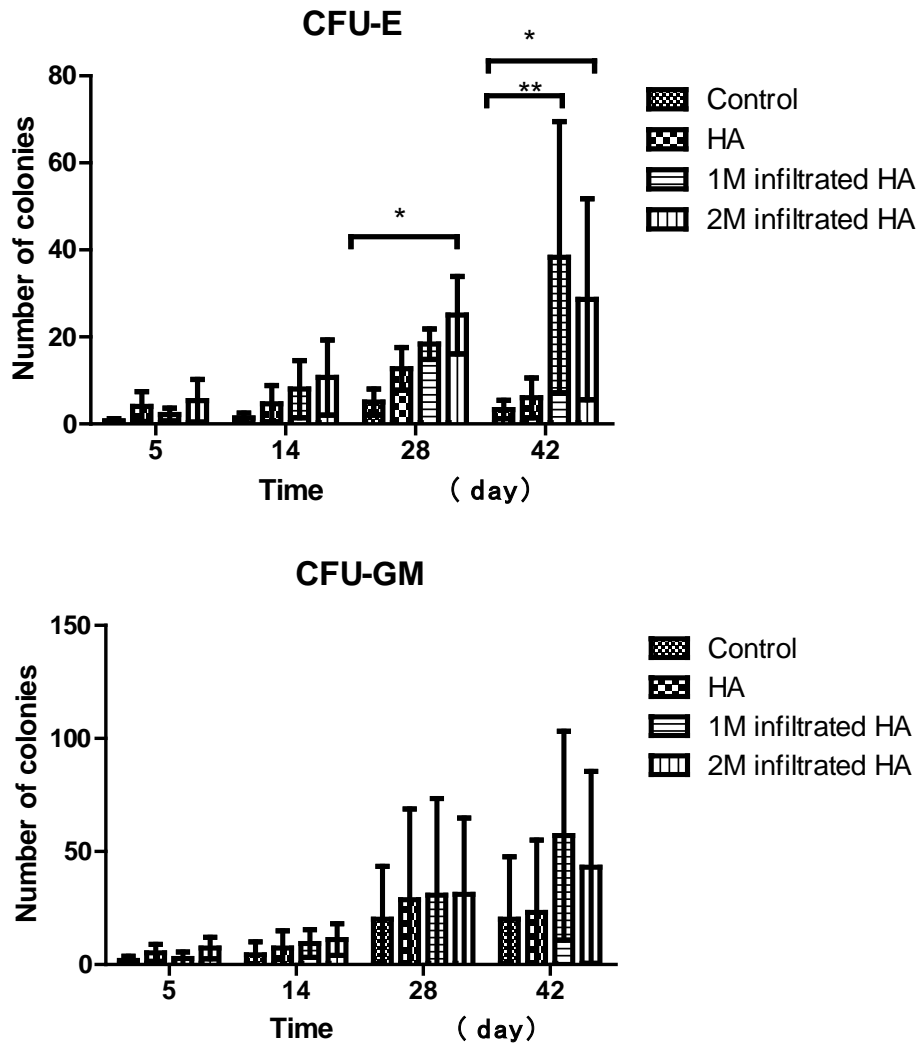


**Figure 6.42** CFU colonies accounting of HSC/Saos-2 in (A) CFU-E and (B) CFU-GM for all the conditions at harvest time points

There were no BFU-E and CFU-GEMM observed for any of the cultured HSCs. CFU-E are erythrocytes colonies, which indicates the HSC progenitors in the culture that have the potential to proliferate and differentiate into erythrocytes. Figure 6.42 (A), shows that after the longer culturing times, there are significant differences between the infiltrated HA scaffolds and the control condition. At day 28, the 2M infiltrated HA condition had significantly more CFU-E colonies than the control condition. Both 1M and 2M infiltrated HA scaffolds conditions gave

significantly higher numbers of CFU-E colonies than the control condition at day 42. The Figure 6.42 (A) provides strong evidence that the infiltrated scaffolds could increase the fraction of HSCs which have the potential to differentiate into blood cells.

For the CFU-GM result, Figure 6.42 (B), there was no significant difference between the conditions at each time point. However, when we group the CFU-GM colony counts for each donor, the infiltrated scaffold conditions have higher CFU-GM colony numbers than the control condition harvested at 42 days.

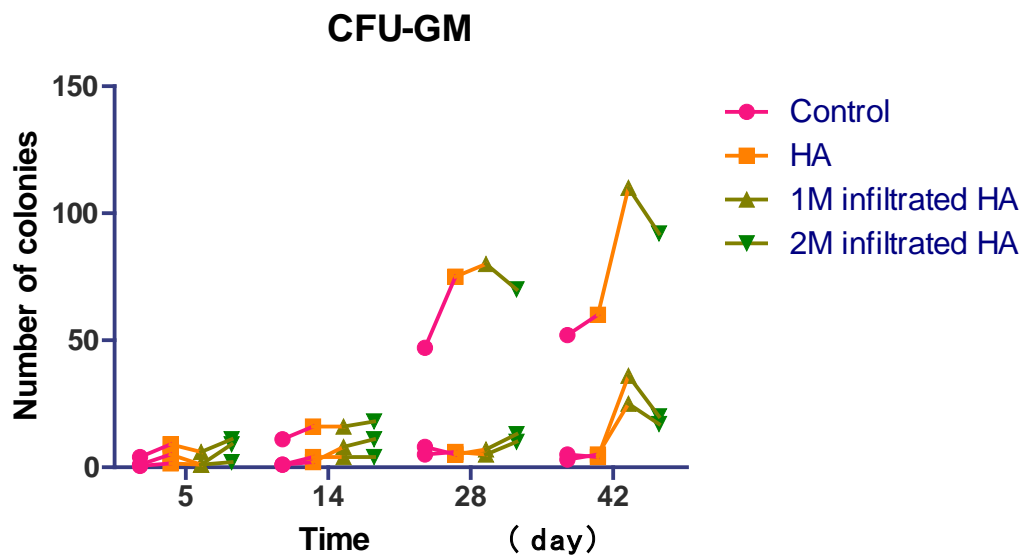


**Figure 6.43** CFU-GM colonies accounting of HSC/Saos-2 of each repeat

In the Figure 6.42, the results for the different scaffold conditions are grouped by donor at each time point. It then becomes clear that the infiltrated HA scaffold conditions enhanced the number of the hematopoietic lineage cell colonies compared to the control. This trend suggests that HSCs cultured in the presence of the scaffolds have a higher probability of differentiating into the hematopoietic cell lineage.

## **7.0 CONCLUSIONS**

### **7.1 EFFECT OF THE INFILTRATION PROCESS ON HA AND CONSEQUENT EFFECT ON DISSOLUTION**

1. A biphasic calcium phosphate ceramic can be created by infiltrating calcium salts into HA scaffolds that has been partially sintered. The infiltration process and consequent heat treatment produce HA with minor amounts of CaO. Exposure to moisture causes the transformation of CaO to  $\text{CaCO}_3$ , another highly soluble Ca-rich phase,
2. The biphasic calcium phosphate ceramic has a higher degradation rate in static tri-buffered saline over at least 28 days. The calcium ion release from the Ca infiltrated HA is consistently higher than that of HA for dense pellets and highly porous foams over 28 days. Therefore this part of the hypothesis was correct.
3. The transformation of CaO to  $\text{CaCO}_3$  on exposure to moisture also caused fragmentation of the ceramic by removing adjacent HA grains leading to relatively large surface defects that grew deeper with exposure time.

## **7.2 PREPARATIONS OF A BIPHASIC CALCIUM PHOSPHATE SCAFFOLD AND THE CULTURING OF HUVECS**

Human umbilical vein endothelial cells (HUVECs) were successfully cultured on HA and infiltrated HA scaffolds over 42 days. When compared to a control with no scaffold, it was found that the presence of HA or Infiltrated HA scaffold increased the expression of HSCs, with a combination marker of CD34+ /CD38-/Lin-, and acquired the expression of CD45 and Lin, two mature hematopoietic cell marker, mainly for lymphocytes . This showed for the first time that calcium phosphate scaffolds can stimulate HUVEC cells, commonly recognized as endothelial progenitors, to acquire HSC character and then differentiate down the hematopoietic lineage. Additionally, the CFU assay test showed that the HSCs derived from HUVEC cells can then differentiate and form erythrocytes colonies and granulocytes/ macrophages colonies. Finally HA scaffold was important to the differentiation to erythrocytes after 42-day culture; whereas the high calcium concentration associated with the impregnated scaffolds may be more important for HUVECs differentiation into lymphocytes. In summary, a small fraction of HUVEC cells can develop HSC character in culture and the scaffolds were found to improve HSC maintenance in long term culture and some increase in HSC cell fraction but there was no evidence of a major expansion of the HSC population derived from HUVEC cells.

### **7.3 PREPARATIONS OF A BIPHASIC CALCIUM PHOSPHATE SCAFFOLD AND THE CULTURING OF HSC/OSTEOBLAST CO-CULTURE**

Hematopoietic stem cells and osteoblasts were successfully co-cultured over 42days in the presence of HA and infiltrated HA scaffolds. The differentiation of the HSC cells was indicated by cell marker for mature hematopoietic cells in FACs. In this study, the biocompatibility of the infiltrated HA scaffolds was shown to be similar to the HA scaffolds. HSCs and osteoblast maintenance during 42 days of co-culture was improved by the presence of the scaffolds.. FACs analysis of erythrocytes marker (CD235a) ,hematopoietic cell maker( Lin) and the CFU assay, showed that the infiltrated HA scaffolds resulted in higher fractions of hematopoietic cells after long term culture and the HSC s cultured on the infiltrate scaffolds showed more potential to differentiate down the hematopoietic lineage compared with the control. Again, there was no major expansion of the HSC population.

## **8.0 SUGGESTED FUTURE WORK**

### **8.1 BIOREACTOR CONSTRUCTION**

The effect of the scaffold materials on the HSC/osteoblast co-culture should be examined under perfusion conditions using bioreactors. This is known to affect the fate of HSC cells making them more susceptible to differentiation. In particular the ability of the scaffolds to maintain the HSC population in long term culture should be investigated for the infiltrated scaffolds.

### **8.2 THE BIOCOMPATABILITY OF THE HIGH CALCIUM CERAMICS WITH HSCS**

The infiltration method only results in minor fractions of the second phase in HA and as a result the dissolution and the fragmentation of the scaffold is slow. To improve the solubility of the scaffolds and their ability to degrade, other methods such as mixed powder techniques should be used to make ceramics with much larger fractions of the CaO second phase. The solubility of these ceramics in saline should then be investigated. If scaffolds can be made to degrade in culture it would allow the cells to remodel the space into tissue like structures.

### **8.3 THE DIFFERENTIATION PATHWAY OF HUVECS TOWARDS HEMATOPOIETIC LINEAGE**

In the study, the biocompatibility of the material has been tested with HUVECs. The positive results of FACs and PCR on the differentiation to hematopoietic cells, demonstrated that the infiltrated HA scaffolds could stimulate certain HUVEC cells into hematopoietic cell linages. If this could be achieved at higher cell fractions it may be possible to use HUVECS as a source of endothelial cells and hematopoietic cells. More cell biology experiments must be conducted on the of the scaffolds and calcium release on the differentiation pathway and the role of hemangioblast character in determining if HUVECS will differentiate to HSCs at higher cell fractions.

## BIBLIOGRAPHY

- [1] T.A. Einhorn. Enhancement of fracture-healing. *J. Bone Joint Surg. Am.*, 77: 940–956, 1995.
- [2] A. Praemer, et al. *Musculoskeletal Conditions in the United States*. The American Academy of Orthopaedic Surgeons, 1992.
- [3] Kenneth R. Keivyon, Scheffer C.G. Tseng, Limbal Autograft Transplantation for Ocular Surface Disorders. *Ophthalmology*, 96(5): 709–723, 1989.
- [4] Jeffrey D Hosenpud, Leah E Bennett, Berkeley M Keck, Mark M Boucek, et al. The registry of the international society for heart and lung transplantation: eighteenth official report—2001. *The Journal of Heart and Lung Transplantation*, 20(8): 805–815, 2001.
- [5] G.Gahrton, B. Björkstrand. Progress in haematopoietic stem cell transplantation for multiple myeloma. *J Intern Med*, 248 (3): 185–201, 2000.
- [6] Saxon, Wolfgang, Robert A. Good, 81, *Founder of Modern Immunology, Dies*. New York Times, 18 June, 2003.
- [7] Betty Ferrell, Marcia Grant, Gerhard M. Schmidt, et al. The meaning of quality of life for bone marrow transplant survivors. *Cancer Nursing*, 15(3):153-160, 1992.
- [8] Alois Gratwohl, Helen Baldomero, Michael Gratwohl, Mahmoud D Aljurf, et al, Quantitative and qualitative differences in use and trends of hematopoietic stem cell transplantation: a Global Observational Study , *Haematologica*, 98(8):1282-1290, 2013.
- [9] A .Tyndall, A. Fassas, J .Passweg, et al. Autologous haematopoietic stem cell transplants for autoimmune disease--feasibility and transplant-related mortality. Autoimmune Disease and Lymphoma Working Parties of the European Group for Blood and Marrow Transplantation, the European League Against Rheumatism and the International Stem Cell Project for Autoimmune Disease , *Bone Marrow Transplant*, 24 (7): 729–34, 1999.
- [10] George Canellos. The Role of Salvage Therapy in Malignant Lymphomas, The *Oncologist*, 2 (3): 181–183, 1997.

- [11] Yucai Xie, Tong Yin, Winfried Wiegaebe, Xi C. He, et al. Detection of functional haematopoietic stem cell niche using real-time imaging. *Nature*, 457:97-101, 2009.
- [12] P Habibovic, K de Groot. Osteoinductive biomaterials--properties and relevance in bone repair. *J Tissue Eng Regen Med.*, 1(1):25-32, 2007.
- [13] Q .Shang, Z .Wang, W .Liu, Y. Shi et al. Tissue-Engineered Bone Repair of Sheep Cranial Defects with Autologous Bone Marrow Stromal Cells. *J Craniofac Surg*, 12(6):586-93, 2001.
- [14] L.Zhu, W. Liu, L. Cui, Y.Cao. Tissue-engineered bone repair of goat-femur defects with osteogenically induced bone marrow stromal cells. *Tissue Eng*, 12(3):423-33, 2006.
- [15] H.Imaizumi, M. Sakurai, O. Kashimoto, et al. Comparative study on osteoconductivity by synthetic octacalcium phosphate and sintered hydroxyapatite in rabbit bone marrow. *Calcif Tissue Int.*, 78(1):45-54, 2006.
- [16] K.G .Marra, J.W .Szem, P, N .Kumta, P.A. DiMilla, et al. In vitro analysis of biodegradable polymer blend/hydroxyapatite composites for bone tissue engineering. *J Biomed Mater Res.*, 47(3):324-35, 1999.
- [17] David T. Scadden. The stem-cell niche as an entity of action. *Nature*, 441 (7097):1075-1079, 2006.
- [18] Shinya Nakamura, Takuya Matsumoto, Jun-Ichi Sasaki, et al. Effect of Calcium Ion Concentrations on Osteogenic Differentiation and Hematopoietic Stem Cell Niche-Related Protein Expression in. *Tissue Engineering: Part A*, 16(8):2467-73, 2010.
- [19] Paul K Chu, Xuanyong Liu. Biomaterial fabrication and processing handbook. *The CPC Press*, 2007
- [20] Mason C, Dunnill P.A brief definition of regenerative medicine. *Regenerative Medicine*, 3 (1): 1–5, 2008.
- [21] *Science and Technology Committee Regenerative Medicine Report*, the Authority of the House of Lords. The Stationery Office Limited, 2013.
- [22] British Standards Institution (BSI): Publicly Available Specification (PAS) 84: *Regenerative Medicine—Glossary*, 2008.
- [23] H. Baharvand and N.Aghdami. *Regenerative medicine and cell therapy*. New York: Humana Press,2013
- [24] F.H. Gage. Cell therapy. *Nature*, 392 (6679 Suppl): 18–24, 1998.

- [25] I .Singec, R .Jandial, A. Crain, G .Nikkhah, E.Y .Snyder. The leading edge of stem cell therapeutics. *Annu. Rev. Med.* 58: 313–28, 2007.
- [26] Jason A. Burdick, and Gordana Vunjak-Novakovic. Engineered Microenvironments for Controlled Stem Cell Differentiation. *Tissue Eng Part A.*, 15(2): 205–219, 2009.
- [27] T.W. James. Continuous Culture of Microorganisms. *Annual Review of Microbiology*, 15: 27–46, 1961.
- [28] John A. Williams. Keys to bioreactor selection. [www.cepmagazine.org](http://www.cepmagazine.org): 34-41, 2002.
- [29] C. Fenge and E. Lullau. Cell Culture Bioreactors. In S.S. Ozturk and W.S. Hu, editors, *Cell Culture Technology for Pharmaceutical and Cell-Based Therapies*. CRC Press, 2006.
- [30] Joel P. Miller and Bruce E. Logan, Sustained Perchlorate Degradation in an Autotrophic, Gas-Phase, Packed-Bed Bioreactor. *Environ. Sci. Technol.*, 34 (14), 3018–3022, 2000.
- [31] Hojae Shim, Shang-Tian Yang. Biodegradation of benzene, toluene, ethylbenzene, and *o*-xylene by a coculture of *Pseudomonas putida* and *Pseudomonas fluorescens* immobilized in a fibrous-bed bioreactor. *Journal of Biotechnology*, 67, (2–3): 99–112, 1999.
- [32] J.C. Gerlach, K Mutig, IM Sauer, P Schrade, E Efimova, T Mieder, G Naumann, A Grunwald, G Pless, A Mas, S Bachmann, P Neuhaus and K Zeilinger. Use of Primary Human Liver Cells Originating from Discarded Grafts in a Bioreactor for Liver Support Therapy and the Prospects of Culturing Adult Liver Stem Cells in Bioreactors: a Morphologic Study. *Transplantation*, 76 781-786, 2003.
- [33] E. Schmelzer, F. Triolo, M.E. Turner, R.L. Thompson, K. Zeilinger, L.M. Reid, B. Gridelli and J.C. Gerlach.Three-Dimensional Perfusion Bioreactor Culture Supports Differentiation of Human Fetal Liver Cells, *Tissue Engineering: Part A*, 16: 2007-2016, 2010 .
- [34] Jason A. Burdick and Gordana Vunjak-Novakovic. Engineered Microenvironments for Controlled Stem Cell Differentiation, *Tissue Engineering Part A*. 15(2): 205-219, 2009.
- [35] E.D., Cearbhail, M.A. Punchard, M.Murphy, F.P. Barry, P.E. McHugh and V. Barron. Response of mesenchymal stem cells to the biomechanical environment of the endothelium on a flexible tubular silicone substrate. *Biomaterials*, 29, 1610–1619, 2008.
- [36] B.C.Isenberg, C. Williams and R.T. Tranquillo. Small-diameter artificial arteries engineered *in vitro* .*Circ Res.*, 98, 25–35, 2006.
- [37] W.L.Grayson, G.P. Chao, D. Marolt, D.L. Kaplan and G. Vunjak-Novakovic. Engineering custom designed osteochondral tissue grafts. *Trends Biotechnol*, 26, 181–189, 2008.

- [38] W.L. Grayson, S. BhumiratanaC. Cannizzaro, et al. Effects of initial seeding density and fluid perfusion rate on formation of tissue engineered bone. *Tissue Engineering Part A*, 14(11):1809-20, 2008.
- [39] V.I. Sikavitsas, G.N. Bancroft, H.L. Holtorf, et al. Mineralized matrix deposition by marrow stromal osteoblasts in 3D perfusion culture increases with increasing fluid shear forces. *PNAS* 100: 14683, 2003.
- [40] X.J. Yu, E.A. Botchwey, E.M. Levine, S.R. Pollack and C.T. Laurencin. Bioreactor-based bone tissue engineering: the influence of dynamic flow on osteoblast phenotypic expression and matrix mineralization. *PNAS* 101: 11203, 2004
- [41] L. Meinel, V. Kareourgiou, R. Fajardo, B. Snyder, V. Shinde-Patil, et al. Bone tissue engineering using human mesenchymal stem cells: effects of scaffold material and medium flow. *Ann Biomed Eng*, 32, 112–122, 2004.
- [42] B. P. Chan and K. W. Leong. Scaffolding in tissue engineering: general approaches and tissue-specific considerations. *Eur Spine J.* (Suppl 4): 467–479, 2008.
- [43] N.R Mohamed, D.E. Daya, BS Balb, et al. Bioactive glass in tissue engineering. *Acta Biomaterialia*, 7, (6): 2355–2373, 2011.
- [44] M. Heughebaert, R.Z. LeGeros, M. Gineste and A. Guilhem. Hydroxyapatite (HA) ceramics implanted in non-bone forming site. Physico-chemical characterization. *J Biomed Mat Res.*, 22:257-268, 1988.
- [45] Olivier Gauthiera, Ralph Müllerb, Dietrich von Stechowb, Bernard Lamy, et al, In vivo bone regeneration with injectable calcium phosphate biomaterial: A three-dimensional micro-computed tomographic, biomechanical and SEM study , *Biomaterials*, 26( 27) :5444–5453, 2005.
- [46] G. Daculsi, Biphasic calcium phosphate concept applied to artificial bone, implant coating and injectable bone substitute , *Biomaterials*, 19 (16): 1473–1478, 1998.
- [47] T. Livingston Arinze, S. Peter, M. Archambault, C. Van Den Bos, S. Gordon et al. Allogeneic mesenchymal stem cells regenerate bone in a critical-sized canine segmental defect. *J Bone Joint Surg Am*, 85-A (10): 1927–1935, 2003.
- [48] S. Kadiyala, N. Jaiswal, S.P. Bruder, Culture-expanded, bone marrow-derived mesenchymal stem cells can regenerate a critical-sized segmental bone defect , *Tissue Eng.*, 3 (2): 173–185,(1997)

- [49] T. Livingston Arinzech T. Tran, J. Mcalary, G. Daculsi, A comparative study of biphasic calcium phosphate ceramics for human mesenchymal stem-cell-induced bone formation , *Biomaterials*, 17(26): 3631–3638,(2005).
- [50] J.L Irigaray, H Oudadesse, E. Jallot, V. Brun, G. Weber and P. Frayssinet. Kinetics resorption after implantation of some hydroxyapatite compounds used as biomaterials. *Materials in clinical applications*, 1998 (Florence, 14-19 June).
- [51] T Noshi, T Yoshikawa, M Ikeuchi, Y Dohi, H Ohgushi,et al. Enhancement of the *in vivo* osteogenic potential of marrow/hydroxyapatite composites by bovine bone morphogenetic protein. *J Biomed Mater Res*, 52 : 621-30 ,2000.
- [52] M. Jarcho. Calcium phosphate ceramics as hard tissue prosthetics, *CORR*, 157:259--278, 1981.
- [53] Simon Storgard Jensen, Michael M. Bornstein, Michel Dard, Dieter D. Bosshardt, Daniel Buser. Comparative Study of Biphasic Calcium Phosphates with Different HA/TCP Ratios in Mandibular Bone Defects. A Long-Term Histomorphometric Study in Minipigs. *Journal of Biomedical Materials Research Part B: Applied Biomaterials*, 90B( 1):171-181, 2008
- [54] Christian Schopper, Farzad Ziya-Ghazvini, Walter Goriwoda, Doris Moser, et al. HA/TCP Compounding of a Porous CaP Biomaterial Improves Bone Formation and Scaffold Degradation—A Long-Term Histological Study. *Journal of Biomedical Materials Research Part B: Applied Biomaterials*, 74B,( 1): 458-467,2005
- [55] U. Ripamonti, P. W. Richter, R. W. N. Nilen and L. Renton. The induction of bone formation by smart biphasic hydroxyapatite tricalcium phosphate biomimetic matrices in the non-human primate Papio ursinus. *J. Cell. Mol. Med.* 12,( 6B) :2609-2621,2008
- [56] M. Schumacher, U. Deisinger, R. Detsch ,G. Ziegler. Indirect rapid prototyping of biphasic calcium phosphate scaffolds as bone substitutes: influence of phase composition, macroporosity and pore geometry on mechanical properties. *Journal of Materials Science: Materials in Medicine*, 21, (12): 3119-3127,2010
- [57] Atsushi Fujita, Makoto Migita, Takahiro Ueda, Rei Ogawa,et al. Hematopoiesis in Regenerated Bone Marrow within Hydroxyapatite Scaffold. *Pediatric Research*, 68: 35–40, 2010.
- [58] S. Bertazzo and C. A. Bertran. Morphological and dimensional characteristics of bone mineral crystals. *Bioceramics*. 309–311 (Pt. 1, 2): 3–10, 2006.
- [59] <http://www.doitpoms.ac.uk/tplib/bones/structure.php>

- [60] Stavros C. Manolagas and Robert L. Jilka. Bone Marrow, Cytokines, and Bone Remodeling — Emerging Insights into the Pathophysiology of Osteoporosis. *N Engl J Med*, 332:305-311, 1995.
- [61] <http://training.seer.cancer.gov/anatomy/skeletal/tissue.html>
- [62] Susan Hall. *Basic Biomechanics (Fifth Edition)*, Dubuque, 2007.
- [63] [http://en.wikipedia.org/wiki/Bone\\_marrow](http://en.wikipedia.org/wiki/Bone_marrow)
- [64] *The Lymphatic System*. Allonhealth.com. Retrieved, 2011.
- [65] G.Vunjak-Novakovic, N. Tandon, A. Godier, R. Maidhof, A. Marsano, T.P. Martens and M. Radisic. Challenges in Cardiac Tissue Engineering. *Tissue Engineering Part B: Reviews* 16 (2): 169, 2010.
- [66] M. S.Thaler, R. D. Klausner, and H. J. Cohen. *Medical immunology*. Lippincott, 1977.
- [67] J. Morrison, Judith Kimble. Asymmetric and symmetric stem-cell divisions in development and cancer. *Nature*, 441(7097):1068-1074, 2006
- [68] S.J. Morrison, I.L. Weissman. The long-term repopulating subset of hematopoietic stem cells is deterministic and isolatable by phenotype. *Immunity*, 1 (8): 661–673, 1994.
- [69] 2001 Terese Winslow, Lydia Kibiuk
- [70] <https://www.stemcell.ucla.edu/blood-hematopoietic-stem-cells-hsc>
- [71] Bladé J, Samson D, Reece D, et al. Criteria for evaluating disease response and progression in patients with multiple myeloma treated by high-dose therapy and haemopoietic stem cell transplantation. Myeloma Subcommittee of the EBMT. European Group for Blood and Marrow Transplant. *Br. J. Haematol.* 102 (5): 1115–1123, 1998.
- [72] S.Z. Pavletic, I.F. Khouri, M. Haagenson, et al. Unrelated donor marrow transplantation for B-cell chronic lymphocytic leukemia after using myeloablative conditioning: results from the Center for International Blood and Marrow Transplant research. *J. Clin. Oncol.* 23 (24): 5788–5794, 2005.
- [73] Locasciulli A, Oneto R, Bacigalupo A, et al. "Outcome of patients with acquired aplastic anemia given first line bone marrow transplantation or immunosuppressive treatment in the last decade: a report from the European Group for Blood and Marrow Transplantation (EBMT)". *Haematologica*, 92 (1): 11–8. (2007).

- [74] Yu Oyama, Robert M. Craig, Ann E. Traynor Autologous hematopoietic stem cell transplantation in patients with refractory Crohn's disease. *Gastroenterology*, 128(3):552 – 563, (2005).
- [75] George P. Canellos, "The Role of Salvage Therapy in Malignant Lymphomas". *The Oncologist* 2 (3): 181–183, (1997).
- [76] Galbraith, W; Wagner, MC; Chao, J; Taylor, DL, et al. Imaging cytometry by multiparameter fluorescence. *Cytometry* 12 (7): 579–596, 1991.
- [77] Russell N, Bessell E, Stainer C, Haynes A, Das-Gupta E, Byrne J. "Allogenic haemopoietic stem cell transplantation for multiple myeloma or plasma cell leukaemia using fractionated total body radiation and high-dose melphalan conditioning". *Acta Oncol*, 39 (7): 837–841, 2000.
- [78] A Gratwohl, J Passweg, C Bocelli-Tyndall, A Fassas, et al. Autologous hematopoietic stem cell transplantation for autoimmune diseases. *Bone Marrow Transplantation*, 35, 869–879, 2005.
- [79] Shannon L. McKinney-Freeman, Kathyjo A. Jackson, Fernando D. Camargo, et al. Muscle-derived hematopoietic stem cells are hematopoietic in origin. *PNAS*, 99: 1341-1346, 2002.
- [80] Masataka Sata, Akio Saiura, Atsushi Kunisato, Akihiro Tojo, et al. Hematopoietic stem cells differentiate into vascular cells that participate in the pathogenesis of atherosclerosis. *Nature Medicine*, 8: 403 – 409, 2002.
- [81] Eric Lagasse, Heather Connors, Muhsen Al-dhalimy, et al. Purified hematopoietic stem cells can differentiate into hepatocytes in vivo. *Nature Medicine*, 6:1229-1234, 2000.
- [82] I.L. Weissman. Translating stem and progenitor cell biology to the clinic: barriers and opportunities. *Science*, 287: 1442–1446, 2000.
- [83] Eric Lagasse, Judith A. Shizuru, Nobuko Uchida, Ann Tsukamoto, Irving L. Weissman, Toward Regenerative Medicine , *Immunity*, 14(4) :425-436, 2001.
- [84] Oostendorp, R. A. et al. Stromal cell lines from mouse aorta-gonads-mesonephros subregions are potent supporters of hematopoietic stem cell activity. *Blood*, 99:1183–1189, 2002.
- [85] R. S. Taichman and S. G. Emerson. The role of osteoblasts in the hematopoietic microenvironment. *Stem Cells*, 16:7–15, 1998.

- [86] Ronald Palacios, Eva Golunski and Jacqueline Smaridis. In vitro generation of hematopoietic stem cells from an embryonic stem cell line (hematopoiesis/stromal cells/cytokines). *Proc. Natl. Acad. Sci. Developmental Biology*, 92: 7530–7534, 1995
- [87] D. Visnjic, et al. Hematopoiesis is severely altered in mice with an induced osteoblast deficiency. *Blood*, 103, 3258–3264, 2004.
- [88] D. Visnjic, et al. Conditional ablation of the osteoblast lineage in Col2.3<sup>sk</sup> transgenic mice. *J. Bone Miner. Res.*, 16, 2222–2231, 2001.
- [89] Anne Wilson and Andreas Trumpp. Bone-marrow haematopoietic-stem-cell niches. *Nature Reviews Immunology*, 6: 93–106, 2006.
- [90] O. Ohneda, et al. Hematopoietic stem cell maintenance and differentiation are supported by embryonic aorta-gonad-mesonephros region-derived endothelium. *Blood* 92, 908–919 (1998).
- [91] W. Li, et al. Primary endothelial cells isolated from the yolk sac and para-aortic splanchnopleura support the expansion of adult marrow stem cells *in vitro*. *Blood*, 102, 4345–4353, 2003.
- [92] T. L. Huber, V. Kouskoff, H. J. Fehling., J. Palis, and G. Keller. Haemangioblast commitment is initiated in the primitive streak of the mouse embryo. *Nature*, 432, 625–630, 2004.
- [93] W. Li, S. A. Johnson, W. C. Shelley and M. C. Yoder. Hematopoietic stem cell repopulating ability can be maintained *in vitro* by some primary endothelial cells. *Exp. Hematol.* 32, 1226–1237, 2004.
- [94] Sergey V. Dorozhkin, Review: Calcium orthophosphates , *Journal of Materials Science*, 42, (4):1061-1095,(2007).
- [95] R.Z Legeros. *Calcium phosphates in oral biology and medicine*. Karger, 1991.
- [96] J.C .Elliot. *Structure and chemistry of the apatites and other calcium orthophosphates*. Elsevier, 1994.
- [97] Z. Amjad. *Calcium phosphates in biological and industrial systems*. Springer: 529 ,1997.
- [98] Sergey V. Dorozhkin. Review: Calcium orthophosphates. *Journal of Materials Science*, 42, (4):1061-1095, 2007.
- [99] W.Cao, L.L. Hench. Bioactive materials. *Ceram Int* , 22:493–507, 1996.
- [100] K. Anselme. Osteoblast adhesion on biomaterials. *Biomaterials*, 21: 667–681, 2000.

- [101] J.E. Davies. In vitro modeling of the bone/implant interface. *Anat Rec*, 245: 426–445, 1996.
- [102] J.L. Ong, D.C.N. Chan. Hydroxyapatite and their use as coatings in dental implants: a review. *Crit Rev Biomed Eng.*, 28:667–707, 1999.
- [103] R.Z. LeGeros and R.G. Craig. Strategies to affect bone remodeling: osteointegration. *J Bone Miner Res*, 8 (Suppl. 2): 583-596, 1993.
- [104] <http://www.algaeinstitute.com/hydroxyapatite.html>
- [105] <http://electronicstructure.wikidot.com/cation-substitutions-in-hydroxyapatite>
- [106] <https://en.wikipedia.org/wiki/Hydroxylapatite>
- [107] Erika Meier, Processing of Calcium Hydroxyapatite Foam
- [108] M.J. Buerger. Crystallographic aspects of phase transformations. In R. Smoluchowski, J.E. Meyer, W.A. Weyl, editors, *Phase transformations in solids*, John Wiley, 1951.
- [109] G. Renaudin, P. Laquerrière, Y. Filinchuk, E. Jallot and J. M. Nedelec. Structural characterization of sol–gel derived Sr-substituted calcium phosphates with anti-osteoporotic and anti-inflammatory properties. *J. Mater. Chem*, 18:3593-3600, 2008.
- [110] P.Ducheyne, S. Radin, and L. King. The Effect of Calcium Phosphate Ceramic Composition and Structure on in vitro Behavior: Dissolution. *J. Biomed. Mater. Res.*, 27: 25–34, 1993.
- [111] N. Kivrak, A.C. Tas. Synthesis of calcium hydroxyapatite-tricalcium phosphate (HA-TCP) composite bioceramics powders and their sintering behavior , *J Am Ceram Soc*, 81 (9):2245 – 2252, 1998.
- [112] I.R. Gibson, I. Rehman, S.M. Best, W. Bonfield, Characterization of the transformation from calcium-deficient apatite to  $\beta$ -tricalcium phosphate , *J Mater Sci.: Mater Med*, 12:799– 804, 2000.
- [113] N. Kotobuki, D. Kawagoe, D. Nomura, Y. Katou, et al. Observation and Quantitative Analysis of Rat Bone Marrow Stromal Cells Cultured in vitro on Newly Formed Transparent Beta-tricalcium Phosphate , *J. Mater. Sci. Mater. Med.*, 17: 33–41, 2006.
- [114] R.G. Carrodeguas and S. De Aza.  $\alpha$  -Tricalcium phosphate: Synthesis, properties and biomedical applications. *Acta Biomaterialia* , 10 (7): 3536-3546, 2011.
- [115] M. Bohner. Calcium orthophosphates in medicine: from ceramics to calcium phosphate cements. *Injury*, 31 (Suppl. D): 37–47, 2000.

- [116] S.V. Dorozhkin. Calcium orthophosphate cements for biomedical application. *J Mater Sci*, 43:3028–3057, 2008.
- [117] Shinya Nakamura, Takuya Matsumoto, Jun-Ichi Sasaki, Hiroshi Egusa, et al. Effect of Calcium Ion Concentrations on Osteogenic Differentiation and Hematopoietic Stem Cell Niche-Related Protein Expression in Osteoblasts. *Tissue engineering: Part A*, 8(16):2467-2473, 2010.
- [118] P. Ducheyne, S. Radin and L. King. The Effect of Calcium Phosphate Ceramic Composition and Structure on in-vitro Behavior. I. Dissolution. *J. Biomed. Mater. Res.*, 39 603-610, 1998.
- [119] <http://ion.chem.usu.edu/~sbialkow/Classes/3600/alpha/alpha3.html>
- [120] M. Bohner. Calcium orthophosphates in medicine: from ceramics to calcium phosphate cements. *J.Care Injured*, 31: D37-47, 2000.
- [121] G. Daculsi, R. Z. Legeros, E. Nery, K. Lynch and B. Kerebel. Transformation of Biphasic Calcium Phosphate Ceramics in-vivo: Ultrastructural and Physicochemical Characterization. *J. Biomed. Mater. Res.*, 23: 883-894, 1989.
- [122] A.E. Porter, N. Patel, J.N. Skepper, S.M. Best and W. Bonfield. Comparison of in-vivo Dissolution Processes in Hydroxyapatite and Silicon-Substituted Hydroxyapatite Bioceramics. *Biomaterials*, 24:4409-4620, 2003.
- [123] Birbrair, A.; Zhang, T.; Wang, Z.-M.; Messi, M. L.; Olson, J.D.; et al, Type-2 Pericytes Participate in Normal and Tumoral Angiogenesis. *Am J Physiol Cell Physiol*, 307(1):C25-38, 2014
- [124] John S. Penn. *Retinal and Choroidal Angiogenesis*. Springer: 119. Retrieved, 2010.
- [125] Li, W. et al. Primary endothelial cells isolated from the yolk sac and para-aortic splanchnopleura support the expansion of adult marrow stem cells in vitro. *Blood*, 102: 4345–4353, 2003.
- [126] Ohneda, O. et al. Hematopoietic stem cell maintenance and differentiation are supported by embryonic aorta-gonad-mesonephros region-derived endothelium. *Blood*, 92: 908–919, 1998.
- [127] M.M. Dvorak, D. Riccardi. Ca<sup>2+</sup>as an extracellular signal in bone. *Cell Calcium*, 35: 249, and 2004.
- [128] Wang, J.F., Liu, Z.Y., and Groopman, J.E. The alphachemokine receptor CXCR4 is expressed on the megakaryocytic lineage from progenitor to platelets and modulates migration and adhesion. *Blood*, 92:756, 1998.

- [129] Peled, A., Petit, I., Kollet, O., Magid, M, et al. Dependence of human stem cell engraftment and repopulation of NOD/SCID mice on CXCR4. *Science*, 283:845, 1999.
- [130] Arai, F., Hirao, A., Ohmura, M., Sato, H., et al, Tie2/angiopoietin- 1 signaling regulates hematopoietic stem cell quiescence in the bone marrow niche. *Cell*, 118:149, 2004.
- [131] Shinya Nakamura, Takuya Matsumoto, Jun-Ichi Sasaki, Hiroshi Egusa, et al, Effect of Calcium Ion Concentrations on Osteogenic Differentiation and Hematopoietic Stem Cell Niche-Related Protein Expression in Osteoblasts , *TISSUE ENGINEERING: Part A*,8(16) :2467-2473, 2010.
- [132] R. Brezny and D. J. Green. Mechanical behavior of cellular solids. In W. Cahn, P. Haasen and E. J. Kramer, editors, *Materials Science and Technology, Vol. II, Structure and Properties of Ceramics*. R VCH, Germany, 1992.
- [133] L.M. Sheppard, Porous Ceramics: Processing and Applications, K. Ishizaki, L. Sheppard, S. Okada, T. Hamasaki, and B. Huybrechts, editors. *Ceramic Transactions, Porous Materials*, The American Ceramic Society, Westerville, 1993
- [134] A.R. Studart, U.T. Gonzenbach, E. Tervoort, et al,, Processing Routes to Macroporous Ceramics: A Review , *Journal of the American Ceramic Society*, 89(6): 1771–1789, 2006
- [135] K. Schwartzwalder and A. V. Somers, Method of making porous ceramic articles. US Patent No. 3:090-094, 1963.
- [136] J.G.P. Binner. Ceramic Foams. In Scheffler M, Colombo P, editors, *Cellular Ceramics: Structure, Manufacturing, Properties and Applications*. Weinheim;Chichester;: Wiley-VCH, 2005.
- [137] H.X. Peng, Z. Fan and J.R.G. Evans. Microstructure of Ceramic Foams. *J. Eur. Ceram. Soc.*, 20:807-813, 2000.
- [138] Andre' R. Studart, Urs T. Gonzenbach, Elena Tervoort, and Ludwig J. Gauckler. Processing Routes to Macroporous Ceramics: A Review. *J. Am. Ceram. Soc.*, 89 (6): 1771–1789, 2006.
- [139] P. Colombo, E. Bernardo, and L. Biasetto, Novel Microcellular Ceramics from a Silicone Resin, *J. Am. Ceram. Soc.*, 87 (1):152–154, 2004.
- [140] O. Lyckfeldt and J. M. F. Ferreira, Processing of Porous Ceramics by Starch Consolidation, *J. Eur. Ceram. Soc.*, 18 (2):131–140, 1998.
- [141] T. J. Fitzgerald, V. J. Michaud, and A. Mortensen. Processing of Microcellular Sic Foams. 2. Ceramic Foam Production. *J. Mater. Sci.*, 30 (4):1037–1045, 1995.

- [142] R. J. Pugh, Foams and Foaming. In K. Holmberg, editor, *Handbook of Applied Surface and Colloid Chemistry*. John Wiley & Sons Ltd, 23–43, 2001.
- [143] U. T. Gonzenbach, A. R. Studart, E. Tervoort, and L. J. Gauckler. Ultrastable particle-stabilized foams. *Angew Chem Int Ed Engl.*, 19; 45(21):3526-3530, 2006.
- [144] S. U. Pickering, Emulsions, *J. Chem. Soc.*, 91: 2001–2021, 1907.
- [145] E. Dickinson, R. Ettelaie, T. Kostakis, and B. S. Murray, Factors Controlling the Formation and Stability of Air Bubbles Stabilized by Partially Hydrophobic Silica Nanoparticles, *Langmuir*, 20 (20):8517–25, 2004 .
- [146] Z. P. Du, M. P. Bilbao-Montoya, B. P. Binks, E. Dickinson, R. Ettelaie, and B. S. Murray, Outstanding Stability of Particle-Stabilized Bubbles, *Langmuir*, 19 (8): 3106–8, 2003.
- [147] B. P. Binks, Particles as Surfactants—Similarities and Differences, *Curr. Opin. Colloid Interf. Sci.*, 7 (1–2): 21–41, 2002.
- [148] S. Barg, C.Soltmann, M.Andrade, D.Koch and G.Grathwohl. Cellular ceramics by direct foaming of emulsified ceramic powder suspensions, *J.Am.Ceram.Soc.*, 91:2823-2829, 2008.
- [149] M.N. Rahaman. Sintering of ceramics. *CRC Press*, Boca Raton, 2008.
- [150] E. Champion. Sintering of Calcium phosphate bioceramics. *Acta Biomaterialia*, 4(9):5855-5875, 2013.
- [151] [http://www.keramverband.de/brevier\\_engl/4/1/4\\_1\\_4.htm](http://www.keramverband.de/brevier_engl/4/1/4_1_4.htm)
- [152] E. G. Youngs. Infiltration measurements—a review. *Hydrol. Process*, 5(3): 309–319, 1991.
- [153] B.R. Marple, D. J. Green.Graded compositions and microstructures by infiltration processing. *Journal of Material Science*, 28:4637-4643, 1993.
- [154] Yung-Jen Lin and Yi-Chi Chen. Cyclic Infiltration of Porous Zirconia Preforms with a Liquid Solution of Mullite Precursor. *Journal of the American Ceramic Society*,84 (1): 71–78, 2001.
- [155] P. Honeyman-Colvin and F F.Lange, Infiltration of porous alumina bodies with solution precursors: strengthening via compositional grading, grain size control, and transformation toughening, *J.Am.Ceram.Soc*, 79(7):1810-1814, 1996.

- [156] A. Rapacz-Kmitaa, C. Palusziewiczab,\* A. S'lo'sarczyka, Z. Paszkiewicza, FTIR and XRD investigations on the thermal stability of hydroxyapatite during hot pressing and pressureless sintering processes , *Journal of Molecular Structure* ,744–747: 653–656, 2005.
- [157] Julius MH, Masuda T, Herzenberg LA. Demonstration that antigen-binding cells are precursors of antibody-producing cells after purification with a fluorescence-activated cell sorter. *Proc. Natl. Acad. Sci. U.S.A.* 69 (7): 1934–1938, 1972.
- [158] Schmelzer E, Finoli A, Nettleship I, Gerlach JC. Long-term three-dimensional perfusion culture of human adult bone marrow mononuclear cells in bioreactors. *Biotechnology and bioengineering*, 112:801-10, 2015.
- [159] Hoshi, H, and W L McKeehan. Brain- and Liver Cell-Derived Factors Are Required for Growth of Human Endothelial Cells in Serum-Free Culture. *Proceedings of the National Academy of Sciences of the United States of America*, 81(20): 6413–6417, 1984.
- [160] <http://www.sigmaaldrich.com/china-mainland/zh/life-science/cell-culture/learning-center/media-expert/calcium.html>
- [161] Fiorio Pla, Alessandra, and Dimitra Gkika. Emerging Role of TRP Channels in Cell Migration: From Tumor Vascularization to Metastasis. *Frontiers in Physiology*, 4: 311, 2013.
- [162] Choi, Ji Sun, Bhushan P. Mahadik, and Brendan A. C. Harley. Engineering the Hematopoietic Stem Cell Niche: Frontiers in Biomaterial Science. *Biotechnology journal*, 10:1529–1545, 2015.
- [163] L.M. Calvi, G.B. Adams, K.W. Weibrech, et al. Osteoblastic cells regulate the haematopoietic stem cell niche. *Nature*, 425 (6960): 841-846, 2003.
- [164] Silver IA, Murrills RJ, Etherington DJ. Microelectrode studies on the acid microenvironment beneath adherent macrophages and osteoclasts, *Exp Cell Res.*, 175(2):266-76, 1988.
- [165] Lorget F, Kamel S, Mentaverri R, Wattel A, Naassila M, Maamer M, Brazier M. High extracellular calcium concentrations directly stimulate osteoclast apoptosis. *Biochem Biophys Res Commun*, 268(3):899-903, 2000.
- [166] J T Buckley and J N Hawthorne. Erythrocyte membrane polyphosphoinositide metabolism and the regulation of calcium binding. *J Biol Chem.* ,247(22):7218-23, 1972